THE MECHANICAL DESIGN ASPECTS OF A SMALL DIAMETER VASCULAR PROSTHESIS

IC MACKELLAR

July 1998

Submitted in partial fulfilment for the requirements of the degree of Master of Science in Mechanical Engineering

---

Department of Mechanical Engineering
University of Cape Town
Rondebosch
7700
South Africa

DECLARATION

I, Iain MacKellar, declare that the work set out in this thesis is essentially my own work and that no part has been submitted for a degree at any academic institution.

Signed by candidate

Signature removed

Iain MacKellar

July1998

ACKNOWLEDGEMENTS

I would like to express my sincere thanks to the following people and organisations:

My Supervisors, Dr. Greg Starke and Professor Daya Reddy for their encouragement and technical assistance

Damian Conway and Dr. Greg Mitchell for their sound advise and assistance.

Deon Bezuidenhout and everybody at the Cardiovascular Research Unit, UCT for their helpful input and valuable suggestions

Colleagues at CERECAM for their encouragement

The Centre for Research in Computational and Applied Mechanics (CERECAM) and the Foundation for Research Development (FRD) for financial assistance.

SYNOPSIS

Failure of medium to small diameter vascular grafts is believed to be in part due to the compliance mismatch between the native artery and the implanted graft. Consequently, designers are examining the use of more compliant materials for their manufacture. Ether free polyurethanes are currently amongst the most popular materials for use in biological implants although these materials are inherently too stiff for use in vascular prostheses. These materials can be made more compliant by introducing porosity. Apart from creating a more compliant overall material, under optimal biological conditions, the porosity may lead to cell ingrowth through the thickness of the graft allowing an endothelial cell layer to form on the inner flow surface. Compliance and cell ingrowth are both important characteristics that determine the successful functioning of the graft.

The current work is part of a collaborative venture with the Cardiovascular Research Unit (CVRU) at the University of Cape Town to design and develop a new polyurethane graft. Finite element models are used to facilitate stress analyses and to evaluate the long-term behaviour and compliance of various graft designs made from a bio-inert thermoplastic polyurethane.

Material properties of the polyurethane are determined from uniaxial tension tests, simple-shear tests and viscoelastic shear tests. The constitutive equations for a compressible, large strain hyperelastic material model with viscoelasticity are implemented in the finite element code using material constants calculated from the test data. The behaviour of the finite element model is verified by using a single element test and comparing results to the material data.

The finite element model is validated for use in more sophisticated problems by comparing axi-symmetric models with *in vitro* experiments. An artery/graft anastomosis is then analysed by modelling the artery as an incompressible hyperelastic material. Further more complex graft designs are analysed with internal growth channels and spiral reinforcing winds. Viscoelastic effects are also examined. The modelling method is discussed and important results are noted.

It was found that an initially compliant, microporous graft with internal growth channels is achievable using the polyurethane. However, the long-term viscoelastic properties of the material predominate and some form of reinforcing is necessary. Analyses

investigating the effect of external reinforcing indicate that most of the compliance is sacrificed when reinforcing is applied. Furthermore, the reinforcing material should not be viscoelastic and should be as compliant as the whole graft structure.

TABLE OF CONTENTS

CHAPTER ONE

INTRODUCTION

Vascular disease in small to medium diameter arteries adversely affects the arterial wall structure. As a result, the blood flow through the vessel is hindered either by the total occlusion or, in the opposite extreme, an acute over dilation of the vessel (aneurysm). Such indications usually require reconstructive or bypass surgery. The most successful replacements at present are autologous grafts (arteries and veins taken from the host), but often these are too diseased or unsuitable for use as an implant. There is thus a great need for the development of a reliable small diameter vascular prostheses.

Over the last 40 years, considerable progress has been made in the development of artery prostheses. The modern era of vascular surgery began in the early 1950's, 40 years after Carrel and Gutherie (1906) demonstrated that autologous veins could be used to replace arteries. With the advent of antibiotics and anticoagulants in ancillary medicine, the development of vascular prostheses prospered. The reversed saphenous vein was soon considered the best artery replacement and was used successfully in femoral artery replacement by Kunlin in 1949. However the need for a larger prosthesis led to further research by Gross and associates involving homografts using sterilised tissue. Although early results were encouraging, the long-term results were still unsatisfactory, with the grafts often failing due to thrombosis and aneurysm. (Burkel 1988)

While pioneers such as Gross *et al.* (1948) worked on with hetero- and homografts, Voorhees made an important observation in 1952 that changed the direction of vascular prosthetic development. After discovering that cells grew on silk thread exposed to blood, he showed the effectiveness of synthetic textile or fabric tubes as arterial replacements. A new era of vascular surgery began and the search for the most suitable material and optimal structure for a textile graft began (Burkel 1988). Experiments until recently investigated factors such as knitted or woven textiles, large or small pores, different surface finishes and crimping and external reinforcing.

Presently, the materials used for vascular implants are tanned natural vessels, textile tubes made from woven or knitted Dacron, or tubes made from e-PTFE. These grafts are successful

for large diameter artery replacement where there is a high blood flow rate; (Sauvage *et al.*, 1974) but they have a much lower success rate in arteries with a diameter less than 6mm. All of the present grafts eventually fail by occlusion due to thrombosis (fibrous tissue build up), or intimal hyperplasia (exuberant muscle growth at the interface between artery and graft).

Factors such as the thrombogenic nature of the graft material, surface roughness, the mechanical and haemodynamic properties of the graft and the condition of the host artery are known to influence the success of the graft (Burkell 1987, How *et al.* 1992). Although the reasons for failure are not fully understood, it is largely agreed that the compliance mismatch between artery and graft is the predominant issue surrounding the failure of small diameter prostheses. (Abbott *et al.* 1987, Baird *et al.* 1977, Hasson *et al.*1985, Hayashi *et al.* 1993, How *et al.* 1992, Lyman *et al.* 1978, Stewart *et al.* 1992, Seifert *et al.* 1979, Sauvage *et al.* 1974, Weston *et al.* 1996). The discontinuity in mechanical properties between the graft and artery alters the blood flow resulting in a fibrous tissue build-up leading to the complete occlusion and hence failure of the graft. (Abbott *et al.* 1987, Burkell 1987, Ballyk *et al.* 1996, Deweese JA, 1985, Flemma *et al.* 1978, Stewart *et al.* 1992).

One of the main reasons for a fibrous build up on the graft is the thrombogenic reaction of the blood with the graft material. Much of the current research involves the development of various polymers – especially polyurethanes, to which biological coatings can be applied to improve the stability of the graft in the body over long periods. Ideally the graft should have an endothelial cell lining on the inner wall. This prevents a reaction by providing a less thrombogenic flow surface for the blood passing through it (Burkel 1988). One way of achieving this is through a porous graft structure. This, in conjunction with suitable biological engineering, can induce cell ingrowth through the wall leading to musculogenesis and the eventual endothelialisation of the inner surface (How *et al.* 1992, Hayashi *et al.* 1987, Hess *et al.* 1986, Sauvage *et al.* 1974).

Autologous grafts, such as the saphenous vein and the internal mammary artery are still considered the best grafts for the reconstruction of small peripheral arteries (Harris *et al.* 1987, Loop 1976, Flemma *et al.* 1976), but these are often too diseased or unsuitable for use as a graft. None of the present textile grafts (PTFE and Dacron) have proved successful for long periods either (Bergen *at al.* 1982, Brewster *et al.* 1983, Burkel 1989). Many new and novel approaches to graft production have been developed in an effort to create a porous polyurethane artery graft. Indeed, it has been shown that it is possible to create an initially compliant porous graft (Hayashi *et al.* 1989, Lyman *et al.* 1987, Mooney *et al.* 1996). However, the long-term patency (success) of such grafts remains to be proven. It has become apparent that the current methods of graft construction are ineffectual and a new approach is necessary.

It is evident that the present small diameter grafts do not provide an acceptable long-term patency. Although the causes for failure are not immediately clear, it is apparent that none of the previous prostheses have the same structure as an artery or behave mechanically as an artery does. Apart from the biological issues, which are arguably the most important and complex issue in graft design, one of the central issues involves understanding the mechanics of arterial behaviour. Recent investigations have addressed the issue of compliance in an effort to create a structurally similar graft, but compliance alone has not proved completely successful. Thus, there is a need to develop a graft that addresses the issue of mechanical behaviour through structure. The graft structure should create an optimal strain environment that will facilitate and encourage the development and maintenance of endothelial and smooth muscle cells in the vessel.

This work is a collaborative effort with the Cardiovascular Research Unit at the University of Cape Town and sets out a design approach for the development of a small diameter vascular prosthesis using a bio-stable segmented polyurethane.

The specific objectives of this work are to:

- Design a new artery graft.
- Adequately characterise a new polyurethane for implementation in the finite element method.
- Show how the finite element method can be used as an effective structural design tool in the process of developing a new graft.

Chapter Two discusses the physical structure and mechanical behaviour of arteries in order to obtain an insight to the complex nature of the vessels. The structural requirements of grafts are reviewed next, followed by an introduction to the behaviour and production of polymeric materials. This is followed by a review of present graft designs. Chapter Three deals with the characterisation of the proposed graft material. This includes a discussion of the theory necessary to describe polymeric behaviour, which can be implemented in the finite element method. Following this is a description of the mechanical tests performed on the polymer to characterise the material. This includes tensile testing, "simple-shear" testing and time dependent viscoelasticity testing. The numerical models are then verified in tests using a single element. Chapter Four begins with a review of some graft design concepts. The numerical model is validated by comparing results from *in vitro* experiments to basic numerical analyses. After this, some more sophisticated graft designs are modelled and relevant results are presented. The results are discussed in Chapter Five.

CHAPTER TWO

THE STRUCTURE OF ARTERIES AND GRAFTS

2.1 INTRODUCTION

Arteries are not only responsible for transporting blood to the organ systems, but also for maintaining regulated pressure and smooth blood flow. The energy of each pulse from the heart must be absorbed by the elasticity of the artery walls to regulate the blood flow and maintain a consistent pressure. When arteries become stiffened through disease and are unable to dilate, the pressure necessary to provide flow through the system increases dramatically, placing enormous strain on the heart and the rest of the arteries. An increased systolic pressure often leads to the over dilation of arteries that have lost their elasticity resulting in aneurysm or heart failure. It is the unique elasticity or contractility of the arteries that ensures the normal functioning of the circulatory system. In the development process of designing a replacement vessel, it is important to study the structure and functioning of arteries to understand the mechanics that characterize this behaviour.

To provide an insight into the purpose and functioning of arteries and to clarify the role of an artery graft, this section briefly introduces the biomechanics of circulation and the form and function of arteries. Aspects of arterial mechanics are then discussed followed by a review of the structural requirements for an artery graft, current biomedical polymeric materials for graft production and current graft structures. The requirements for a successful graft are detailed in the last section of the chapter.

2.2 BIOMECHANICS OF THE CIRCULATING SYSTEM

The heart supplies pressure for blood flow and connects the two vascular beds that form the circulatory system (Figure 2.1). The chambers on the left side of the heart supply oxygenated blood to the systemic circulation and the chambers on the right side of the heart supply blood to the pulmonary circulation. The left ventricle pumps blood into the aorta where arteries and arterioles branching from the aorta transport the blood to the capillary networks of various organ systems. Here oxygen and nutrients are absorbed and exchanged across the capillary membrane. Veins and venules collect the blood, which flows back into the right atrium via the vena cavae. The right ventricle pumps blood to the pulmonary arteries and into the pulmonary capillaries where the exchange of oxygen takes

place with the atmosphere. The oxygenated blood flows through the pulmonary venous system back into the left atrium.

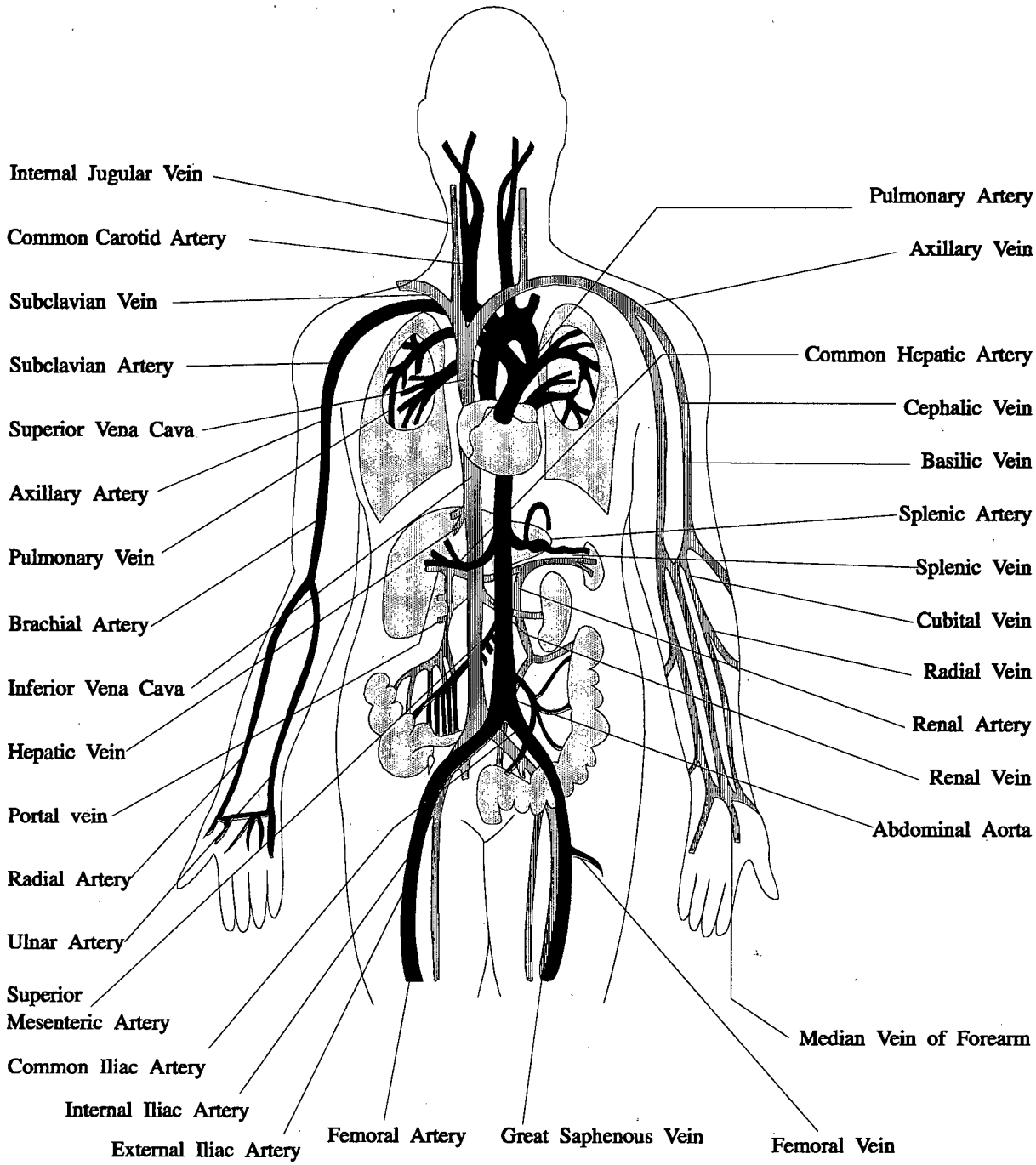

Figure 2.1 Arteries and veins of the human circulatory system. (CorelDraw v.7)

2.3 THE STRUCTURE OF ARTERIES

There are generally two types of arteries, elastic and muscular. Elastic arteries are mostly large diameter vessels such as the aorta, pulmonary artery and common carotids. Muscular arteries include the femorals, cerebrals and coronary arteries and are smaller in diameter. The size varies along the aortic tree, with the larger elastic arteries near the heart and the smaller muscular arteries near the capillaries. The further away from the heart, the smaller and more muscular the arteries become.

The arterial wall can be divided into three distinct layers or tunica, the intima, media and adventitia (Figure 2.2). The intima is similar for most arteries and consists of a single layer of endothelial cells lining the innermost surface of the artery. A thin sheet of elastin separates the intima from the media. In elastic arteries, the media consists mainly of alternating layers of smooth muscle cells and elastic lamina, all connected by a ground substance gel matrix. The smooth muscle cells are generally oriented in a helical arrangement although this can become almost circumferential in some places. The smooth muscle in muscular arteries appears as a single thick layer and is also generally helically oriented. The adventitia is the outermost layer and consists mostly of ground substance with bundles of elastin, collagen, nerves, some fibroblasts, macrophages and vasa vasorum. (Humphery, 1995)

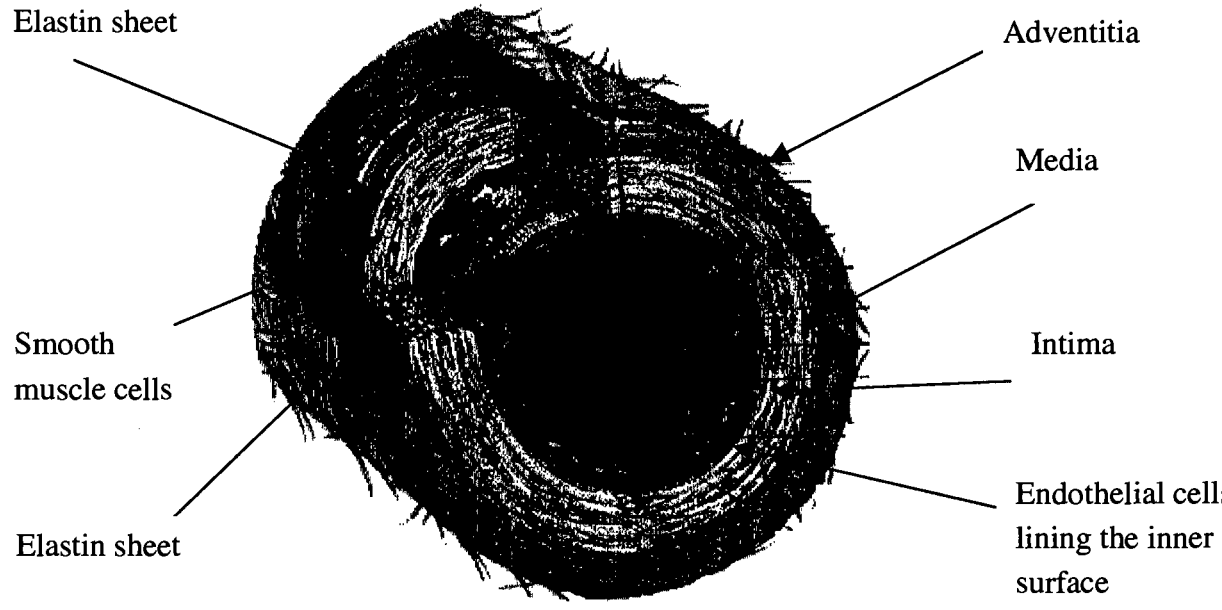

Figure 2.2 A muscular artery showing the various layers and structure of the arterial wall.

2.3.1 Arterial mechanics

An artery is thus not merely a conduit that supplies blood, but a complicated synergy of organic fibres that regulate the blood flow and optimise the function of the cardiovascular system. The composite nature of arteries suggests that their mechanical behaviour is not trivial. Helical muscle growth, stiff inextensible collagen and rubber-like elastin all combined in an optimally designed structure gives rise to a host of mechanical issues that need to be considered when characterising arterial behaviour. The walls are structurally anisotropic, incompressible and highly deformable, exhibiting a non-linear stress strain response. In order to fully characterise their behaviour, the following section deals with the mechanical and structural aspects of arteries.

2.3.2 Incompressibility

An artery is a composite material consisting of layers of elastin, collagen and smooth muscle in a fluid or gel matrix. The high fluid content suggests that arterial walls are incompressible. This implies that the volume is preserved during deformation or that the ratio of shear modulus to bulk modulus is very large. Carew *et al.* Lawton, Dobrin, Rovick (Humphery 1995) have all shown that arteries deform approximately isochorically. Choung and Fung (1984) measured fluid extrusion during compression on rabbit aorta segments and reported results similar to Carew *et al.* The results of these investigators indicate that the assumption of incompressibility is reasonable for arteries under normal physiological loading. By assuming incompressibility, the stress / strain analysis of the artery is simplified. The deformation in the radial direction is solely determined by the deformation in the longitudinal and circumferential directions.

2.3.3 Pre Stress

The stress distribution through a thick walled cylinder due to an internal pressure varies considerably. There is a peak stress at the inner surface that decays exponentially throughout the thickness to the outer surface. In arteries this stress through the wall thickness is reduced to a more uniform state by pre stressing. This pre stressing is evident in the way an artery will spring open if a section is cut along its axis. Figure 2.3 shows a rat artery (a) pressurised – this represents the zero load state in the artery, (b) un-pressurised – the artery has a bunched up appearance due to the internal compressive stress, and (c) cut open along its axis. The compressive pre stress results in the artery opening up when it is cut open. Pre stress reduces the peak stress at the internal surface due to an internal pressure and moderates the stress through the thickness so that the artery operates at a lower overall stress state. Several researchers (Choung and Fung 1986, Fung *et al.* 1992) have examined pre-stressing. The degree of pre-stress is usually determined by measuring the angle made by the artery when it springs open. The angle gives an indication of the amount of compressive stress present in the arterial wall.

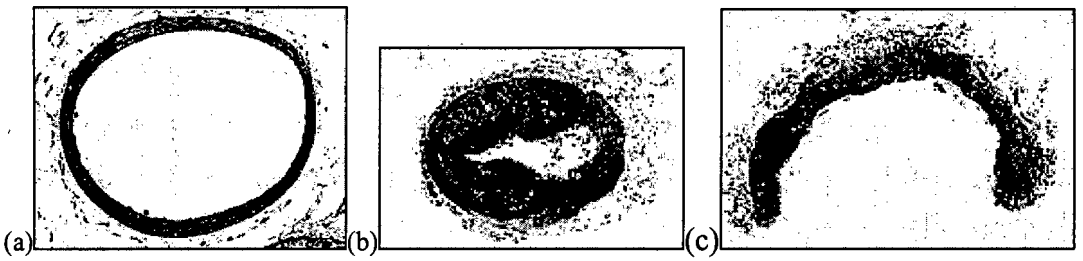

Figure 2.3 Sectional geometry of the rat pulmonary artery at (a) *in vivo* loading of 15mmHg, (b) *no-load* and (c) *no stress* (Fung *et al.*, 1992).

2.3.4 Non Linear Behaviour

Perhaps the most important mechanical feature of arteries is their non-linear stress strain behaviour. The mechanical behaviour of most biological tissues is highly non-linear and arteries are no exception. In terms of mechanical behaviour, the intima and media can be grouped together as one layer and the adventitia as a second. The adventitia layer has an elastic modulus that is an order of magnitude higher than the intima–media layer. During normal physiological conditions, arteries are subjected to cyclic pressure loading between 10 and 16kPa (75 – 120 mmHg). The response in this range is largely linear elastic as the load in the wall is absorbed initially by the intima-media layer. At higher pressures, from about 20kPa (150mmHg), more of the load is transferred to the adventitia. As the loose bundles of collagen fibres align themselves and as more fibres are recruited, the wall experiences marked stiffening. This mechanism prevents over inflation or aneurysm at excessive pressures.

2.3.5 Anisotropy

It is reasonable to assume that arteries are anisotropic. Many investigators have shown that the arterial wall is stiffer in the circumferential direction than in the axial direction (Cox 1975, Sato *et al.* 1979, Vosshougi and Wiezsacker 1985, Dobrin 1986) but others have found the opposite (Gentile *et al.* 1988, Papageorgio and Jones 1988). Discrepancies have been attributed to differences in methodology, animal species and arterial sites. Some investigators have shown that longitudinal force is independent of internal pressure and that over an averaged physiological range of internal pressures and axial forces the arterial walls are isotropic (Wiezsacker and Pinto 1988, Dobrin 1986). In the absence of active smooth muscle, arteries exhibit hysteresis under cyclic loading, stress relaxation under constant extension and creep under constant loads. These findings indicates that arteries are viscoelastic

2.3.6 Viscoelasticity

As long as 40 years ago, investigators realised that biological soft tissues, including arteries displayed viscoelastic behaviour. Fung (1972) found that arterial tissue does indeed exhibit a delayed response to loading. He found that stiffness increased with increased loading rate, but the amount of lag associated with the hysteresis was fairly insensitive to strain rate. Using data from tests done on canine aortas, Fung was able to postulate a fairly simple continuous modulus function for arterial behaviour that assumed linear viscoelastic behaviour. Later studies by Hutchinson (1974), Newan (1975) and Greenwald (1982) were consistent with this result. However, these tests were done on animal species and more recent work done by Langewouters *et al.* (1984; 1985) has shown that human arterial wall tissue has a non-linear viscoelastic response (i.e. the viscoelastic parameters vary significantly with varying strain). There now appears to be consensus in the literature that the true viscoelastic behaviour of biological soft tissues (including arterial tissue) is indeed non-linear (Haut *et al.*, 1972, Young *et al.*, 1977; Dehoff, 1978; Decraemer *et al.*, 1980; Wu and Lee, 1984; Demiray, 1996; Johnson *et al.*, 1996).

2.4 Graft Structural and Mechanical Requirements

A host of requirements determine a grafts overall success. Most of these are biological factors that limit or compliment a grafts performance in the body, but the structural and mechanical issues must be examined to determine the most effective manner in which to support this biological framework. Much has been learned from past innovative and novel designs in the search for a successful prosthesis creating a knowledge base of information. The following section outlines some of the prominent issues relevant to the structure and mechanics of artery grafts.

2.4.1 Compliance matching

Compliance in arteries is thought by many researchers to be the most important issue in small diameter graft design (Weston *et al.* 1995, Lyman *et al.* 1988, Kidson *et al.* 1978, Abbott *et al.* 1987, Baird *et al.* 1976, and White *et al.*1983). Compliance is necessary to maintain a regular blood flow and to provide a steady pressure pulse to the peripheral arteries. Many investigators have identified a positive link between arterial compliance and performance of grafts (Courtman 1994, Trubel *et al.* 1994), while others have found no significant difference. However, most surgeons now agree that grafts that are compliance matched and have matching mechanical properties ought to perform better haemodynamically.

A discontinuity in elastic properties between artery and graft results in a discontinuous pressure pulse. The pressure pulse is attenuate by the relatively stiff or non-compliant grafts like Dacron and PTFE (Figure 2.4). A stiffer graft has a smaller effective diameter,

which influences the local haemodynamics causing turbulence and flow separation downstream of the anastomosis creating high wall shear stresses. Abnormally high or low wall shear stresses have been associated with intimal hyperplasia, the build up of fibrous tissue that leads to long term failure (Ishibashi *et al.* 1996, Dobrin *et al.* 1989, Friedman *et al.* 1981, Binns *et al.* 1989). When a relatively stiff graft is implanted in a compliant artery, the restriction in movement imposed by the graft causes high stresses at the suture line. This may be the cause of anastomotic aneurysms and intimal hyperplasia, which have been observed with the use of stiff artery grafts. (Ojha *et al.* 1996)

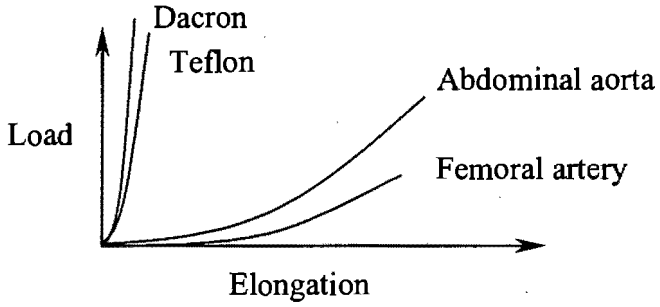

Figure 2.4: Stiffness comparison of Dacron and Teflon to femoral and abdominal artery.

Hayashi *et al.* (1980) proposed an equation to describe pressure-diameter relations of arteries in the physiological pressure range (60 –160mmHg).

$$\ln\left(\frac{P}{P_s}\right)=\beta\left(\frac{D_0}{D_s}-1\right), \tag{2.1}$$

where P_s is the arbitrarily chosen standard pressure (for example, 100mmHg), and D_s the wall diameter at pressure P_s. The coefficient β, which is called the stiffness parameter, represents the stiffness of an arterial wall and can be very useful when evaluating elastic properties of arteries since the stiffness can be compared independent of pressure. The most common measure of vascular compliance, C_v, is usually quantified by the following expression, according to AAMI (1994)

$$C_v=\frac{\Delta d}{d_0\Delta P}\cdot 10000 \tag{2.2}$$

where Δd is the change in diameter due to a change in pressure, ΔP. The units are percent per 100mm mercury.

It is however questionable to match the graft compliance with that of a healthy artery, when in most cases the host artery is probably diseased. Langewouters *et al.*, (1984) compared the compliance of diseased arteries and found no significant differences over the physiological pressure range. Of course, the compliance will also be affected by the amount of tissue ingrowth and many originally compliant grafts have failed because of the ingrowth of various proteins and fibrous tissue, which serve to reduce the effective compliance. Compliance values of some graft materials, veins and arteries are presented in Table 2.1.

VESSEL	DIAMETER (mm)	COMPLIANCE (%/100mmHg)	REFERENCE
Woven Dacron	10	0.08	Hokanson *et al.*, 1968
Knitted Dacron	8	2.0	Usui *et al.*, 1988
Expanded PTFE	6	1.2	Hanel *et al.*, 1982
Polyurethane	4	7.0-19.0	How *et al.*, 1984
Human umbilical vein		3.7	Walden *et al.* 1980
Human saphenous vein		4.4	Walden *et al.* 1980
Human femoral artery		5.9	Walden *et al.* 1980

Table 2.1 Compliance of vascular prostheses, saphenous vein graft and femoral artery (How *et al.* 1992)

The size of the graft is important when considering the effects it will have on the through flow and attenuation of the pulse energy. It should be as close to the diameter of the host artery as possible so as not to affect the fluid flow properties and allowance should be made for pseudo intimal build up on the inner surface as well as creep swelling and initial compliance.

2.4.2 The importance of porosity

In the early 1950's, Voorhees *et al.* suggested using a porous conduit made from fabric as a prosthesis. Recently, the idea of a porous graft has been well researched and today woven textiles, porous polyurethane and Gortex (ePTFE) are among the latest innovations. A porous conduit made from synthetic fabric provides scaffolding for the blood to clot around and form a compacted fibrin lining. It is widely accepted that the ultimate non-thrombogenic surface is endothelial cell lining. Although current grafts when implanted in animals become completely endothelialised, in man the endothelialisation only extends a few millimetres from the anastomosis (How *et al.* 1992, Sauvage *et al.*1974).

Many investigators have experimented with pore size and more recently, have been developing grafts of variable porosity, pore size and orientation in an attempt to improve graft patency. Lyman *et al.* and Hyashi *et al.* (1989) have successfully produced compliant porous grafts. More recently, Doi *et al.* (1996) developed a small diameter vascular prosthesis with a radial pore structure created by a laser. Mooney (1996) produced porous sponges with large porosities and pore sizes up to 100μm.

Campbell *et al.* (1973) with Matsumoto and associates reported excellent patency rates using Gore-Tex in dogs and noted that higher porosity produced higher patency rates.
The size of the pores also plays an important role in the amount and type of ingrowth. Pore sizes less than 30μm limit the tissue ingrowth to a depth of less than 50μm leaving the rest of the wall free of fibrous tissue (White *et al.* 1988). The type and amount of collagen that infiltrates the pores is sensitive to pore size (How *et al.*, 1992)

2.4.3 Flow surface finishes

Knitted and woven grafts do not have a smooth flow surface finish. Sauvage *et al.* (1974) found that a fibrous inner surface was more successful for graft healing and the development of an endothelial lining than a smooth inner surface. Fibrin and cellular materials are deposited to a thickness greater than the height of the roughness (Hamlin *et al.* 1978). Crimping exaggerates the effective roughness and causes problems leading to occlusion in these grafts by reducing the cross sectional area.

Sauvage et al (1987) penned the term Thrombotic Threshold Velocity (TTV) which is the velocity below which thrombus formation develops. It has been suggested that if the flow is greater than 6-8ml/sec per cm^2, no further fibrin build up will occur. In large diameter grafts, the velocity is almost three times faster than the TTV and thus the fibrin lining stabilises without developing to a point that would hinder the flow, resulting in excellent patency rates after 5 years. A similar fibrous layer in a small diameter graft can reduce the flow by as much as 75% and 5-year patency rates are accordingly much lower.

2.4.4 Buckling (kinking) resistance

In below knee femoropopliteal bypasses, the graft is subjected to small radius bending during knee flexion. It is important that the graft handles this flexion without buckling or obstructing the flow of blood. A circumferential crimping or slightly helical corrugation is introduced to prevent this. This crimping provides radial stiffness and reduces tensile and compressive stresses on the inner and outer walls. It also has an influence on the longitudinal extensibility and lateral flexibility of the graft, thereby improving its handling. The height of the corrugations influences the blood flow especially in small diameter grafts where this height becomes more pronounced. Another form of buckle prevention is the use of an external helical coil fused to the surface. This reinforcing prevents buckling and compression during knee flexion, and produces higher patency

results than corrugated prostheses (Kowligi *at al.* 1988). Leidner *et al.* (1983) calculated the kink resistance as a function of wind angle in polyurethane grafts.

2.5 BIOMEDICAL POLYMERIC MATERIALS

Many polyurethanes are ether based polymers and have been widely used in medical devices due to their excellent blood compatibility. However, ether based polyurethanes have been shown to biodegrade *in vivo* leading to microcracking and potential failure. Polyurethane elastomers are being increasingly accepted as the chosen biomaterial in applications that require compliance with soft cardiovascular tissues since they can achieve a wide range of mechanical properties and can be very biostable. Many of the most advanced medical devices are currently being made from ether-free biostable polyurethane elastomers because these polymers offer a combination of strength, performance and ease of manufacture. (Reed *et al.*, 1994)

Polyurethane elastomers are multi-phase block co-polymers that consist of blocks of hard and soft segments and are thus referred to as segmented polymers. A high content of hard segments increases the modulus and strength and decreases the ultimate elongation. Increasing the molecular weight of the soft segment increases the ultimate elongation and reduces the modulus. Polyurethane elastomers are synthesised by the rearrangement polymerisation of a diisocyanate and specific active hydrogen containing compounds. The main constituents of any polyurethane elastomer are a diisocyanate, a long chain hydroxy terminated macroglycol (e.g. an ether or an ester) and a chain extender (e.g. Glycol or a diamine). (Reed *et al.*, 1994)

Polyurethane is a generic term that refers to polymers containing the –NH-COOH- - repeating linkage within the molecular chain. The name gives no scientific information about the precise chemical composition of the molecular chain. Polyurethanes have been categorised into three major categories: thermoplastics, thermosets and virtually crosslinked materials. The same group of materials can also be categorised in terms of their mechanical performance i.e. materials that display plastic behaviour and those that behave as rubber-like materials.

2.5.1 Thermoplastics

Long chain-like molecules are held together by relatively weak Van der Waals forces (Figure 2.5). When the material is heated, the intermolecular forces are weakened and the material becomes soft and flexible and flows in the manner of a highly viscous liquid (melt flowable). When the material cools again, it solidifies. This heating and cooling process can be repeated indefinitely. Thermoplastics can be subdivided further depending on whether the structure is crystalline (ordered) or amorphous (random). Crystalline

synthetic polymers are partly crystalline and partly amorphous, thus the term crystalline implies partially crystalline. Crystalline materials are generally harder and denser due to the closer packing of the molecules. Thermoplastic materials are viscoelastic. Thus, when the material is stressed, it exhibits elastic deformation (energy storage) and viscous flow (energy dissipation). The degree of viscoelasticity largely depends on the amount of crystalinity in the material. Nylon, PTFE (Teflon) and PET (Dacron) fall under the category of semi-crystalline plastics and are very tough, resistant to chemicals and have a low friction coefficients.
Thermoplastic: Non crosslinked, linear segmented, melt flowable

2.5.2 Thermosets

These are produced by a chemical reaction that has two stages. The first stage produces long chain-like molecules similar to those present in thermoplastics, but still capable of further reaction. The second stage of the reaction produces crosslinking and usually takes place under the application of heat and pressure. This process makes thermosets ideally suited to moulding applications. Crosslinking creates a close network structure interlinking the molecular chains by strong chemical bonds that cannot be softened again with the application of heat. Crosslinked polymers are therefore quite rigid and their mechanical properties are not heat sensitive.
Thermoset: Highly crosslinked (intentionally) branched, not melt flowable, insoluble.

2.5.3 Elastomers

These are rubber-like materials and are a member of the polymer family in that they consist of very long, amorphous, chain-like molecules. The long polymer chains form entanglements or points where the long chains become knotted. This allows the material to undergo large deformations. The molecules slide past one another irreversibly, except at areas of entanglement and on unloading, the entanglements provide anchors for the long chains to return to their original shape. To prevent the sliding, the molecules can be anchored together by a curing process known as vulcanization. The long chains are effectively crosslinked much like those of a thermoset using sulphur (Figure 2.5). The material is able to undergo large deformations due to the uncoiling of the polymer chains, but returns to its original shape on unloading because the molecules have not slid past one another.

Thermoplastic polyurethanes are linear segmented structures with no intentional chemical crosslinking inherent in the structure. These materials are heat mouldable and processable. They are soluble in organic solvents and possess a wide range of mechanical properties, Thermoset polyurethanes are intentionally branched, segmented structures, which possess a high level of covalent crosslinking. As a result they are non-heat processable and are not soluble in organic solvents, although they still possess a range of mechanical properties. Virtually crosslinked materials are formed by the presence of the urethane and urea bonds

that make a secondary level of molecular interaction possible. These short-range interactions have a high degree of hydrogen bond character and are often referred to as virtual or pseudo crosslinks (Figure 2.5).

Virtually crosslinked: Virtually crosslinked, melt softening, soluble in certain solvents.

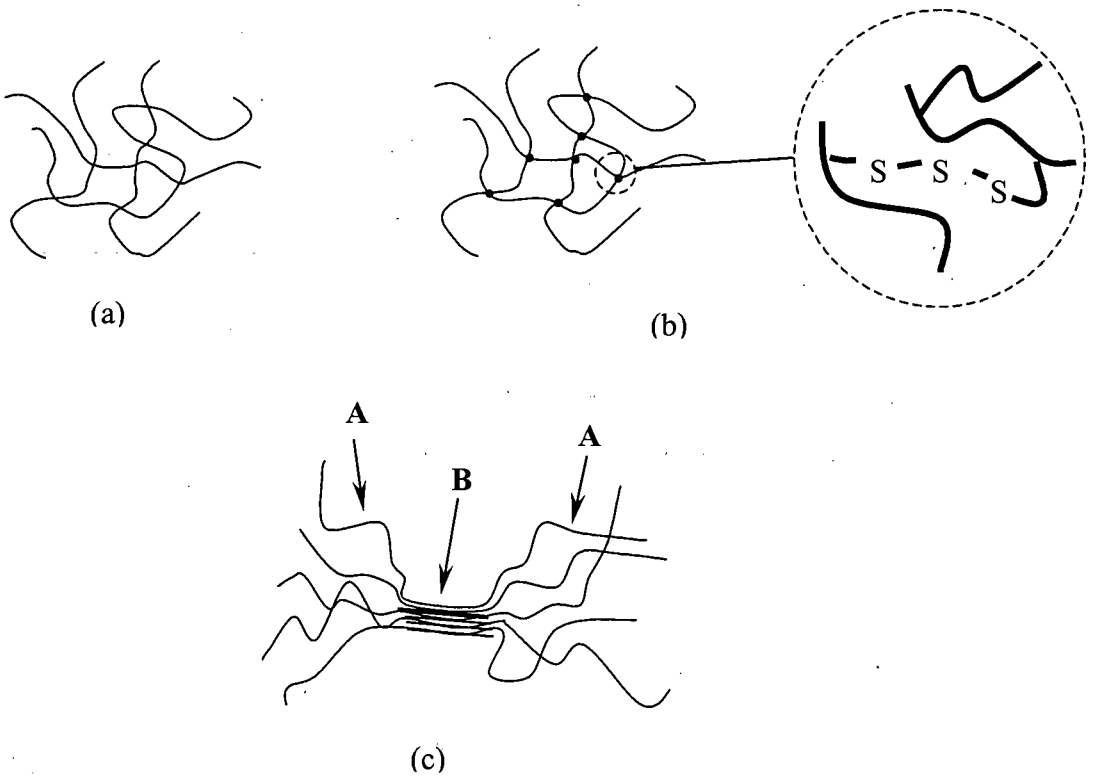

Figure 2.5: (a) Un-crosslinked polymer with weak van der Vaals bonds, (b) Sulphur bonds form physical crosslinks in vulcanised rubbers, (c) Block segmented polyurethane with "virtual" cross links. **A** represents a soft segment and **B** represents a hard segment.

The determination of the mechanical properties of polymers is very sensitive to the testing conditions. A polymer can show all the features of a glassy, brittle solid or an elastic rubber or a viscous liquid depending on the temperature, rate of loading and time scale of the test (Figure 2.6).

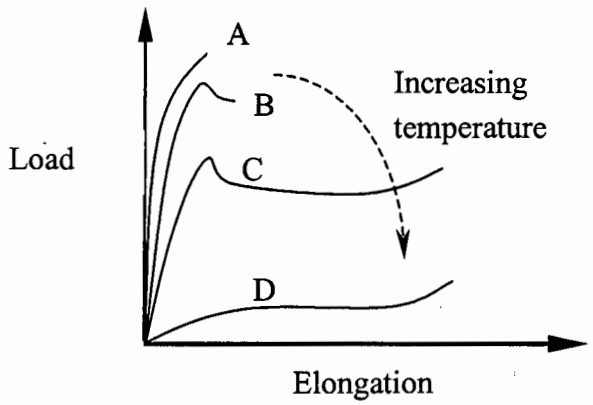

Figure 2.6: The variation in mechanical properties of a polymer as temperature increases

Polymers and in particular polyurethanes are described as viscoelastic materials, which emphasizes their intermediate position between viscous liquids and elastic solids. At low temperatures or high frequencies, the polymer may display glass like characteristics associated with a brittle material i.e. low breaking strains and high elastic modulus. At high temperatures or low frequencies, the same polymer may display rubber like qualities, withstanding large strains without permanent deformation and at even higher temperatures the same polymer behaves like a viscous liquid (Figure 2.7).

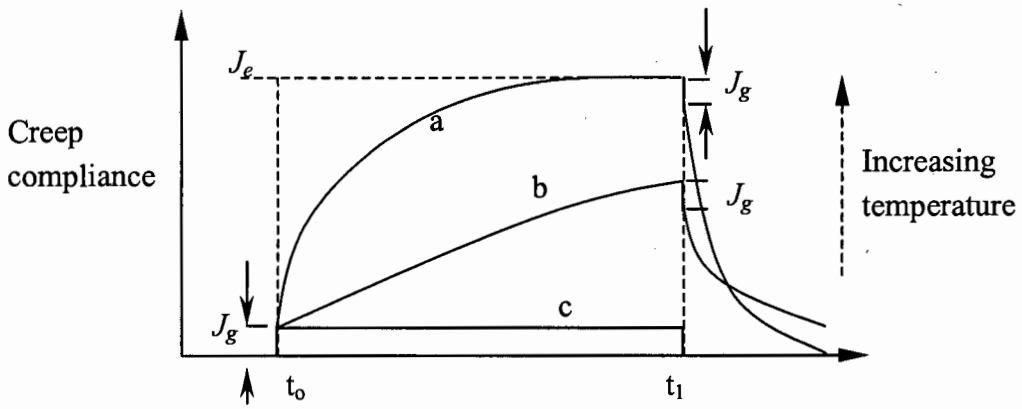

Figure2.7: The time dependent nature of polymers as temperature increases. a) glassy response at temperature well below glass transition; b)transition region viscoelastic response; c)transition to rubbery equilibrium.

There is an intermediate temperature called the glass transition temperature, Tg, where the material is neither glassy nor rubber-like, is viscoelastic and withstands large

deformations. Below this temperature, the material behaves like an elastic solid and above, it approaches rubbery equilibrium or viscous flow (Figure 2.7).

2.5.4 Forming of Polymers

Thermoplastics soften when heated, allowing them to be formed by techniques such as injection moulding, extrusion, blow moulding and compression moulding. Thermosets, on the other hand, are formed and cured simultaneously usually by compression moulding. Rubbers and elastomers are formed like thermosets, by pressing and heating a mixture of polymers. The polymers can be forced through fine nozzles (spinnerets) when molten and spun into fibres that can be woven or knitted into a fabric. Other techniques include extrusion through a fine orifice (Leidner *et al.* 1983), electrostatic spinning (Annis *et al.* 1978), spraying techniques and spinning fibres on a rotating mandrel. To date much attention has been paid to the development of thermoplastic materials to be used in pellet form for extrusion and injection moulding. Polymers can be expanded into foams by making use of blowing agents. This can be done by expanding a dissolved gas into bubbles by reducing the pressure or by using chemicals that release gas bubbles into the molten polymer. Dissolvable solids such as salt can also be mixed into the molten polymer and dissolved out using an acid or water creating a porous structure.

2.6 GRAFT DESIGNS

Most of the recent work has involved the development of segmented polyurethanes because of their low thrombogenicity and wide range of mechanical and chemical properties. Their tensile strength is lower than that of Dacron and PTFE and their fatigue resistance is good. There are also many different manufacturing techniques being developed for the forming of polyurethanes. Solid tubes historically do not perform well since they do not promote cell ingrowth and are generally not compliant at all. Fibrillar grafts are spun, woven or knitted and can create a range of porosities but without any specific orientation and limited compliance. Porous polyurethane grafts are particularly versatile since there are many ways of producing porous polyurethane grafts. The following section evaluates the present graft structures.

2.6.1 Fibrillar Prostheses

In the early 1970's woven and knitted prostheses were introduced to promote better healing and incorporation into the surrounding tissue. Woven prostheses are produced by spinning fibres on a rotating mandrel or by standard mat weaving techniques. They are strong and stiff both radially and longitudinally and are thus structurally sound. They have a low porosity and don't have to be pre clotted which means they are useful in trauma. However, it is important to promote cell ingrowth through porosity, thus woven prostheses are not ideal in this regard. In addition, they have a tendency to fray at the cut ends.

Knitted prostheses are produced by looping yarn around needles and are more porous than woven grafts. The size of the needles and the yarn size define the extent of the porosity. They must therefor be pre clotted before implantation. Weft and warp knit are the terms used for circumferentially or longitudinally oriented knits respectively (Figure 2.8). The type and variation of knit allow the designer to create a certain amount of compliance through the 'slack' between stitches in the knit. Structural integrity can be achieved by using either a stiff thermoplastic or a strong elastomer. Knitted grafts are more comfortable, easier to suture and less susceptible to fraying. High porosity and low tensile strength are drawbacks of velour fabrics. The regular pattern inherent in a weave or knit implies that it is difficult to produce a specifically oriented pore structure in the graft wall with either of the techniques.

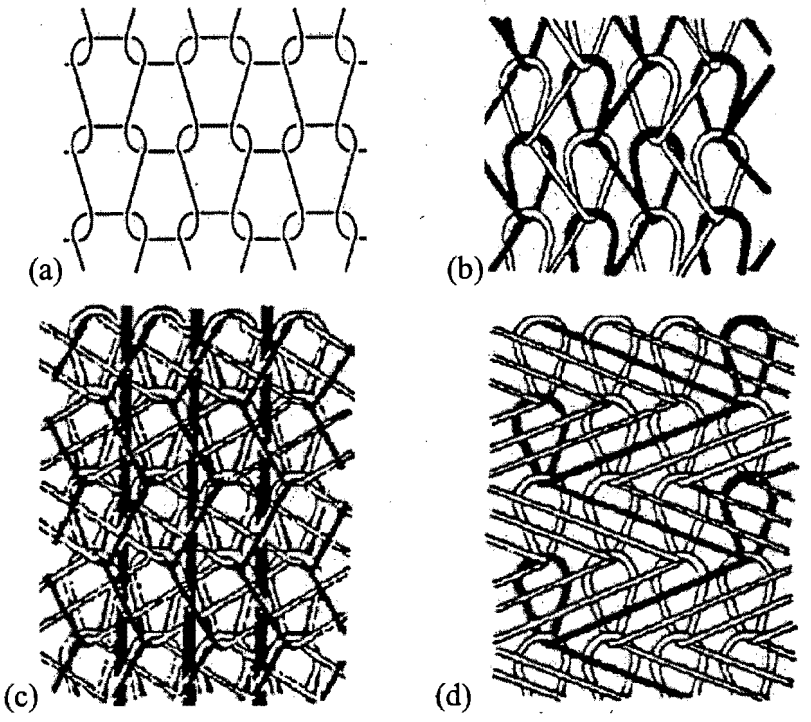

Figure 2.8 Different types of knitted textile. a) Weft knit, b) Warp knit c) Warp knit with weft inserted yarns d)Warp knit with interlocking underlaps

De Cooman *et al.* (1996) used a solution spinning technique to create oriented fibre porosity. They found they could prepare porous composite fibres with a closed external skin by a single extrusion. Since the outer side is closed, there is no cell ingrowth from the surrounding tissue. Ze Zhang *et al.* (1996) and Kowligi *et al.* (1988) developed fibrous prostheses made from a unique polycarbonate urethane using a spraying technique onto a rotating mandrill. This created commuting pores in the wall structure, but no orientation was induced. All explanted prostheses had failed due to kinking or graft artery mismatch. Lyman *et al.* produced a Dacron reinforced porous prosthesis using a coagulation process. The Dacron reinforcing caused an anisotropy where the longitudinal strength was three times the circumferential strength.

After studying the mechanical properties of the human common carotid artery, Gupta *et al.* (1997) developed a hybrid woven textile graft. The graft was a two-layer construction made from two different elastic materials. The inner layer was polyurethane filament with a low elastic modulus and the outer layer was made from a polyester yarn with a high elastic modulus. The graft design was based on the structure observed in the arteries they had studied. The inner weave represents the elastin and smooth muscle structure and the external weave, which is a much stiffer material, was more loosely woven and represents the collagen reinforcing. The structure led to unique pressure-circumferential stretch ratio curve, displaying sudden stiffening at higher pressures. A compliant graft was achieved with this structure and tubes of 4-6mm diameter were constructed. Promising results were reported for preliminary *in vivo* studies in dogs.

2.6.2 Expanded PTFE prostheses (Gore Tex)

ePTFE prostheses were introduced in 1975. PTFE is extruded under high pressure with a lubricant into tubes. These tubes are stretched at a high temperature producing a strong expanded material with high porosity. The pores are elongated spheres, 5-10μm wide, 5-100μm long and are interconnected by longitudinal fibrils less than 0.5μm diameter (Figure 2.9) (Lenox and Baker 1976). This porosity provides the material with an inherent resistance to buckling and an induced anisotropy. It is much stronger in tension than compression and is structurally very sound. However, the pores or nodes in ePTFE are created during the expansion phase and it is thus not possible to create an oriented pore structure. Initially there were problems with material creep and dilation, which were overcome by introducing a reinforcing layer of fibrous ePTFE (Gore Tex), or by using thicker graft walls. Both of these measures sacrifice a degree of compliance however, new methods of expanding PTFE suggest that compliance might also become achievable in the near future.

2.6.3 Foamed prostheses

The latest developments in prostheses involve polymeric materials because of their excellent blood compatibility and mechanical properties. It is relatively easy to introduce porosity in polyurethanes and many techniques have recently been developed. Hayashi *et al.*, (1989) produced a polyurethane prosthesis with silicon rubber added (Figure 2.9). He used a phase separation technique to create porosity and used a woolly polyester net for reinforcement. This created a similar porous structure to that of Lyman. Lyman used a precipitation method with a polyester reinforcing mesh on the outer surface. The elastic modulus was largely linear up to strains of 100%, but was far lower than that of the femoral artery. The wall thickness had to be increased to obtain the same compliance. The external reinforcing mesh was necessary because the strength was too low without it. White and co-workers (1972) have developed a novel process termed replamineform for fabricating microporous prostheses. In this process the calcite structure of sea urchin spines is replicated. Tubes of 4-6mm internal diameter with a wall thickness of 1mm were

machined out of the urchin spines and a polymer solution is injected into the calcite structure. The calcite is then dissolved leaving a microporous polyurethane structure with a pore size of between 18-25μm. The maximum length of the graft is obviously limited to the length of sea urchin spine. Another graft design called the Mitrathane graft is a microporous conduit made from a segmented polyurethane that is very strong but also stiff (non compliant) and was rejected for use in humans after 59% of those implanted in dogs failed due to occlusion.

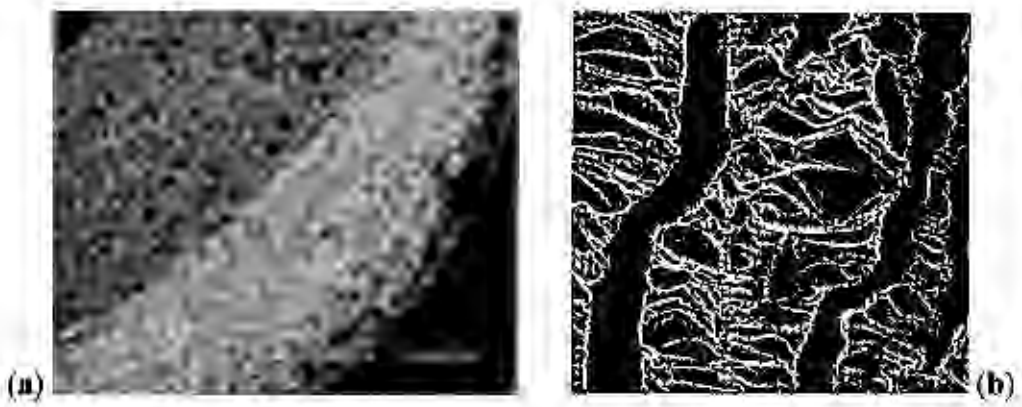

Figure 2.9 a) A Porous graft structure (Hyashi *et al.* 1989) b) expanded Teflon structure.

2.7 Finite Element Analysis of Arteries and Grafts

Much research has focussed on the development of mathematical models to describe the behaviour of arterial vessels (Fung 1977, Patel and Vaishnav 1972, Carmines 1991, Simon 1993, von Maltzahn 1981, Takamizawa and Hayashi 1993, Chuong and Fung 1983, Bergel 1961). Recently, these and other models have been developed and adapted for use in the finite element method. Finite element studies have been used to study aspects of mechanical and structural behaviour of arteries and grafts. Chandran *et al.* (1992) used a linear elastic finite element model to evaluate the distribution of stress and compliance in the vicinity of the artery graft anastomosis. They reported a hypercompliant zone on the arterial side of the anastomosis and high tensile stress on the graft side. Ballyk *et al.* (1995) developed a large strain linear elastic finite element model for vascular mechanics. Later (1996) they used this to determine the suture line stress distribution at an artery-vein anastomosis. They related the stress at the sutures to the development of atherosclerotic plaques. Beattie *et al.* (1996) coupled results from histological and experimental data to a finite element model to predict the formation and distribution of calcification, lipid accumulations and plaque build up in diseased vessels according to the intramural stress distribution. Most research centres on modelling the artery and its mechanical properties

using large strain theory with hyperelasticity. No research was found that described the behaviour of the graft as a hyper – viscoelastic foam.

2.8 REQUIREMENTS FOR A SUCCESSFUL GRAFT

To summarise the chapter, the requirements for the development of a successful artery graft can be defined. The development of a successful prosthesis is largely dependent on the development of biological technology. The mechanical aspects, which are emphasised here, need to accommodate the biological development and provide a framework for the optimal biological environment for cell ingrowth and musculogenesis. With this in mind, the requirements for a successful graft can be drawn from the review on arterial structure and the presently available graft designs and fabrication techniques.

From the review, it can be seen that one of the most important mechanical factors in graft design is matched compliance. The graft must also have a suitable flow surface finish and should be resistant to small radius buckling. Other requirements include the materials resistance to fatigue, the materials biostability to prevent thrombogenic reaction and resistance to long term biodegradation.

Compliance is affected by the material used and the structure of the graft. The material needs to be highly deformable and completely elastic i.e. the material should not show any retarded elastic behaviour (viscoelasticity) and all deformation should be fully recoverable. The type of graft structure i.e. woven, knitted or porous polyurethane can enhance the compliance and influence the amount and type of ingrowth. Most recent work has shown that initial compliance is achievable through a number of techniques, but the long-term results are still unacceptably low. Work has been done investigating various flow surface finishes and the effect of porosity on the success of the grafts. However, very few of the latest designs consider a graft that is structurally similar to an intact artery. It is the aim of this project to investigate the compliance and structural integrity of graft structures that induces cell ingrowth and musculogenisis through an oriented porous structure.

The remainder of this thesis is concerned with the development of such a graft. The material chosen for the development is a biostable segmented thermoplastic polyurethane. The object is to create a commuting (open) cell wall structure with oriented ingrowth channels to promote musculogenesis and cell ingrowth. The structural analysis is performed using finite element software and *in vitro* experiments. This involves characterizing the polyurethane and forming an accurate hyper – viscoelastic material model. This project is part of an ongoing work and the findings in this thesis will be used to further develop and improve future graft designs. The next chapter deals with the formulation of a theoretical framework for analysis and the material characterisation of the polyurethane in order to model the graft numerically using finite element software.

CHAPTER THREE

MATERIAL CHARACTERISATION

3.1 INTRODUCTION

Failures of grafts typically occur in the graft or in the region of the anastomosis. Any mechanical model will require the constitutive response of both the graft and the natural artery, and thus, a review of the fundamentals of the mechanical response of compliant materials is necessary.

Compliant materials deform appreciably under load and their behaviour is thus described by large (finite) strain theory. Polymers, especially rubber-elastic polymers, sustain large strains, may be anisotropic and are often incompressible and viscoelastic. Most soft tissues also sustain large strains, are generally non-linear in their constitutive response, exhibit either transverse isotropy or more general forms of anisotropy and are either incompressible or nearly so.

To describe the mechanical behaviour of both polymers and soft tissue, a hyperelastic (Green elastic) strain energy function of the local deformation or strain is used. The existence of a strain energy function for a material implies that, regardless of deformation path, equal work is done in going from one deformation state to another. In order to characterise compliant materials, appropriate strain energy functions, W, need to be formulated. First, a framework with which to describe the deformations, strains and stresses must be developed.

While the material constants that characterise the natural artery are taken from data in published literature, the polyurethane to be used for the manufacture of these grafts has yet to be characterised. This section serves not only to develop the constitutive laws that describe the materials behaviour, but also to characterise the polyurethane through physical testing. The experimental results of tensile, simple shear and viscoelastic tests are used specifically for the purpose of characterising the constants in the material law for implementation in the numerical analysis. The numerical model to be implemented is verified through simple tests.

3.2 THEORETICAL FRAMEWORK

It is clear that graft materials and arteries are both highly deformable and display time dependent (viscoelastic) behaviour. Hence, a constitutive law for their behaviour must be formulated. This section provides a framework for the theory of finite strain, the derivation of a hyperelastic material law and the fundamental theory of linear viscoelasticity. These principles can be cast into numerical format for use in the finite element code.

3.2.1 Finite Strain

Detailed formulations of the theory can be found in numerous texts such as Crisfield [16] or Malvern [63]. Presented here is a summary of the theory relevant to the work.

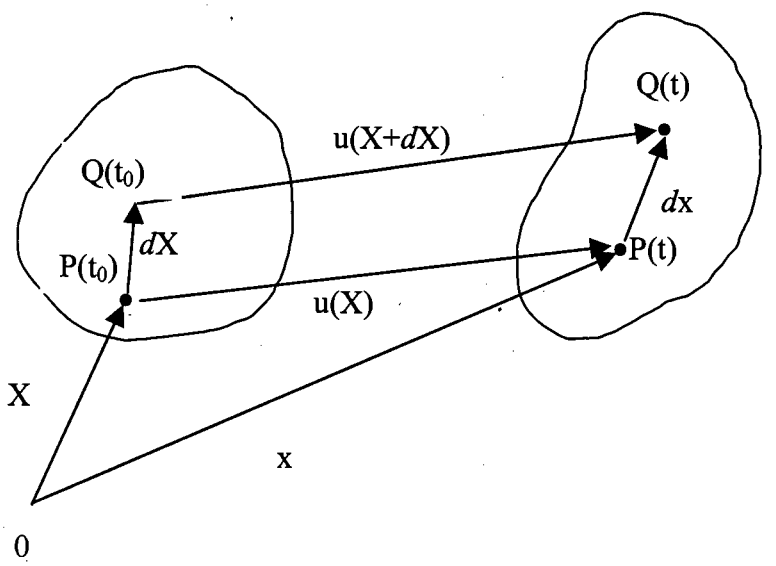

Figure 3.1 Material points in a material undergo finite deformation.

The motion of a material can be described as a mapping that defines the position of a particle in a material. Referring to Figure 3.1, a material has a particular configuration at some reference time, t_0, and deforms to another configuration at time t. A typical material point P undergoes a displacement, u, so that it arrives at the point $P(t)$

$$\boldsymbol{x} = \boldsymbol{X} + u(\boldsymbol{X}, t) \tag{1}$$

Similarly, a point Q, originally at $\boldsymbol{X} + d\boldsymbol{X}$ arrives at $\boldsymbol{x} + d\mathbf{x}$ which is related to $\mathbf{X} + d\mathbf{X}$ by

$$\mathbf{x} + d\mathbf{x} = \mathbf{X} + d\mathbf{X} + \mathbf{u}(\mathbf{X} + \mathbf{X}d\mathbf{X}, t) \tag{2}$$

Subtracting 1 from 2, the result becomes

$$d\mathbf{x} = d\mathbf{X} + (\nabla \mathbf{u})d\mathbf{X} \tag{3}$$

This deformation can be characterised by the deformation gradient tensor, **F**, defined by

$$\mathbf{F} = \mathbf{I} + \nabla \mathbf{u}, \tag{4}$$

where **I** is the identity tensor and $\nabla \mathbf{u}$ is the displacement gradient tensor, **H**. The components of **F** and **H** are given respectively by

$$F_{ij} = \frac{\partial x_i}{\partial X_j}, \text{ and } H_{ij} = \frac{\partial u_i}{\partial X_j}. \tag{5}$$

F can also be described in terms of the stretch ratios relative to the principal axes, viz. $\mathbf{F} = \begin{bmatrix} \lambda_1 & 0 & 0 \\ 0 & \lambda_2 & 0 \\ 0 & 0 & \lambda_3 \end{bmatrix}$ for uniaxial tension and $\mathbf{F} = \begin{bmatrix} 1 & \gamma & 0 \\ 0 & 1 & 0 \\ 0 & 0 & 1 \end{bmatrix}$ for simple shear, where γ is the shear strain and λ_i are the principal stretch ratios, where the stretch ratio is defined as the ratio of the deformed length to the original length i.e.

$$\lambda = \frac{|dx|}{|dX|}$$

Both the deformation gradient tensor and the displacement gradient tensor characterise the deformation at the point ***X***. The deformation gradient tensor **F** also contains information about the local rotation. However, since it is necessary to relate the strain energy function, *W*, to deformation alone, the right and left Cauchy-Green deformation tensors, $\mathbf{C} = \mathbf{F}^T\mathbf{F}$ and $\mathbf{B} = \mathbf{F}\mathbf{F}^T$, are defined respectively. These depend on the deformation only (not the rotation) at any point in the material. Strain is also a measure of deformation independent of rotation used to characterise the strain energy function. The Lagrangian strain, **E**, is defined here by

$$\mathbf{E} = \tfrac{1}{2}\left[\mathbf{F}^T\mathbf{F} - \mathbf{I}\right] = \tfrac{1}{2}\left[\mathbf{H} + \mathbf{H}^T + \mathbf{H}^T\mathbf{H}\right]. \tag{6}$$

Since deformations and rotations are finite, the definitions of stress need to be precise. The true, or Cauchy, stress is the symmetric second-rank tensor, σ, (with components σ_{ij}) which relates the load to the current area. Since the Second Piola-Kirchhoff stress, **S**, considers the reference configuration, it is more easily measured in experiments and is related to the Cauchy stress by

$$\sigma_{ij} = F_{ik} S_{kl} F_{jl}, \tag{7}$$

where repeated indices are summed from 1 to 3.

Finite strain accounts for the physical nature of the material deformations, rotations and stresses in the material, but describes nothing about the specific material behaviour. The mechanical constitutive description of compliant materials assumes that they are hyperelastic, which means they can be described by a strain-energy function. The

following section highlights the salient features of hyperelasticity and leads on to the definition of different strain energy functions for elastomers and soft tissues.

3.2.2 Hyperelasticity

Hyperelastic materials are generally described by a strain energy function that defines the strain energy stored in the material as a function of the strain at that point in the material. Following the work of Humphry, Strumpf and Yin (1990), the simplest strain-energy functions describe isotropic materials, that is, the behaviour of the material is independent of orientation, and the strain energy is a function of three invariants of the Cauchy-Green deformation tensor, i.e. $W = W(I_1, I_2, I_3)$, where

$$I_1 = \mathrm{tr}(\mathbf{C}), \tag{8a}$$

$$I_2 = \tfrac{1}{2}\left[(\mathrm{tr}\,\mathbf{C})^2 - \mathrm{tr}(\mathbf{C}^2)\right], \tag{8b}$$

$$I_3 = \det \mathbf{C}. \tag{8c}$$

For incompressibility, $I_3 = 1$ and $W = W(I_1, I_2)$ only. Also, the hydrostatic stress is not determined by the material deformation but is set by the boundary conditions and the equations of equilibrium. The deviatoric stress is determined by the strain energy, so that, the Cauchy stress, for a material with a strain energy function dependent on two invariants, $W = W(I_1, I_2)$, becomes

$$\boldsymbol{\sigma} = -p\mathbf{I} + 2W_1\mathbf{B} - 2W_2\mathbf{B}^{-1} \tag{9}$$

where W_1 and W_2 are the derivatives of the strain energy function with respect to their respective invariants.

For transversely isotropic materials with a single preferred orientation defined by the unit vector $\mathbf{N}$ in the reference configuration, and for an incompressible material, the strain energy is dependent on four invariants, i.e. $W = W(I_1, I_2, I_4, I_5)$, where

$$I_4 = \mathbf{N}\cdot\mathbf{C}\,\mathbf{N} = \alpha^2 \tag{10a}$$

$$I_5 = \mathbf{N}\cdot\mathbf{C}^2\,\mathbf{N}. \tag{10b}$$

Equation (10a) defines the stretch α^2, in the direction $\mathbf{N}$, so that, this material description is appropriate for muscle, where $\mathbf{N}$ is the muscle fibre orientation and α^2 the muscle fibre stretch. The Cauchy stress is given by

$$\boldsymbol{\sigma} = -p\mathbf{I} + 2W_1\mathbf{B} - 2W_2\mathbf{B}^{-1} + \tfrac{1}{\alpha}W_\alpha\mathbf{F}(\mathbf{N}\otimes\mathbf{N})\mathbf{F}^T \tag{11}$$

where W_1, W_2 and W_α are the derivatives of the strain energy function with respect to these arguments and $\mathbf{N}\otimes\mathbf{N}$ is the tensor product of the two unit vectors.

3.2.3 Strain Energy Functions

There are many forms of hyperelastic strain energy potentials available for modelling approximately incompressible, isotropic materials; two commonly used forms are the polynomial form and the form due to Ogden. The polynomial form is a function of the first and second deviatoric strain tensors, and the Ogden form is a function of the principal stretches. For compressible hyperelastic materials like elastomeric foams and compressible porous media, the strain energy functions must allow for compression. The ABAQUS elastomeric foam material model characterises the elastic behaviour of the foam based on a modified form of Ogden's strain energy function

$$W = \sum_{i=1}^{N} \frac{2\mu_i}{\alpha_i^2}\left[\hat{\lambda}_1^{\alpha_i} + \hat{\lambda}_2^{\alpha_i} + \hat{\lambda}_3^{\alpha_i} - 3 + \frac{1}{\beta_i}((J^{el})^{-\alpha_i\beta_i} - 1)\right], \tag{12}$$

where N is a material constant, μ_i, α_i and β_i are temperature dependent material constants and $\hat{\lambda}_i$ is related to λ_i by the thermal volume ratio so that $\hat{\lambda}_i = (J^{th})^{-1/3}\lambda_i$. The elastic volume ratio $J^{el} = \hat{\lambda}_1\hat{\lambda}_2\hat{\lambda}_3$ and λ_i are the principal stretches. The material constants are determined from test data (detailed later in this chapter).

Numerous researchers have focussed on the development of constitutive laws to describe the mechanical behaviour of arterial vessels (Hayashi *et al.* 1993, McAfee *et al.* 1994, Fung *et al.* 1977, Vaishnav *et al.* 1973, and Carmines *et al.* 1991). There are generally three accepted forms of strain energy function that have been used to describe arterial behaviour.

Vaishnav *et al.* (1973) proposed a polynomial function to describe a cylindrical vessel subjected to an internal pressure. This is the simplest function, usually has seven coefficients and is written as

$$W = aE_{\theta\theta}^2 + bE_{\theta\theta}E_{zz} + cE_{zz}^2 + dE_{\theta\theta}^3 + eE_{\theta\theta}^2E_{zz} + fE_{\theta\theta}E_{zz}^2 + gE_{zz}^3, \tag{13}$$

where *a, b, c, d, e, f,* and *g* are material constants, and $E_{\theta\theta}$ and E_{zz} are the strain components in the circumferential and axial directions respectively.

Fung *et al.* (1977) proposed an exponential function of the form

$$W = C\exp\left(a_1E_{\theta\theta}^2 + a_1E_{zz}^2 + a_1E_{\theta\theta}E_{zz}\right) \tag{14}$$

where C, a_1, a_2 and a_4 are the material constants, which are determined from experimental data.

Takamizawa and Hayashi (1993) proposed a logarithmic function, which again has four coefficients.

$$W = -C\ln\left[1 - \tfrac{1}{2}a_{\theta\theta}E_{\theta\theta}^2 - \tfrac{1}{2}a_{zz}E_{zz}^2 - a_{\theta z}E_{\theta z}^2\right] \tag{15}$$

where $C, a_{\theta\theta}, a_{zz}$ and $a_{\theta z}$ are material constants.

To implement Fung's form of the strain energy function in ABAQUS, the software requires the user to input derivatives of the strain energy function with respect to its invariants. However, Fung's form of the equation is defined in terms of Lagrangian strains and not strain invariants. The equation must therefor be rewritten in terms of strain invariants. ABAQUS can only handle an isotropic strain energy function so Fung's equation must be simplified to an isotropic form first, since it is does not consider radial strains and is thus anisotropic as it stands. The isotropic form of the equation can be re-written as

$$W = C\exp\left[\alpha_1\left(E_{\theta\theta}^2 + E_{zz}^2 + E_{rr}^2\right) + 2\alpha_4\left(E_{\theta\theta}E_{zz} + E_{zz}E_{rr} + E_{\theta\theta}E_{rr}\right)\right] \tag{16}$$

With $E_i = \frac{1}{2}\left(\lambda_i^2 - 1\right)$, the strain energy function can be written in terms of the stretch ratios. Since the invariants can be defined in terms of the stretch ratios,

$$I_1 = tr\left(F \cdot F^T\right) = \left(\lambda_\theta^2 + \lambda_z^2 + \lambda_r^2\right) \text{ and} \tag{17a}$$

$$I_2 = \tfrac{1}{2}\left(I_1^2 - tr\left(B \cdot B\right)\right) \text{ where } B = F \cdot F^T, \tag{17b}$$

The strain energy function can be written in terms of the invariants, $W = W\left(I_1, I_2\right)$ and the appropriate derivatives can be taken. The values for the constants used were taken from data obtained by Fung *et al.* (1977) from experiments on rabbit cardiac and iliac arteries.

The strain energy functions can be cast in terms of the Lagrangian strain components, E_{ij}, since these are easy to measure in experiments. The Second Piola-Kirchhoff stress is then given by

$$S_{ij} = \frac{\partial W(\mathbf{E})}{\partial E_{ij}} \tag{18}$$

for compressible materials, and by

$$S_{ij} = -pF_{ik}^{-1}F_{jk}^{-1} + \frac{\partial W(\mathbf{E})}{\partial E_{ij}} \tag{19}$$

for incompressible materials.
For any non linear material, the increment in stress, dS_{ij}, is related to the increment in strain, dE_{ij} through

$$dS_{ij} = \frac{\partial^2 W}{\partial E_{ij}\partial E_{kl}} dE_{kl} = D_{ijkl}\, dE_{kl}. \tag{20}$$

3.2.4 Viscoelasticity

Viscoelastic behaviour can be described using simple spring and dashpot models (Figure 3.2). A linear spring is used to describe the purely elastic response in the material, where stress, σ, is directly proportional to the strain, ε. The spring element stores elastic energy. The energy loss in the material or viscous component can be modelled using a dashpot, where the stress is proportional to the strain rate $\dot{\varepsilon}$. Here k is the spring constant and η is the viscosity constant.

(a). (b).

Figure 3.2: (a) Linear spring with $\sigma = k\varepsilon$, (b) Dashpot with $\sigma = \eta\dot{\varepsilon}$

Since viscoelastic materials combine elastic and viscous effects, different combinations of spring and dashpots in series and parallel can be used to approximate material behaviour. The Kelvin-Voigt and Maxwell models are two of the simplest models, illustrated in Figure 3.3.

Kelvin-Voigt Maxwell

Figure 3.3: Kelvin-Voigt and Maxwell viscoelastic models.

In the Kelvin-Voigt model, the strain is the same in both the spring and the dashpot, and the stresses in each element are summed to balance the applied load. Thus the equilibrium equation is:

$$\sigma = k\varepsilon + \eta\dot{\varepsilon} \tag{21}$$

In the Maxwell model the elements are connected in series, hence the strains are additive while the stress is constant throughout, thus:

$$\dot{\varepsilon} = \frac{1}{k}\dot{\sigma} + \frac{1}{\eta}\sigma \tag{22}$$

The Maxwell equilibrium is written in terms of strain rate since the dashpot equilibrium is defined in terms of strain rate.

Solving these two differential equations yields the retarded strain at time, t, for a constant stress applied at time, $t = 0$, that is,

$\varepsilon(t) = \frac{\sigma_{t=0}}{k}\left(1 - e^{-t/\tau}\right)$ for the Kelvin-Voigt model where $\tau = \frac{\eta}{k}$

and, $\sigma(t) = k\varepsilon_{t=0}e^{-t/\tau}$, the relaxation stress at time, t, for a constant strain applied at time, $t = 0$, for the Maxwell Model.

The relaxation time, τ, is the time taken for the stress to relax by a factor $e^{-1} \approx 0.37$ of the initial value.

(a) (b)

Figure 3.4 (a) Retarded strain for the Kelvin-Voigt model and (b) stress relaxation of Maxwell model.

The Kelvin-Voigt and Maxwell model are too simple to model viscoelastic behaviour accurately. Consider a load suddenly applied to each model. The Kelvin-Voigt model is initially constrained from any movement by the dashpot, which cannot react immediately, so at time $t=0$, an infinitely large stress is induced in the system. The Maxwell model on the other hand is a purely viscous model, which, once stressed, allows an infinite strain. However a combination of the two models, giving the 3-element or standard linear models shown in Figure 3.5, will accommodate the characteristics of a viscoelastic material.

Figure 3.5: Standard linear viscoelastic models.

Since the stress relaxation and retarded elastic response in most viscoelastic materials are defined by a range of time scales, it is sometimes necessary to combine a number of models in series or parallel in order to capture the full spectrum. However, the major viscoelastic trends can be satisfactorily characterised with three or four component models. Time constants for these models are calculated by curve fitting to delayed elastic

or stress relaxation experimental data. Since these are usually shear tests, strain measured is shear strain and stress is shear stress.

For a multi-element Maxwell model (with N units), the stress relaxation under a constant strain is:

$$\sigma(t) = \varepsilon_0 G(t) \tag{23}$$

where

$$G(t) = G_\infty + \sum_{n=1}^{N} G_n e^{-t/\tau}, \tag{24}$$

where G_∞ is the long term shear modulus calculated from the hyperelastic strain energy function, and G_n is the instantaneous shear modulus of element n.

For a continuous spectrum of relaxation times, the relaxation modulus can be written:

$$G(t) = \int_0^\infty S(\tau) e^{-t/\tau} d\tau \tag{25}$$

where $S(\tau)$ is the relaxation spectrum. Experimentally, the determination of this $S(\tau)$ is easier than finding discrete time scales and moduli from creep test data.

Thus far, only the time-varying response to a constant load applied at some time in the past has been considered. To calculate the response to a time-varying load, the principle of linear superposition (Boltzman, 1874) can be used. Assuming linear viscoelastic behaviour, the strain response to a complex loading history is merely the sum (superposition) of the individual strains due to each step in the load.

$$\varepsilon(t) = \sum_{i=0}^{N} \frac{\sigma_i}{G(t-\tau)}, \tag{26}$$

where σ_i is a step change in stress occurring at time $t_i = \tau$. A similar superposition for the stress response to strain increments applied at time τ yields

$$\sigma(t) = \sum_{i=0}^{N} \varepsilon_i G(t-\tau). \tag{27}$$

If the change in stress is continuous rather than a step function, with increments of strain applied at time τ, $d\varepsilon = \dot{\varepsilon} d\tau$ or with increments of stress applied at time τ, the superposition yields the sum of the elastic responses to all the past increments in load from time -∞ to t,

$$\sigma(t) = \int_{-\infty}^{t} \frac{d\varepsilon(\tau)}{d\tau} G(t-\tau) d\tau \tag{28}$$

and

$$\varepsilon(t) = \int_{-\infty}^{t} \frac{1}{G(t-\tau)} \frac{d\sigma(\tau)}{d\tau} d\tau \tag{29}$$

Changing the integration variable to the time laps, s, where

$$s = t - \tau \text{ and } ds = -d\tau \tag{30}$$

Integrating by part yields

$$\sigma(t) = G_0 \varepsilon(t) + \int_{-\infty}^{t} \frac{dG(s)}{ds} \varepsilon(t-s) ds, \tag{31}$$

where G_0 is the so-called *glassy* or *instantaneous* modulus.

Similarly, the delayed strain response to a smooth stress function of time is

$$\varepsilon(t) = J_0 \sigma(t) - \int_{-\infty}^{t} \frac{dJ(s)}{ds} \sigma(t-s) ds \tag{32}$$

where , $J(t) = \int_0^{\infty} S(\tau)(1 - e^{-t/\tau}) d\tau$ and $S(\tau)$ is the retardation spectrum.

Equations (31) and (32) are constitutive laws for a linear viscoelastic material. They can be implemented in a numerical algorithm, such as the finite element method, to predict the deformation history of any body with a continuum viscoelastic material behaviour subjected to a time-varying stress or strain.

The 1-D viscoelasticity case detailed above can be expanded to the general 3-D case for calculating the viscoelastic response of a continuous media. The finite element code ABAQUS uses a time domain generalisation of the hyperelastic constitutive model for finite strain viscoelasticity. The instantaneous response of the material is assumed to follow from the hyperelastic constitutive equations. The basic hereditary integral for linear isotropic viscoelasticity is transformed to the general case using integration by parts and a variable transformation. After separating the deviatoric and hydrostatic parts, ABAQUS uses the following form of the basic hereditary integral formation

$$\sigma(t) = \mathbf{S}_0(t) + \int_0^{\tau} \frac{\dot{G}(\tau')}{G_0} \mathbf{S}_0(t-t') d\tau' + \mathbf{I}\left(p_0 + \int_0^{\tau} \frac{\dot{K}(\tau')}{K_0} p(t-t') d\tau' \right) \tag{33}$$

where σ is the Cauchy stress (nominal stress), $\mathbf{I}$ is the identity tensor and G_0 and K_0 are the small strain instantaneous shear and bulk moduli respectively and $\dot{G}(\tau') = \frac{dG(\tau')}{d\tau'}$ and $\dot{K}(\tau') = \frac{dK(\tau')}{d\tau'}$.

In Equation 30, the instantaneous stress applied at time *t-t'* influences the stress at time *t*. Therefore it is necessary to map the stress that existed in the configuration at time *t-t'* into the configuration at time *t*. ABAQUS uses a mixed 'push-forward' transformation with the relative deformation gradient $\mathbf{F}_{t-t'}(t)$,

$$\mathbf{F}_{t-t'}(t) = \frac{\partial x(t)}{\partial x(t-t')}. \tag{34}$$

For finite strain viscoelasticity, ABAQUS suggests the following generalisation of the integral formulation

$$\tau(t) = \tau_0(t) + \mathrm{SYM}\left[\int_0^{\tau} \mathbf{F}_t^{-1}(t-t') \cdot \left(\frac{\dot{G}(\tau')}{G_0}\tau_0^D(t-t') + \frac{\dot{K}(\tau')}{K_0}\tau_0^H(t-t')\right) \cdot \mathbf{F}_t(t-t')d\tau'\right], \tag{35}$$

where $\tau(t)$ is the Kirchoff stress state and $\mathbf{F}_t(t-t')$ is the deformation gradient of the state at *t-t'* relative to the state at time *t*.

For time history analysis, ABAQUS assumes that the material is defined by the Prony series expansion of the relaxation modulus:

$$g_R(t) = 1 - \sum_{i=1}^{N} g_i^P (1 - e^{\frac{-t}{\tau_i}}), \tag{36}$$

where N, g_i^P, and τ_i, i = 1,2,3...,N, are material constants. This yields a linear viscoelastic model since the dimensionless stress relaxation function is independent of the magnitude of the deformation. The Prony series expansion, in combination with the finite strain expression for the stress, produces the following large strain model:

$$\tau = \tau_0 - \sum_{i=1}^{N} \tau_i, \tag{37}$$

where

$$\tau_i = \mathrm{SYM}\left[\frac{g_i^P}{\tau_i^G}\int_0 e^{\frac{-s}{\tau_i^G}} \mathbf{F}_t^{-1}(t-t') \cdot \tau_0(t-t') \cdot \mathbf{F}_t(t-t')dt'\right]. \tag{38}$$

The τ_i are interpreted as state variables that control the stress relaxation. When the hyperfoam model is used to define the instantaneous behaviour, the deviatoric and volumetric constitutive behaviour are coupled. Viscoelastic material definition is

accomplished using the instantaneous elastic moduli from the hyperelastic material definition (ABAQUS Theory manual, HKS, 1996).

For the numerical solution of systems involving all types of material behaviour, the equilibrium statement, written as the principle of virtual work, is solved. For equilibrium, the internal virtual work is equal to the external virtual work done.

To find the tangent modulus of the non-linear equilibrium equations for the Newton incremental solution procedure, the variation of the virtual work statement is taken. In order to solve these equations, a constitutive law is required for the stress and the stress rate in terms of the strain and strain rate. The deviatoric and hydrostatic parts of the constitutive law can be separated into two hereditary integrals. Time integration of the hydrostatic and deviatoric stress yields the total stress at the end of the increment, assuming that the stress varies linearly with the reduced time over the increment. This includes a component that considers the current stress state plus the contribution of the stress history on the current stress state which is given by the corotational constitutive rate equations.

The complete tangent modulus matrix can then be defined as the sum of the small displacement stiffness matrix which contains the increment in stress for the increment, the initial stress matrix which contains the stress at the start of the increment and the load stiffness matrix.

3.3 MATERIAL TESTING

The material tests need to characterise the expected range of loads and the predominant mode of loading in the model i.e. if tension is dominant, then tensile data alone is sufficient characterisation. However, when more than one mode of loading is expected, further tests are required to adequately account for any synergistic effects in the material behaviour. The following section describes how the material was produced, how the tests were performed and how the results were prepared for use in the numerical models.

3.3.1 Preparation of the Polyurethane

The polymer is a biostable segmented aliphatic thermoplastic polyurethane and was prepared by a polymerist at the Cardio Vascular Research Unit at the University of Cape Town. Porous samples were produced by forming a paste consisting of the polymer, a solvent for the polymer and an extractable filler material. The polymer is then precipitated in a non-solvent by a phase inversion process and the fill material is extracted to leave voids of the required size and shape. The porosity can be varied according to the ratio of fill material to polymer and is given by the volume fraction of voids to solid polymer. The size of the pores is generally between 90 and 120 μm but using different size fill particles

can easily vary this. During the precipitation process, the solvent in the polymer is also dissolved and creates tiny micropores in the material.

Figures 3.6a and b, are scanning electron micrographs of the porous polyurethane with pores produced by dissolving salt crystals from the polyurethane paste. The voids are slightly irregular in shape due to the different shape of the salt crystals. Figure 3.6c shows the porous polyurethane with pores produced using dissolvable microbeads. These beads have the advantage of forming a regular cell structure and pattern due to their consistent geometry. The tiny micropores due to the inversion process are also clearly visible.

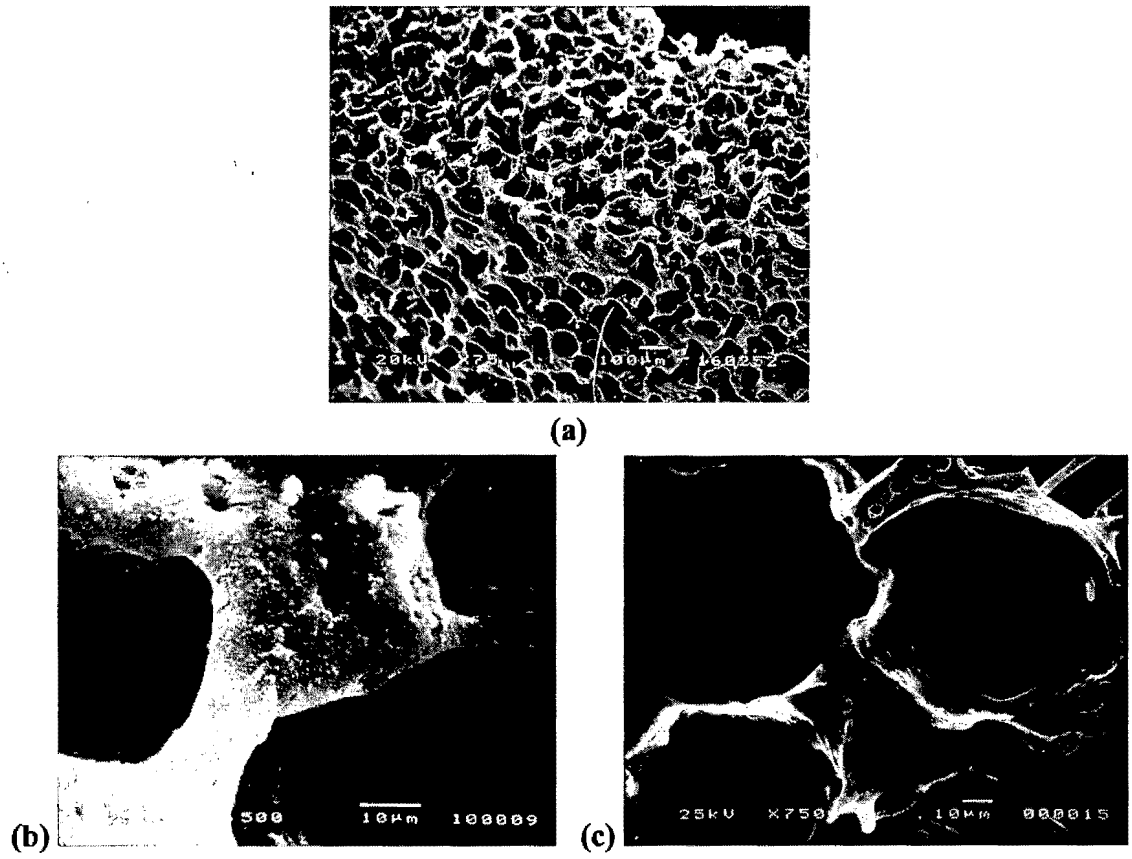

Figure 3.6 Scanning Electron Micrographs (SEM) of porous polyurethane with pores created using dissolvable fill material. [Magnification factor; a) x75, b) x500, c) x750]

Initially, a range of porosities was produced. Ratios of 1:1, 3:1, 5:1 7:1 and 10:1 salt : polymer were made. The lower range (1:1, 3:1) were not porous enough to create an open cell foam (interconnecting cells), and it was thus decided that these ratios were unsuitable for the purposes of artery tissue development and were not considered further.

3.3.2 Tensile, Simple Shear and Viscoelastic Material Tests

The characterisation has been structured towards use as input in the finite element software ABAQUS, and as such, it is important to provide a range of test data that covers the expected modes of loading. Although the predominant mode in the vascular system is tensile due to the induced hoop stress, a certain amount of shear behaviour is present due to the combination of the hoop and axial stresses in the wall. This behaviour is best characterised through bi-axial tests, but if simple shear data is used together with uniaxial test data, the material can be accurately approximated. An ABAQUS subroutine determines the material specific coefficients for the chosen strain energy function according to a least squares fit to the data. Since most polymers are highly viscoelastic, time dependent tests are undertaken to account for the creep response of the material. ABAQUS requires time dependent shear test data in the form of normalised shear modulus as a function time.

All the material tests were done as close to physiological conditions as possible. Thus, the tests were dynamic (as opposed to quasi-static) to represent the cyclic nature of the loading, in a thermostatically controlled environment at 37° C, in a phosphate buffer solution with a neutral pH (AAMI, 1994). The test results are detailed in the following section.

Tensile testing

By varying the ratio of dissolvable salt to solid polymer in the mixing process, a variety of porosities are possible. 'Dog bone' tensile test specimens were cut from mats of the porous polyurethane (Figure 3.7). Six specimens were cut from each mat and the tests were repeated for three different porosities. In order to establish the effects of pre-conditioning, and to simulate the material operating conditions, the material was initially cyclically strained 30%. Apart from the viscoelastic effects or retarded elastic response, it was noted that the material did not suffer any damage and that cyclic pre-conditioning did not significantly alter the material behaviour.

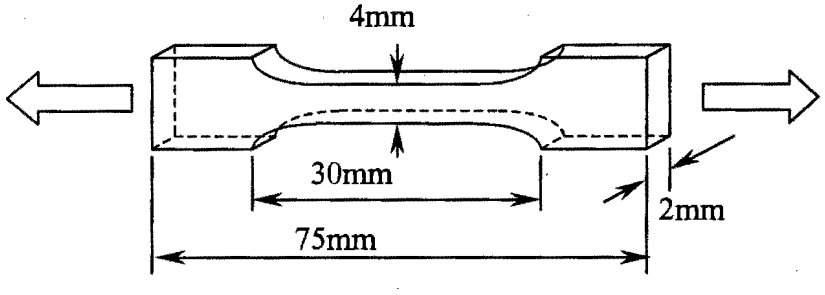

Figure 3.7. Dimensions of the 'dog bone' tensile test specimen used for the tensile tests

In accordance with the American Association for Medical Implants (AAMI 1994) on cardiovascular implants, the strain rate and temperature were held constant at 200mm/min and 37°C respectively for all tests. A best-fit curve was obtained for the results and the correlation coefficient, standard error and the ultimate breaking strain was determined for each material. Initially, the tests were done at room temperature (24° C). The tests were then re-done in the controlled environment in order to examine the effect of temperature on the material behaviour.

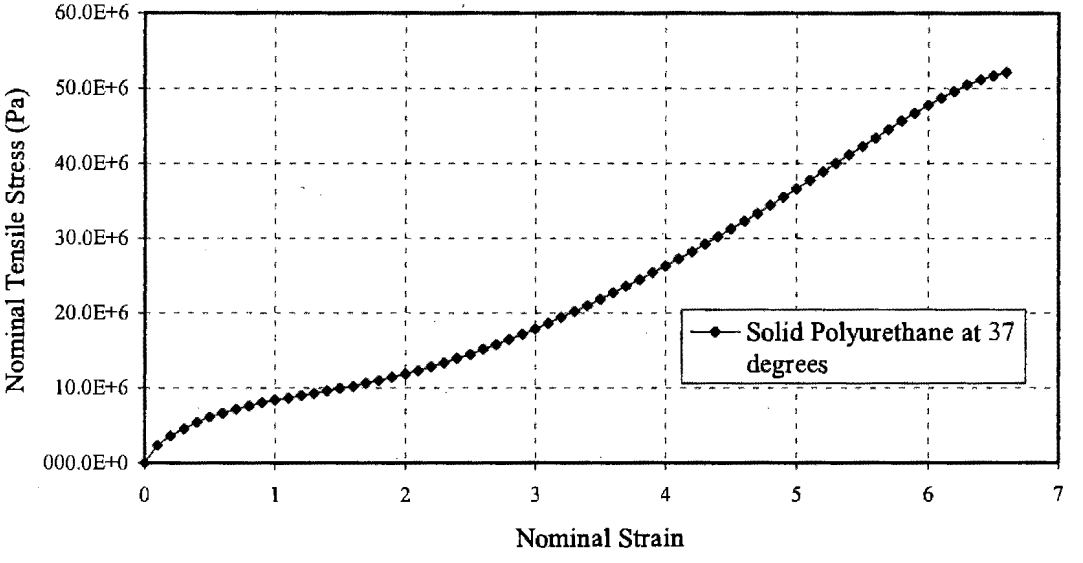

Figure 3.8 The stress –strain characteristics of solid polyurethane in tension at 37 C

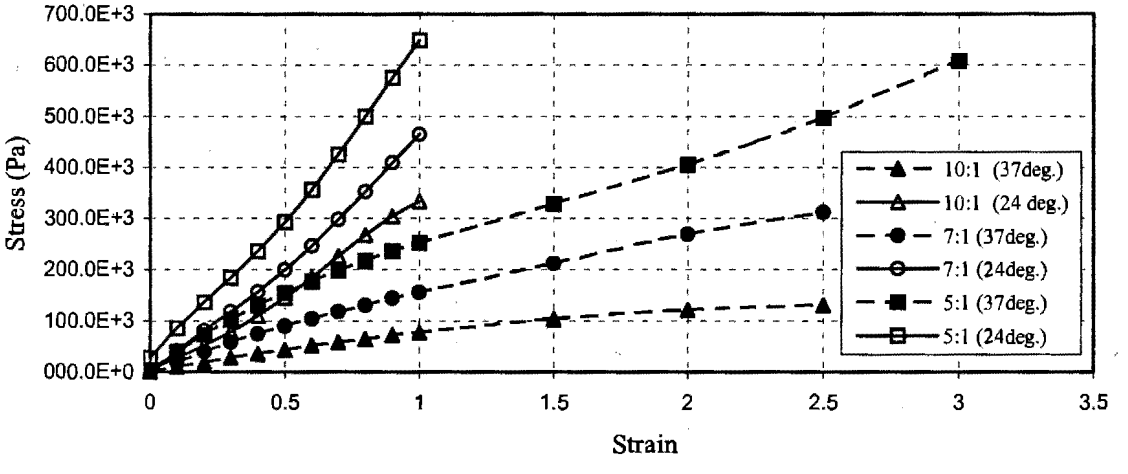

Figure 3.9 Stress-strain characteristics of porous forms of the polyurethane in tension.

The solid polyurethane displays a non-linear stress strain response (Figure 3.8) and is predictably very much stronger than porous versions of the same material. The material is also highly deformable, exhibiting strains up to 700%. From Figure 3.9, it is clear that the porous material displays a strong temperature dependancy. The material also displays a slightly sigmoidal, non-linear behaviour. Comparing the tensile stress at 100% strain, for the same porosity material, the stress in the material at room temperature (24 degrees) is approximately 2.5 to 3 times higher than the material at 37 degrees in each case. Looking at the strain at fracture, the ultimate tensile stress is still in the same range, but the strain at fracture is again almost 2.5 to 3 times greater in the material at body temperature. So the ultimate strength and the moduli of the materials are reduced at higher temperatures. The average ultimate failure stress for the materials are; 615kPa for 5:1, 305kPa for 7:1 and 145kPa for the 10:1 porosity materials.

Simple Shear Testing

Simple shear tests were performed on various porosity materials using the Zwick tensile testing machine (Figure 3.10). For this test, a central pillar is attached between the two specimens. The outer pillars are fixed and the central pillar is pulled. The tan of the angle made by the free face of the specimen is the shear strain. (Figure 3.11).

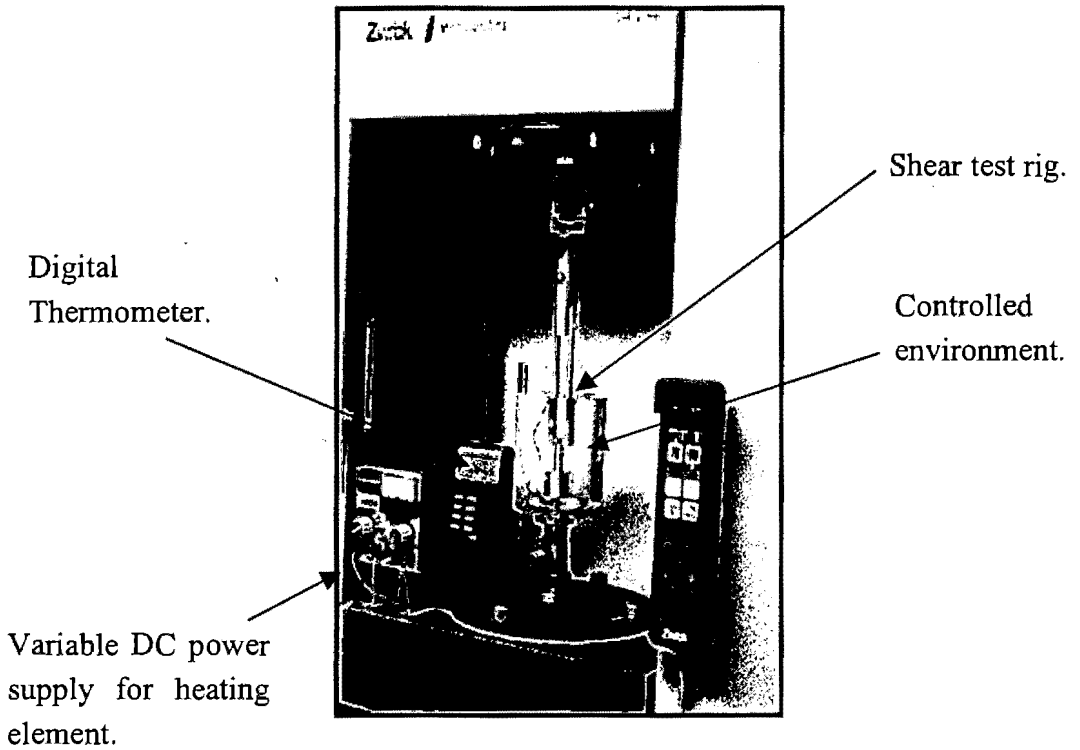

Figure 3.10: The Zwick tensile testing machine with the simple shear test rig.

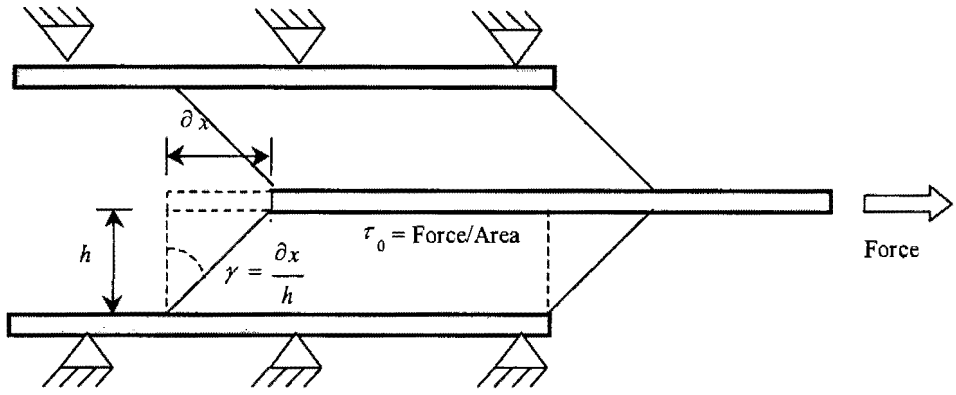

Figure 3.11 Simple shear test schematic. Two specimens are bonded to fixed plates on their outer surfaces and to a central pillar on their inner surfaces. The central pillar is displaced, thereby shearing the specimens.

The specimens are bonded to the test rig using cyanoacrylate glue. The glue was chosen since it provided a good bond strength and displayed poor gap bridging qualities (minimal absorption by the test specimen). The test specimens are 10mm high by 10mm wide and 2mm thick.). These dimensions are reduced from a specimen 5mm thick, since it proved difficult to create a homogenous specimen of the specified thickness. In the curing process, the salt tends to settle to the bottom, and the porosity in the specimen varies through the thickness. As a result, a band of larger pores form in the centre of the specimen. This induces a weaker shear band in the middle of the specimen and thus an unrealistic shear stress would be measured for the material. This geometric effect induced an unrealistic hypercompliance in the shear behaviour. Thus, the size of the specimens was reduced to a more realistic size equivalent to the geometry of the graft wall.. When the specimen were reduced to half the size, a much more consistent result was achieved. Best-fit curves were fitted to the data (Figure 3.12) and the result was used as input for the ABAQUS 'hyperfoam' model.

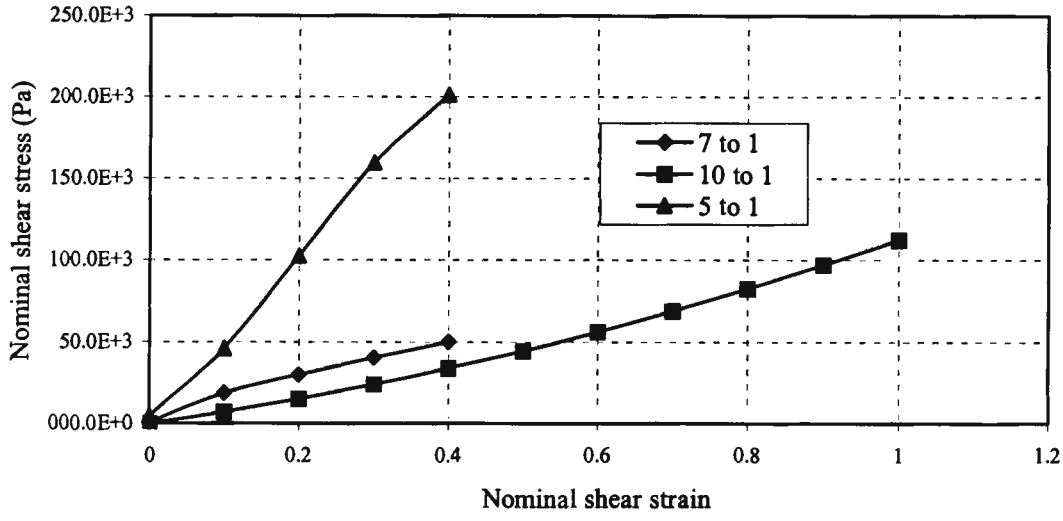

Figure 3.12 Shear stress vs. Shear strain for porous polyurethane.

The result shows the lower porosity of 5 to 1 to be stiffer in shear when compared to the other two lower porosities. The 7 to 1 and 10 to 1 are approximately linear after about 20% strain and have similar moduli, but a much lower modulus than the 5:1 porosity. The material generally fails at strains greater than 40%.

Viscoelastic Testing

Time domain viscoelastic tests were performed using a simple-shear testing device, shown in Figures 3.13 and 3.14, to determine the creep (retarded elastic) response of the material. Specimens were cut from mats of porous polyurethane. Each specimen was 10mm wide, 10mm long and 2mm thick. The tests were constant load simple shear tests where the load was applied by hanging a known mass on a lever arm. A load is chosen that is approximately 20% higher than the highest expected operating load. This load is kept constant and the strain is monitored as a function of time.

The vertical displacement of the specimen is measured by a linear variable differential transformer (LVDT) and plotted as a function of time using a continuous chart recorder. The displacement is used to calculate the shear strain (see Figure 3.11). The shear stress is calculated from the applied force divided by the specimens cross sectional area. The normalised shear compliance is calculated from values recorded in the experiment and implemented in ABAQUS as normalised shear compliance as a function of time. The normalised shear compliance is defined as $js(t) = G_0 J_S(t)$, where $J_S(t) = \frac{\gamma(t)}{\tau_0}$ is the shear compliance, $\gamma(t)$ is the total shear strain and τ_0 is the constant shear stress. G_0 is the instantaneous shear modulus [Hibbit *et al.* 1996].

ABAQUS automatically calculates terms for a Prony series from this data (Figure 3.16).

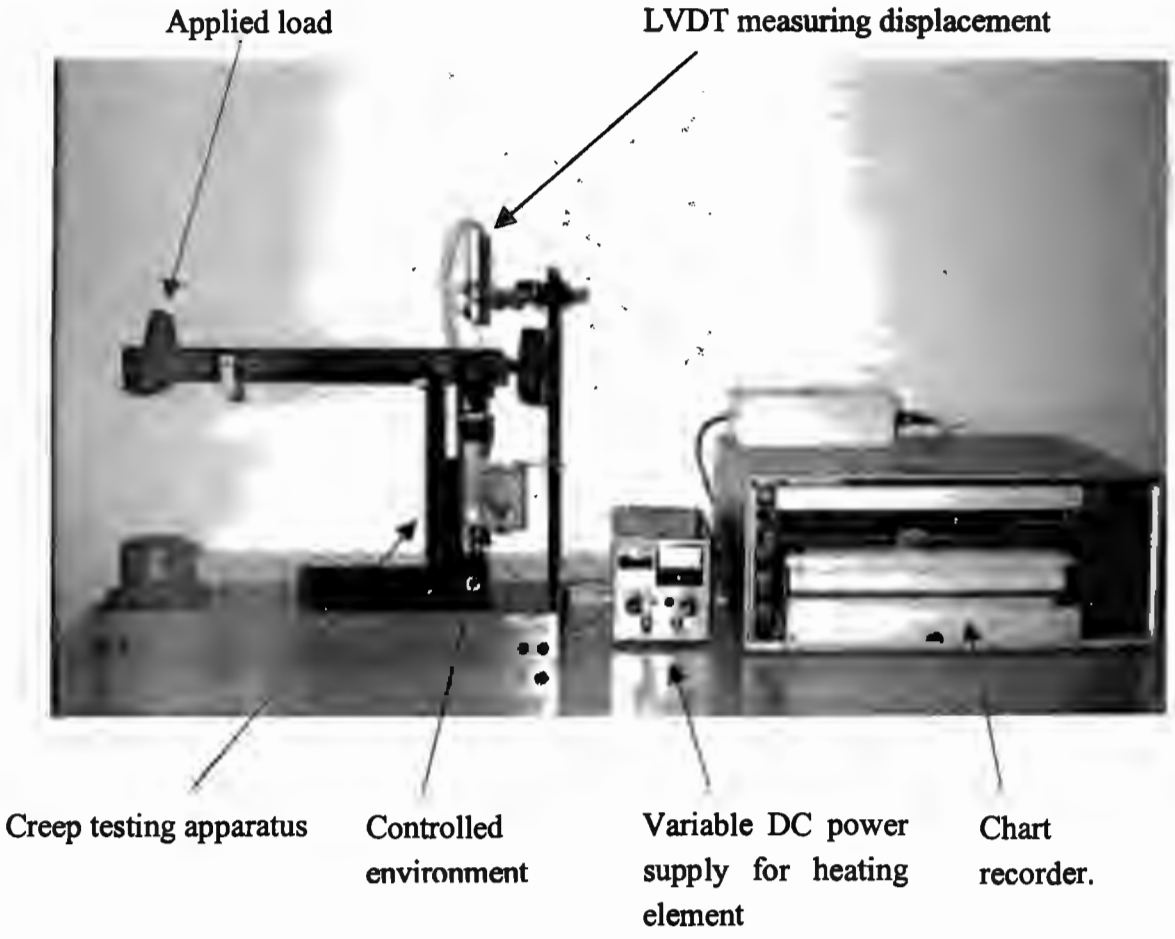

Figure 3.13 Photograph of the viscoelastic testing apparatus.

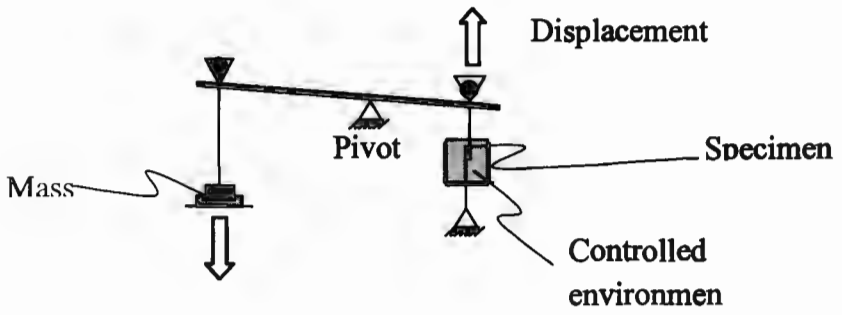

Figure 3.14: Schematic showing the viscoelastic testing rig.

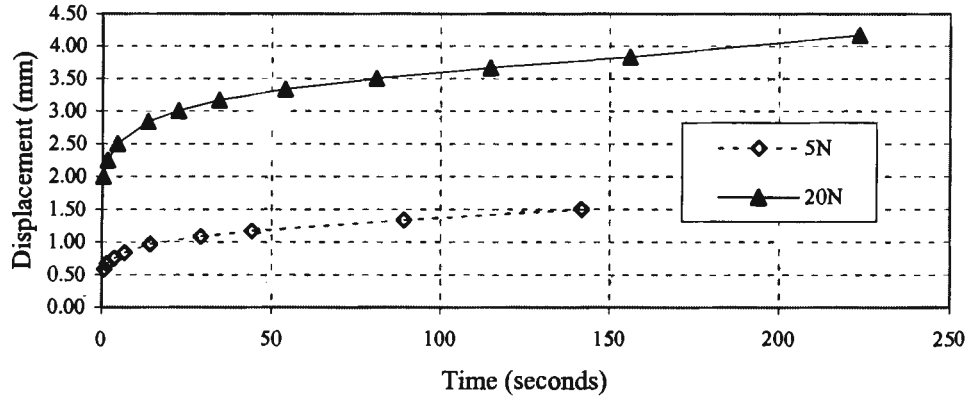

Figure 3.15 Displacement measured at the specimen.

Figure 3.15 shows the displacement response to a constant load. Tests were done at two loads and the result shows that the creep response is proportional to the applied load. The lowest load that could be applied with confidence was 5N; thus it was necessary to extrapolate from the two curves a new curve that predicts the creep at a lower load. This lower load creates a stress in the test specimen that is in the range expected in the numerical model. The shear stresses expected are in the order of 20kPa, requiring a 2N load in the viscoelastic test rig. Such a load could not be accurately applied on the experimental equipment. In order to overcome this problem, linear viscoelasticity was assumed and the behaviour of the material under a 2N load was extrapolated from the curve at 20N and 5N using linear extrapolation since the creep curves are proportional to the load.

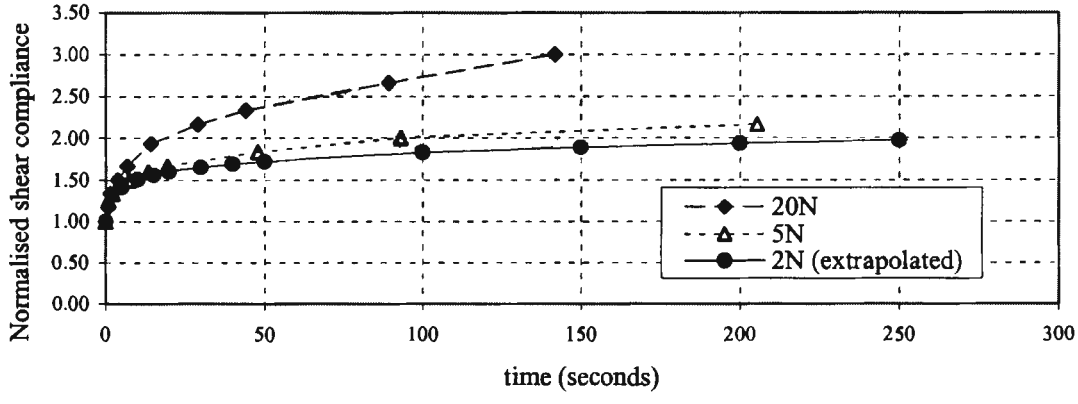

Figure 3.16 Normalised shear compliance for two loads plotted against time.

ABAQUS uses the normalised shear compliance in conjunction with the instantaneous shear behaviour based on the hyperefoam model to create a time dependant modulus. The shear modulus is effectively 'softened' by the normalised shear compliance and the retarded elastic response is reflected in the model as an increasing displacement over time, or 'creep'. This emphasises the importance of performing the viscoelastic tests at loads within the range of loading expected in the model. If the tests are done at loads much higher than those expected in the model, the normalised modulus would exaggerate the softening effect and hence skew the results.

The log time compliance curve (Figure 3.17) gives an indication of the linearity of the viscoelastic behaviour. At the higher load, the creep behaviour is slightly more non-linear than the lower load. However, linear viscoelasticity is still a valid assumption.

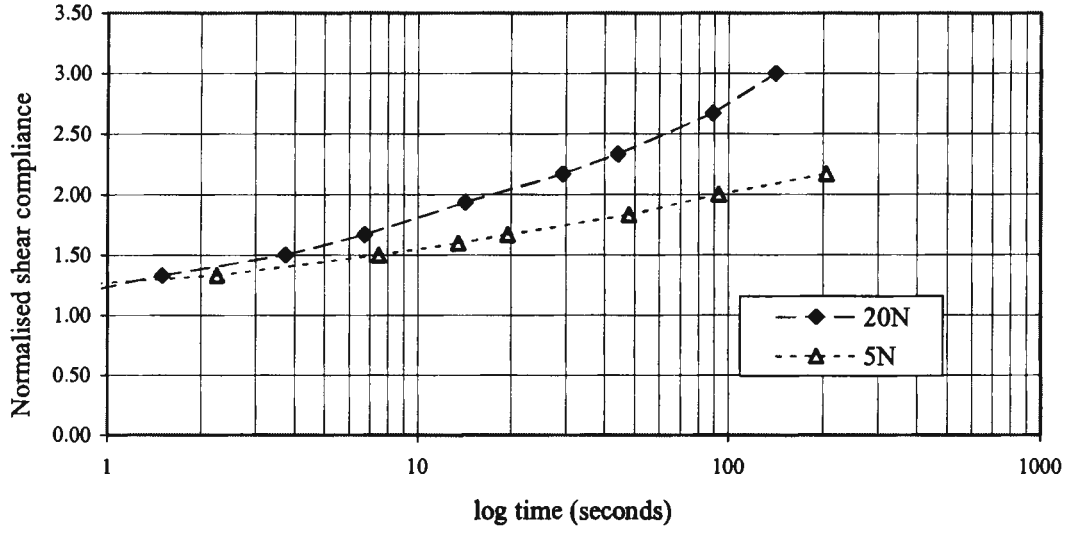

Figure 3.17 Viscoelastic creep response plotted on a log time scale

3.4 MODEL VERIFICATION

To verify the ABAQUS fit to the test data, simple shear and tensile tests were simulated on a single, plane stress element with unit volume (Figure 3.18).

The element was strained 100% and the loading history was plotted and compared to the test data. For the tensile test, nominal stress is plotted against nominal strain and in the simple shear test, shear stress is plotted against shear strain (Figure 3.19). ABAQUS predicts a least squares fit error of 25.5% for a hyperfoam model with N=6 terms. Using less than N=6, the reported error increased to around 40%.

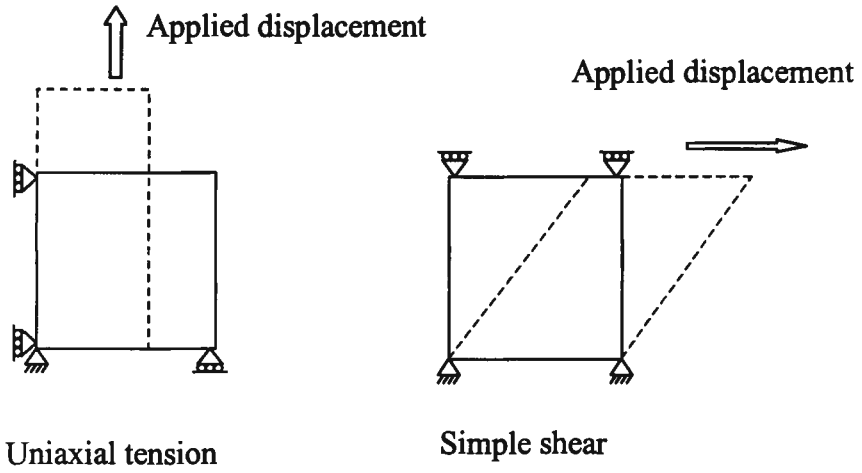

Figure 3.18: Single element tests for uniaxial tension and simple shear

The results of the single element tests show that the ABAQUS hyperfoam fit is valid up to a strain of about 35% for the shear data and up to 65% strain for the tensile data. This is indeed accurate enough to predict compliance in an artery graft, since an artery reaches a maximum strain of around 30% under normal physiological loading conditions. However, this result shows that since the actual and predicted stress values diverge at higher strains, using this model for failure analysis would be unreliable.

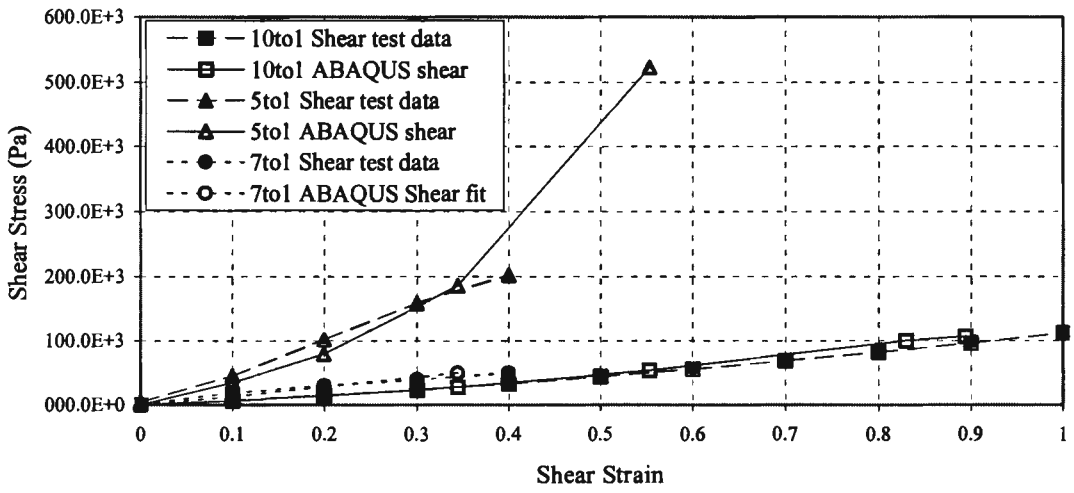

Figure 3.19 Single element simple shear stress. Verification of ABAQUS fit to the test data.

The tensile behaviour is particularly poorly approximated for the 5 to 1 porosity under uniaxial tension (Figure 3.20). This is also the case for the simple shear test, with the accuracy departing at around 30% strain. With the exception of the approximation of the 5 to 1 porosity, the numerical solution has approximated the behaviour consistently accurately to strains of more than 40% for shear strain and around 65% strain for the tensile tests. These results show that the ABAQUS material behaviour correlates with the input data and is accurate to 40% strain for shear strain and 65% strain for uniaxial tension.

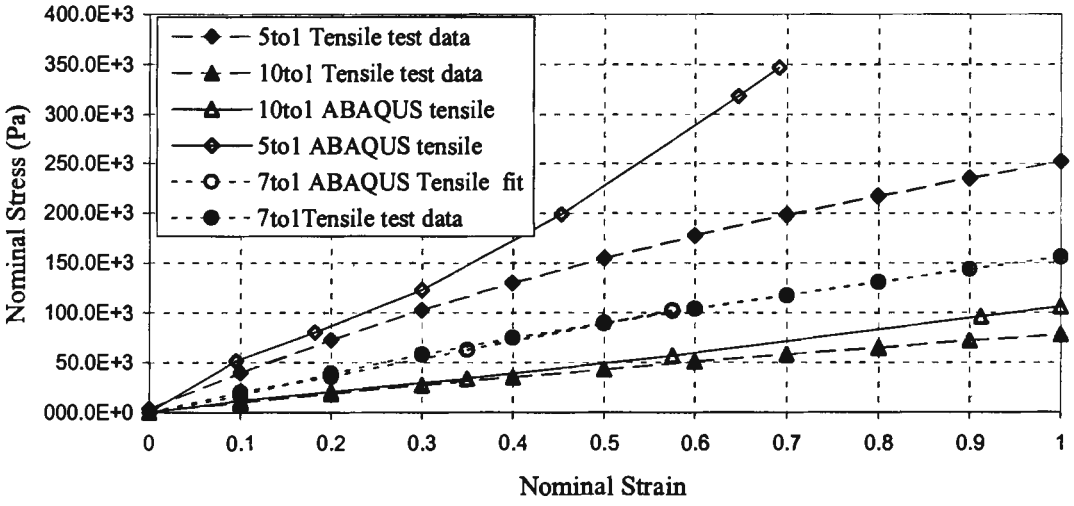

Figure 3.20 Single element tensile test results. Verification of the ABAQUS fit to the test data

A constant shear load was applied to the top surface of the element. The load produced the same shear stress in the element as that experienced in the viscoelastic test (20kPa). From the displacement of The normalised compliance was calculated for the element and the experiment and the results are displayed in Figure 3.21. The correlation between the normalised compliance result in ABAQUS and the test data is very good. The error tolerance for the fit was 3% after 200 seconds. However, it appears that the slope of the Prony series tends to flatten out sooner than the experimental data. This could be a source of error in very long-term displacement predictions.

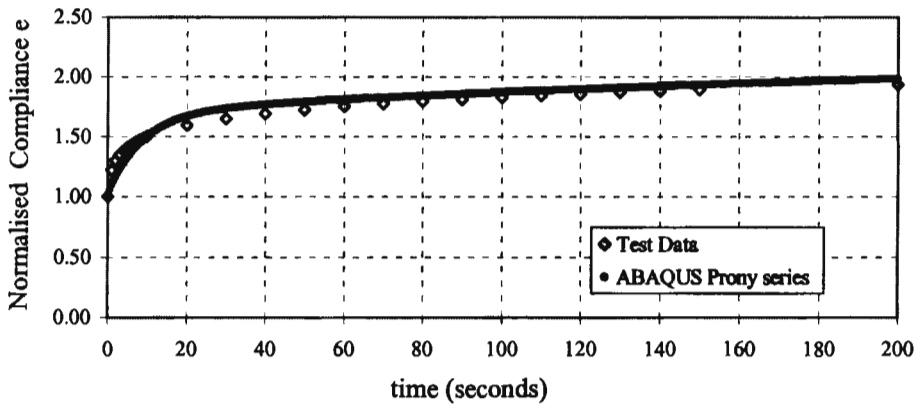

Figure 3.21 Single element Creep test. Verification of ABAQUS fit to the normalised shear compliance.

CHAPTER FOUR

GRAFT DESIGN: NUMERICAL AND *IN VITRO* ANALYSIS

4.1 INTRODUCTION

Having physically tested the polyurethane and outlined the constitutive theory to describe the material behaviour in the previous chapter, it is necessary to verify the numerical model for a problem of the order and magnitude expected. Before the numerical model is tested some design concepts are reviewed. These are drawn out from the structure of the natural artery and from the requirements for successful musculogenesis and cell ingrowth outlined in Chapter two. The numerical model is then evaluated by comparing results from axi-symmetric finite element models with in vitro experiments. Once a correlation between the numerical and physical problems has been established it is possible to explore and develop the design concepts. Finite element models of various graft designs are used to investigate the influence of different structures and material properties on the overall compliance and mechanical behaviour.

4.2 GRAFT DESIGN CONCEPTS

The main objective of this work is to create a compliant, microporous, polyurethane artery graft that enhances cell development through structured ingrowth channels and encourages musculogenesis providing contractility. The success of the graft will depend on the compliance, the type and amount of cell ingrowth and musculogenesis that develops in the wall structure, and the flow surface finish on the inner surface. The graft should be resistant to failure due to over distension, creep, buckling (kinking), fatigue failure and failure due to biodegradation.

The important structural characteristics that were identified from the natural artery are the spiral orientation of the smooth muscle in small diameter arteries and the loose bundles of collagen that act as reinforcing at elevated pressures. The development of organised cell proliferation through porosity and ingrowth channels is a crucial part of the graft structure since this will eventually lead to a completely endothelialised inner flow surface and, if the correct cells develop, provide the necessary contractility through musculogenesis.

Starting with the basic form of bulk, bio-inert polyurethane described in Chapter 3, it is possible to develop some preliminary design concepts. There are many possibilities and

methods for creating graft structures that fulfil the requirements set out previously. Three design concepts are suggested and reviewed here.

Design 1: Radial channels with circular shapes that start at the inner surface and end at the outer surface.

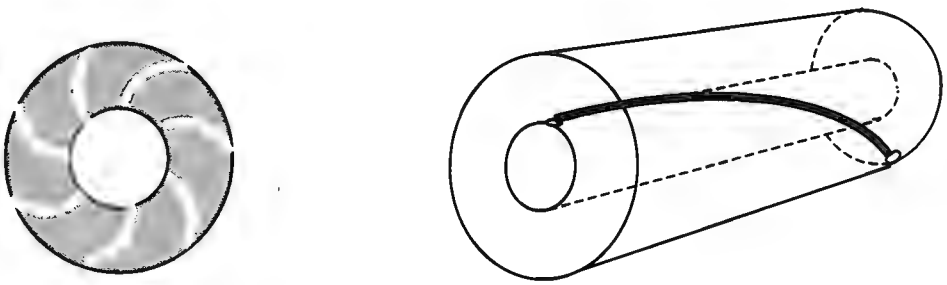

Design 2: Radially expanding spiral channels that start at the inner surface and end at the outer surface.

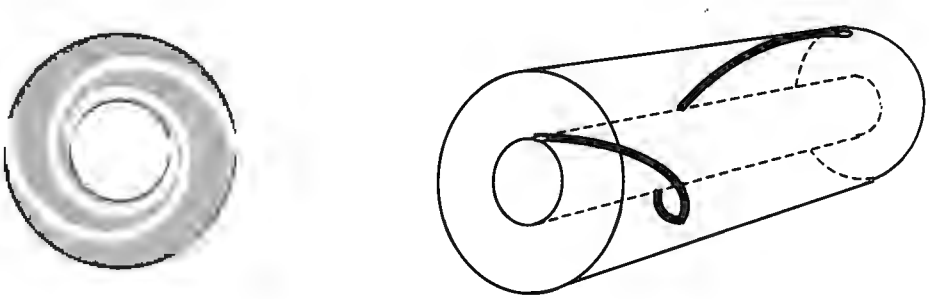

Design 3: Fixed radius spiral channels.

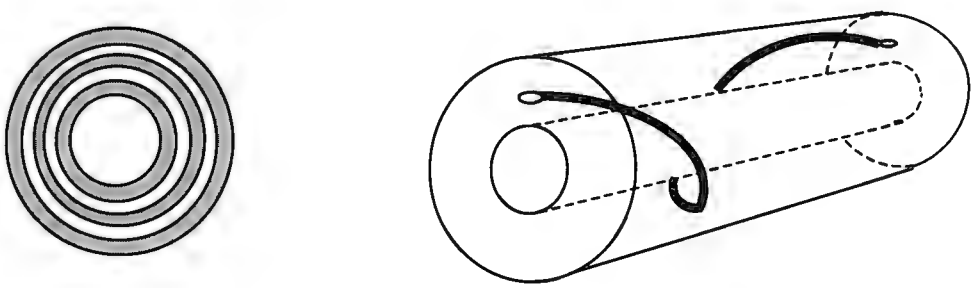

Another design could involve a combination of porous polyurethane and a type of woven structure. Similar to the design of Gupta *et al.* (1997) who used a combination of two types of woven elastic fibres, the inside weave with a low modulus and the outside weave with a higher modulus. This mimics the media and adventitia in the arterial wall. However, the woven structure does not allow for oriented cell ingrowth or musculogenisis.

This design could be improved upon using porous polyurethane on the inside and a loose external weave (Figure 4.1). A compliant graft with an oriented pore structure can be created in the inside layer providing a structure for cell ingrowth and a loosely woven external reinforcing with a higher modulus would prevent excessive dilation at higher pressures.

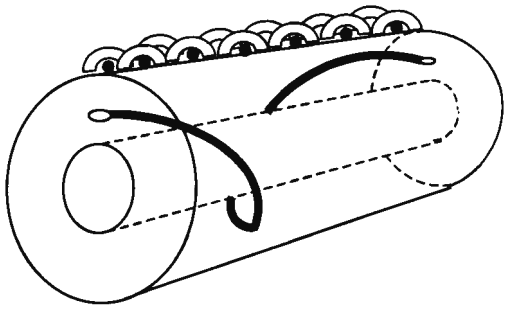

Figure 4.1 Hybrid design concept similar to Gupta *et al.*, (1997) with an internal channel and loosley woven external reinforcing.

Designs one and two are quite similar in that they both involve pores connecting the outer surface to the inner surface. If the graft is made from solid (non-porous) polyurethane, porosity can be achieved by increasing the number radial pores. They connect the inner surface to the outer surface allowing cell ingrowth and a possible endothelial cell lining on the flow surface. The pitch of the pores can be altered to control the circumferential orientation of the pores.

However, in the spiralling concept, there is a limit to the number of spiralling pores that a tube can contain due to the very acute angle made by the pore at the inner surface. The spirals also diverge from each other as they expand towards the outer surface, leading to a variable porosity through the thickness, with the outer half being less porous than the inner half. This could be used to some advantage if that effect was desired. The problem with both of these concepts is the difficult manufacturing technique required to produce pores that start at the inside and end at the outside.

The third design concept is simpler and has the desired effect of creating a circumferentially oriented ingrowth channels and the possibility of an endothelial lining on the inner surface, if a porous polyurethane is used as the bulk material. The manufacturing technique is simple and winding a soluble thread in the graft at intervals during the graft production can create more than one layer of spiral channels. In this way, porosity can be achieved through a combination of material porosity and varying the diameter and thickness of the spiral pores. Changing the pitch of the spiral wind can vary the pore's circumferential orientation.

In order to analyse these structures, it is necessary to test and develop each concept. Testing can be done using finite element models and experimenting with grafts *in vitro*. The constitutive laws for the material have previously been verified using simple, single element tests but there is no evidence that the models will be accurate for all geometries. It is therefore necessary to verify the numerical model's accuracy by modelling a simple graft configuration numerically and comparing results with *in vitro* experiments. Once a correlation between the results has been established the accuracy of the numerical models can be gauged and used as a reference when analysing the results of other numerical models.

The next section begins by comparing and evaluating the numerical analysis of a basic porous graft to in vitro experiments of the same graft. Then, an artery-graft anastomosis is modelled numerically to compare the compliance of basic grafts with a natural artery. This gives an indication of which porosities are most suitable for initial compliance. Next, internal channels in the graft wall are modelled and the effect on the overall compliance of the structure is analysed. The viscoelastic behaviour is investigated last.

4.3 Evaluation of Numerical Models

The implementation of a non-linear hyperelastic material model in a finite element code is not a trivial task. The accuracy and relevance of results predicted using such a model need to be carefully considered. Factors such as the extent of loading and the geometry and deformation in the final state can have a significant effect on the accuracy. Having examined the performance of the numerical model using a single element test, it is now necessary to validate the material model on a more realistic problem. To this end, simple numerical models are compared to *in vitro* experiments and evaluated to gauge the accuracy of the models.

4.3.1 Experimental Procedure

Grafts were prepared at the CVRU at the University of Cape Town, 6mm internal diameter with a 1mm wall thickness, from porous polyurethane with a salt:polymer ratio of 7:1. These were tested in a compliance-testing rig shown in Figures 4.2 and 4.3. Since the graft is a highly porous tube, a very thin latex inner tube is inserted into the graft before it is pressurised to prevent any leakage (AAMI 1994). The graft is attached to the test rig at either end by circular clamps. The experiments were carried out at 37 C.

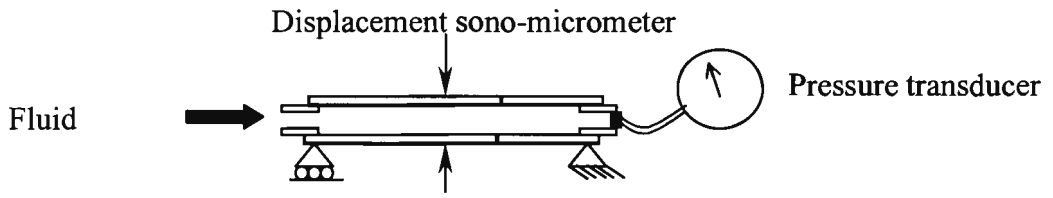

Figure 4.2: Schematic of the in vitro compliance testing device.

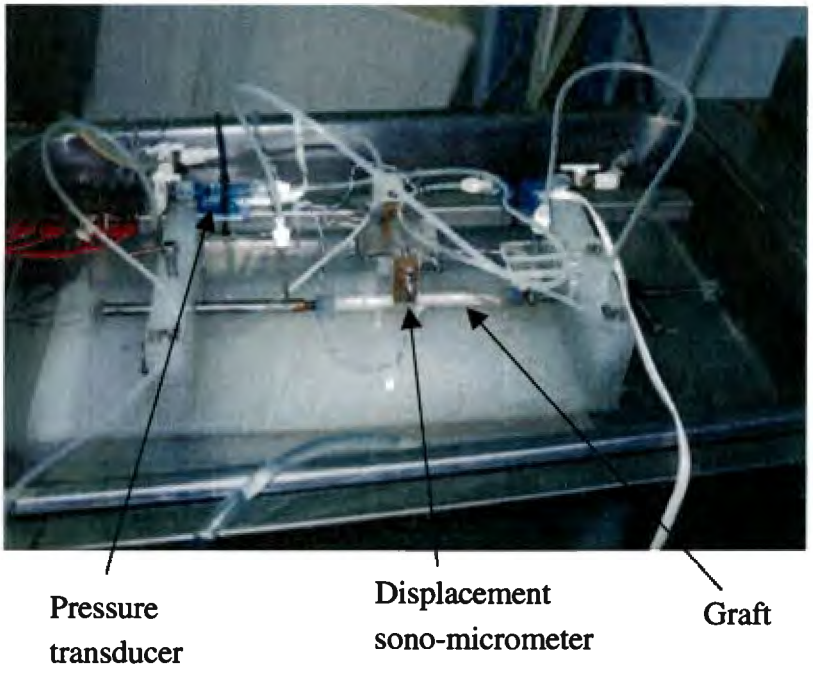

Figure 4.3 Photograph of the *in vitro* testing apparatus.

Two types of constraint were investigated, the first considers the graft fixed axially at both ends, and the second considers one end fixed and the other end free to move axially.

Two loading conditions were considered; first, to investigate the radial compliance, the graft is gradually pressurised by a step loading and the change in diameter is measured at each increment of pressure.
Secondly, to measure the viscoelastic response of the graft, an internal pressure was applied and held constant. A history of the change in diameter was recorded for a length of time, which produces a curve reflecting any retarded elastic (creep) response in the graft.

4.3.2 Numerical Modelling

The *in vitro* experiment described above is simulated using a finite element model. Making use of the rotational symmetry of the graft, axi-symmetric models, geometrically identical to the graft, were created using four noded axi-symmetric elements. The material model used was the "hyperfoam" strain energy function with $N=6$ terms and a Poisson's ratio of 0.2 (Gibson and Ashby, 1988). The model calculates material coefficients from data for simple shear and uniaxial tensile behaviour of the foam in question i.e. the material with 7 to 1 salt:polymer ratio. The models are accurate only up to the strains detailed in Chapter three. Once these strains have been exceeded, the solution becomes unstable and results in this range should be treated carefully. Displacements measured in the physiological pressure range are valid, however failure predictions at elevated pressures are not accurate.

As in the *in vitro* experiment, two boundary conditions are considered. The graft is modelled with both ends fixed for the first model and with one end constrained axially and the other end free to move for the second model. To impose these boundary conditions, the edge nodes at both ends are constrained by radial and axial restrictions (Figure 4.4). The thin latex inner tube is assumed not to have a significant affect on the results and is therefor not modelled.

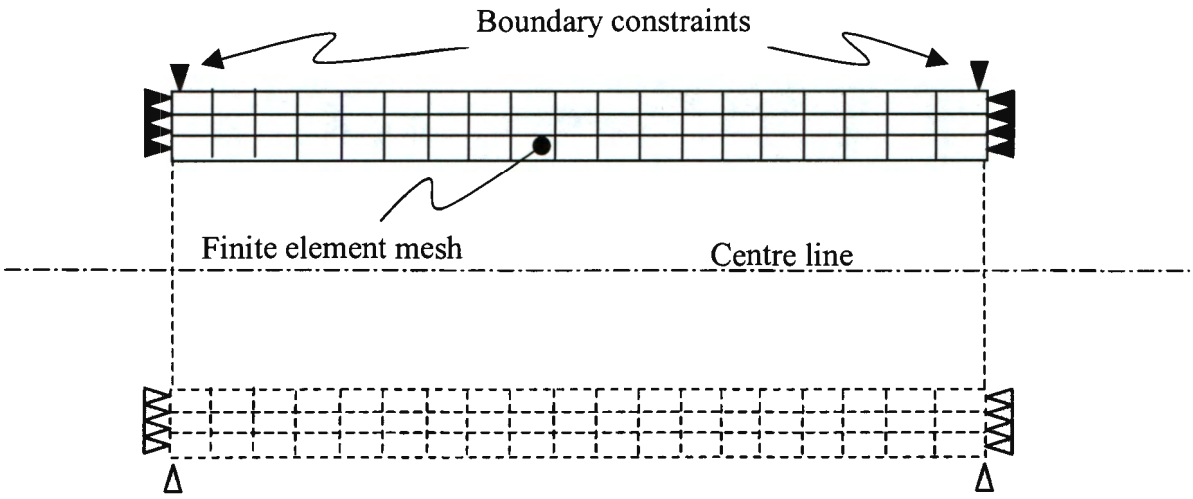

Figure 4.4 Axi-symmetric finite element mesh showing boundary conditions

In the static analysis of the axi-symmetric model, an internal pressure load is applied by ramping the load up over a single time step from 0 –100 mmHg (13kPa). A displacement history of the middle node in the outer surface of the model is recorded and plotted at regular intervals.

In the viscoelastic analysis, the pressure load is ramped up and held constant for a period of time. A load of 13.3kPa (100mmHg) was chosen since this is the mean pressure between systole and diastole pressure. The outer node displacement history is plotted.

4.3.3 Results and Discussion

Compliance is a measure of the change in diameter, D, to an applied pressure, ΔP, measured as $C = \frac{\Delta D}{D_0 \Delta P} \cdot 10000$ and has units %/(100mmHg) (AAMI 1994). This implies that compliance is measured in increments of pressure of 100mmHg, which is not the case in all experiments. It does however define the compliance of a graft at one particular point, that being 100mmHg. What is not apparent from this information is the stiffening behaviour of the arteries under increasing pressure, which is clearly non-linear and it is thus useful to have the compliance of a vessel covering a range of pressures. A more useful representation of the compliance would be a graph covering the physiological range

of pressures measured purely in %/kPa (or mmHg). However, to comply with the standard AAMI, units of %/(100mmHg) have been used here.

Comparing the results in Figures 4.5a and 4.6a, it can be seen that the ABAQUS numerical solution for displacement and compliance are representative of the experimental values for two different loading situations.

Although there is a fairly wide scatter of experimental results, the numerical solution appears to approximate the trend of the experimental data points to a satisfactory level. The numerical results under predict the behaviour in the early stages. In the physiological pressure range (80 – 120mmHg), the compliance results are more accurate. In both boundary condition cases, there is a good correlation of results for displacement (Figures 4.5b and 4.6b), but the results are less accurate when describing the compliance. The compliance of the model constrained at both ends reflects a greater increase in diameter than the graft with one end free to move. At 100mmHg, the unconstrained graft has expanded to 9mm diameter while the constrained graft has expanded to 10mm diameter at the same pressure. This can be attributed to the change in volume of the graft. The graft that is constrained axially dilates more than the graft that is free to elongate.

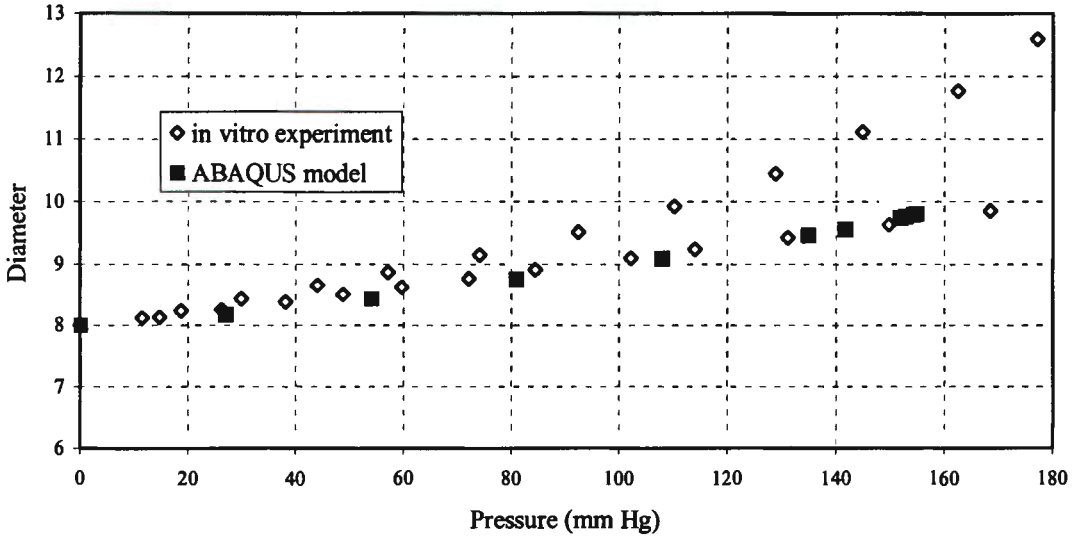

Figure 4.5a Comparison of diameter change to an incremental pressure of a graft constrained at one end only.

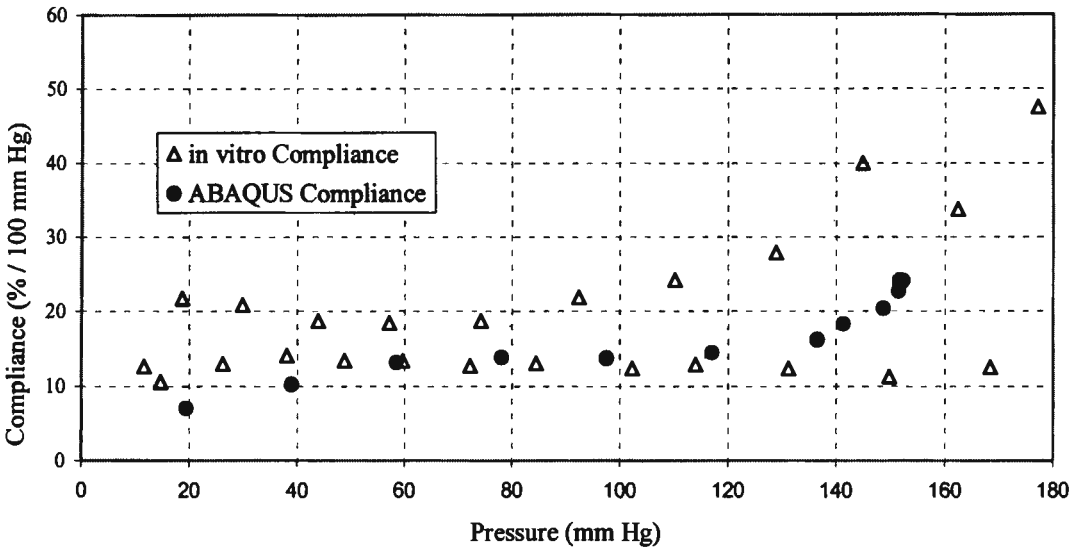

Figure 4.5b Compliance comparison of a graft constrained at one end only.

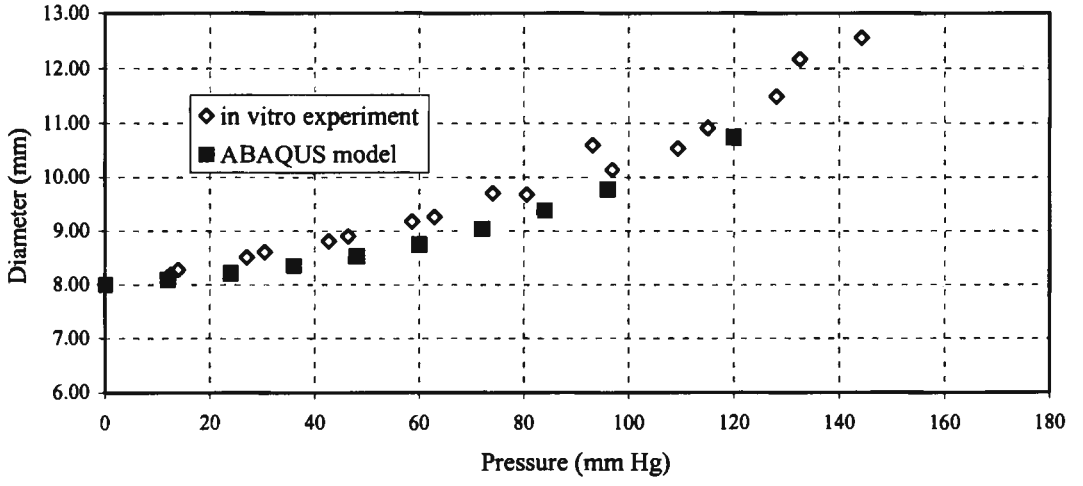

Figure 4.6a Comparison of diameter change of a graft constrained at both ends.

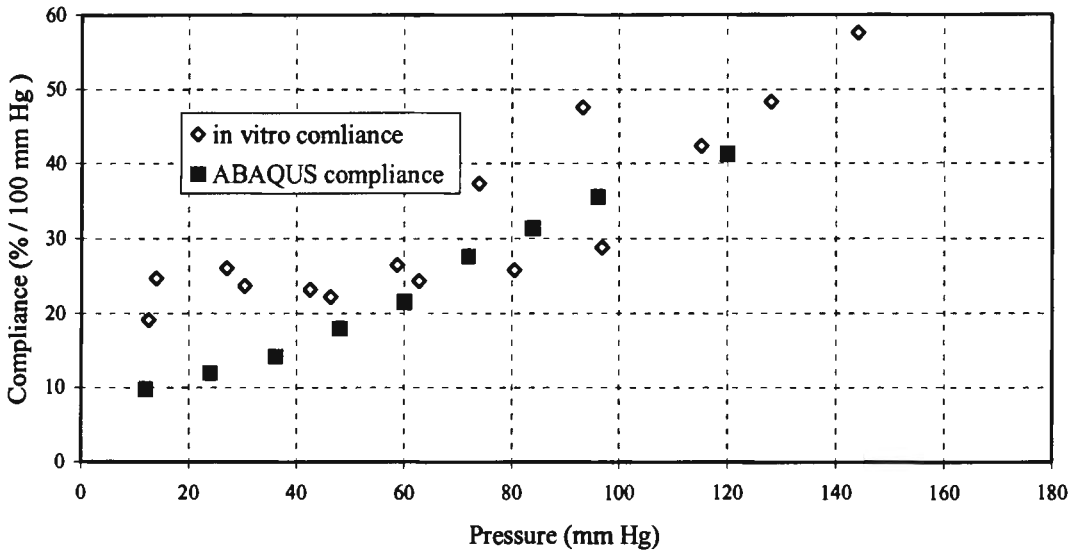

Figure 4.6b Compliance comparison of a graft constrained at both ends.

A sono-micrometer mounted on a lever arm measures the displacement in the experiment. As the graft expands, the arms are forced apart, thus measuring displacement. The more the graft expands, so the error in reading is magnified since the transducers are mounted on a pivot (Figure 4.7).

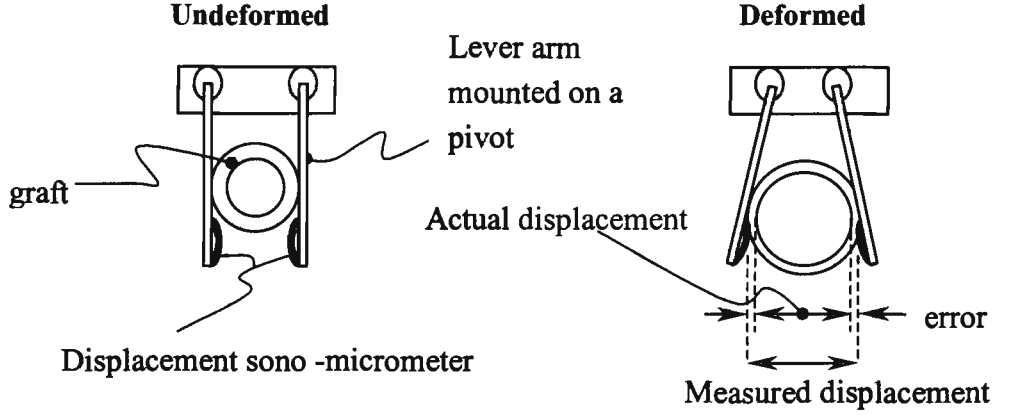

Figure 4.7 Error caused by pivoting lever arms.

The inconsistency in the material properties between different batches of polymer is a significant factor. Most noticeably, a membrane forms on the outer surface of the graft due to the nature of the curing process. This, along with other material inconsistencies from batch to batch may produce a wide scatter of results. The data used in ABAQUS was

averaged from a variety of tests. It is thus significant that, although different batches of the same polymer display slightly different mechanical properties, the material behaviour can be reasonably accurately predicted through a numerical model.

Referring to Figure 4.8, the highest stresses in the model will be the circumferential (hoop) stress due to the fact that the hoop stress in any cylindrical pressure vessel is usually twice as high as the longitudinal stress. This can be shown from the relation, $p \times area = \sigma \times area$, where the internal pressure, p, in the vessel acts over an area, πr^2, axially and $2\pi rl$ circumferentially. The stress due to the internal pressure acts over an area $2\pi rt$, axially and $2tl$ circumferentially. So, the axial or longitudinal stress can be determined from $p\pi r^2 = \sigma 2\pi rt$, solving for stress, the axial stress is $\sigma_{zz} = \frac{pr}{2t}$. In the same way the hoop stress can be determined from $p2\pi rl = \sigma 2tl$ so that $\sigma_{\theta\theta} = \frac{pr}{t}$. Thus, hoop or circumferential stress is twice the longitudinal or axial stress.

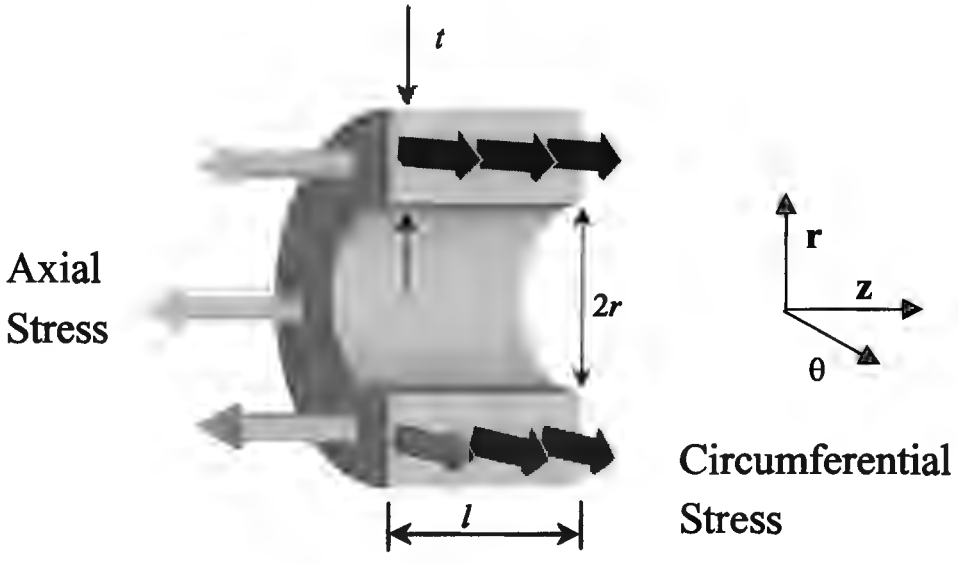

Figure 4.8 The circumferential and axial stress induced in a pressurised tube.

The hoop stress induced by an internal pressure of 100mmHg (13kPa) varies through the thickness of the graft, with a maximum of around 80kPa at the inner surface gradually decaying to around 65kPa at the outer surface. The hoop stress is a minimum at the ends and stress values of between 5 and 10kPa are reported (Figure 4.9).

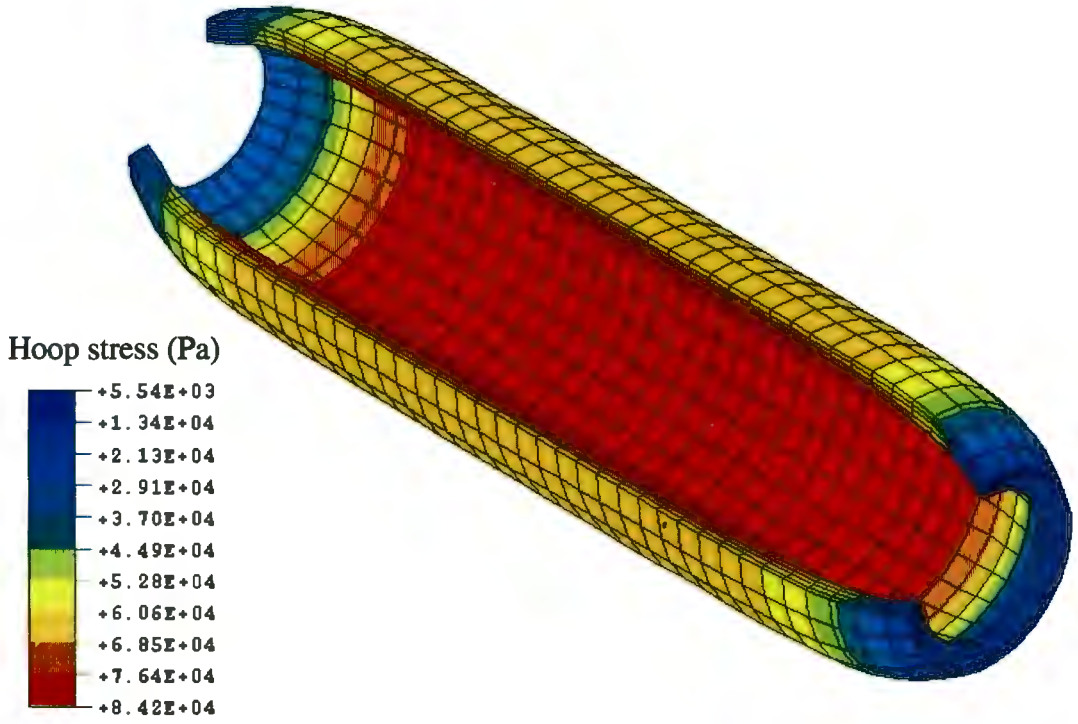

Figure 4.9 Hoop stress induced by an internal pressure of 100mmHg (13kPa) in a graft free to move axially at one end

Creep Response

The viscoelastic material model is introduced which uses a time generalisation of the "hyperfoam" constitutive equation for the material behaviour. The normalised creep compliance at the 2N load case was used. This data was extrapolated from the tests done at higher loads using linear extrapolation (Chapter 3). The long-term behaviour of the material can be seen in Figure 4.10. The left-hand axis of Figure 4.10 is the pressure axis. The pressure was ramped up to 100mmHg over a 20-second time interval. The right hand axis of Figure 4.10 is displacement and a displacement history of a point in the middle of the graft is shown. The displacement of a node on the ABAQUS viscoelastic finite element model is shown here too.

The numerical approximation under predicts the creep displacement by about 7%-10% in the long term. When normalised creep compliance from the 5N test was used, the result was a large over prediction, indicating the importance of the correct testing conditions. It is encouraging that the rate of creep is almost identical for both the experiment and the model. This indicates a strong correlation between the numerical model and the experiment.

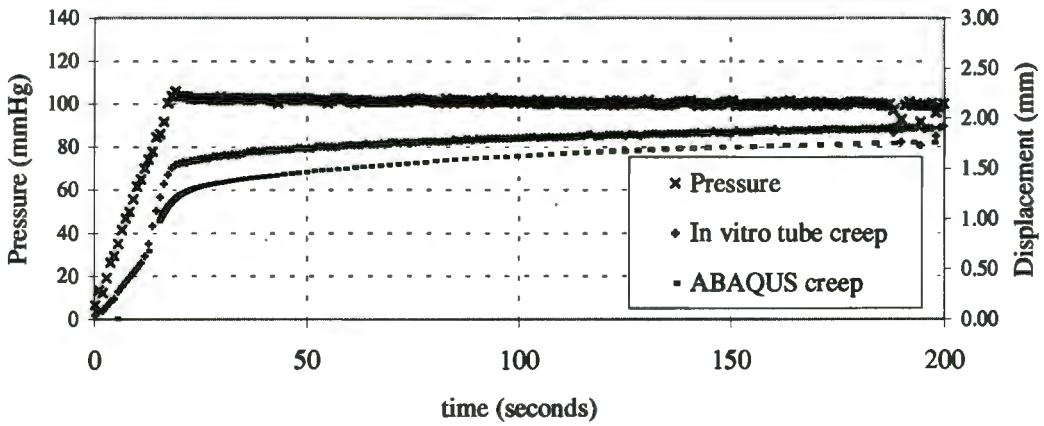

Figure 4.10 Comparison of retarded elastic response of a graft ***in vitro*** and ABAQUS prediction.

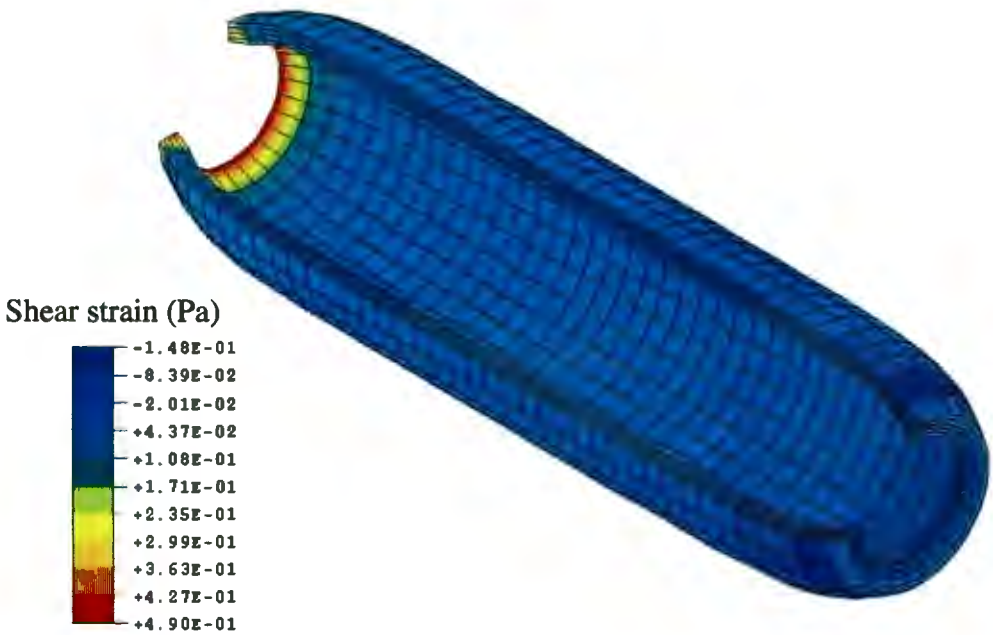

Figure 4.11 Shear strain in a graft pressurised to 100mmHg (13kPa)

Since it is the shear strain in the material that will determine the creep response of the graft, the shear strain is shown in Figure 4.11, and is predictably concentrated at the ends of the graft. At the constrained end the maximum shear strain is tensile and about 42% whereas at the free end the shear strain is compressive and around 14% strain. These shear strains will have the greatest effect on the creep response in the model and over a long time period, this may lead to excessive dilation. Excessive dilation *in vivo* causes aneurysms in the graft and alters the haemodynamics of the blood flowing through it.

4.4 Numerical Modelling of an Artery - Graft Anastomosis

The axi-symmetric numerical model has shown a sufficient degree of accuracy that makes it possible to continue with more complex models with some confidence. The artery – graft anastomosis (end-to-end) is a point of interest and a simple model can be developed to describe the interaction between the two materials. The compliance of the two vessels can be compared relative to one another from the direct comparison of their behaviour. In order to model the anastomosis between a graft and an artery, it is necessary to define suitable strain energy functions for both materials. For this model, the graft is modelled using the same "hyperfoam" strain energy function as in the previous experiment, and the artery is modelled using a hyperelastic material law identified by Fung (outlined in Chapter 3). The model is an isotropic approximation of the original form.

The graft and artery are modelled using 4-noded axi-symmetric elements (Figure 4.12). The elements making up the artery are hybrid elements since these are elements best suited for the analysis of incompressible materials[1].

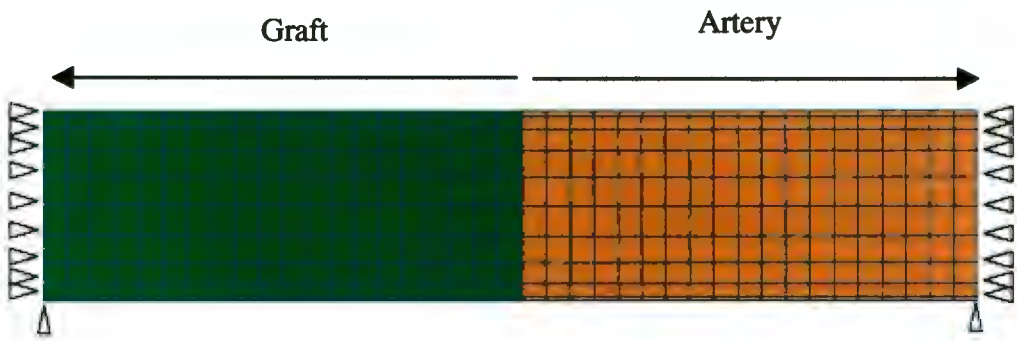

Figure 4.12 Finite element model of the artery-graft anastomosis showing boundary conditions.

The artery and graft are each constrained from axial displacement only, enforcing a symmetrical boundary condition and mimicking the *in vivo* conditions. The sutures normally present at the anastomosis between graft and artery are omitted here as they are assumed to tie the two vessels together, affecting the anastomosis locally but not influencing the overall behaviour significantly. This is however a generalisation and should be investigated in more detail.

[1] In the case of incompressibility, the solution to a problem cannot be obtained in terms of displacement history only, since a purely hydrostatic pressure may be added without changing the displacements. For these materials, a small change in displacement creates an extremely large change in pressure, making a displacement-based solution too sensitive to be useful numerically. The pressure stress in hybrid elements is treated separately and coupled to the displacement solution through the constitutive theory. (Hibbet *et al.* 1996).

An internal pressure is gradually applied to the artery – graft model from zero pressure to 200kPa. In the case of the 7 to 1 and 10 to 1 grafts, the solution is accurate until the limiting strains reported in Chapter three are exceeded. After that, the solution becomes unstable.

Discussion of Results

The compliance of a natural artery, (represented by the isotropic version of Fung's strain energy function) and the polyurethane graphs with three different porosities are shown in (Figure 4.13). The compliance of the artery with Fung's model is almost 5%/100mmHg at 100mmHg, which compares favourably to values of compliance for the human femoral artery of 5.9%/100mmHg reported by Walden *et al.*, (1980). This corresponds to a diameter change of 0.5mm for a graft originally 8mm diameter, which is reflected in Figure 4.14.

It can be seen that the salt polymer ratio of 10 to 1 is hypercompliant in its behaviour over the pressure range exhibiting a compliance of 60% at 80mmHg, which is not suitable for the manufacture of a compliant graft. The 5 to 1 salt polymer ratio is the most suitable in the physiological range between 75 and 120 mmHg and displays compliance of approximately 5%/100mmHg, equal to the artery compliance at a pressure of 90mmHg. The compliance of the 7 to 1 graft is almost three times that of a natural artery in the physiological range, displaying a value of 15% at 90mmHg compared to 5% at the same pressure reported for an artery and the 5 to 1 graft. Before the point where the artery and 5 to 1 grafts compliance coincide (pressure = 90mmHg), the artery is much more compliant than the graft, reaching a peak at 20mmHg reporting a compliance of about 7.5%/100mmHg, almost three times higher than the corresponding graft compliance. After the point at 90mmHg the artery compliance decreases and that of the graft increases until the graft compliance is almost 6 times higher than that of the artery.

In contrast, the 7 to 1 graft follows the same compliance path as the artery at low pressures (<20mmHg). After this point, the graft and artery compliance diverge with the graft becoming more compliant, reaching a maximum of 20%/100mmHg at a pressure of 140mmHg. After this the graft result becomes unstable due to the excessive strain.

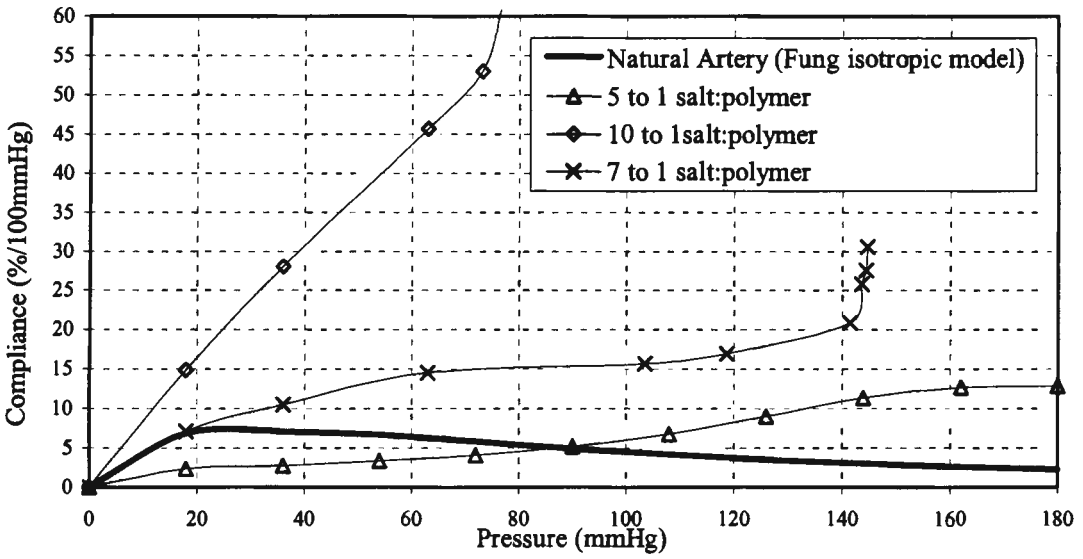

Figure 4.13 Compliance of a natural artery modelled using an isotropic version of Fung's strain energy function and different porosity grafts.

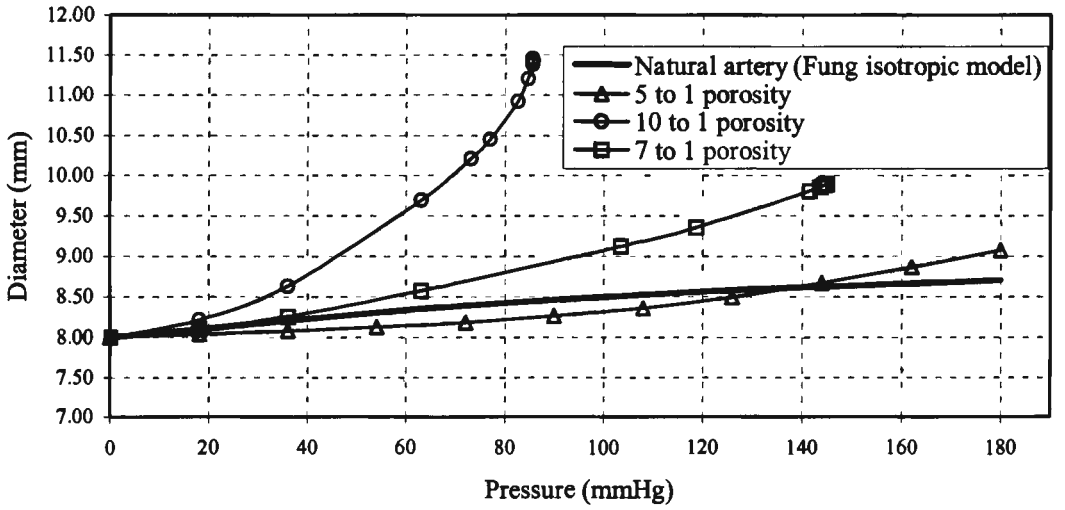

Figure 4.14 Comparison of diameter change in porous grafts compared to the natural artery (Fung model)

The most significant feature of the diameter change displayed in Figure 4.14, is the stiffening exhibited by the artery and the softening of the polyurethane grafts at higher pressures. The 7 to 1 and 10 to 1 grafts both display a sharp increase in compliance at pressures in the range of 140mmHg and 70mmHg respectively. At this point, the accurate limit of the numerical material model has been exceeded and the solution becomes unstable here (discussed in Chapter 3.).

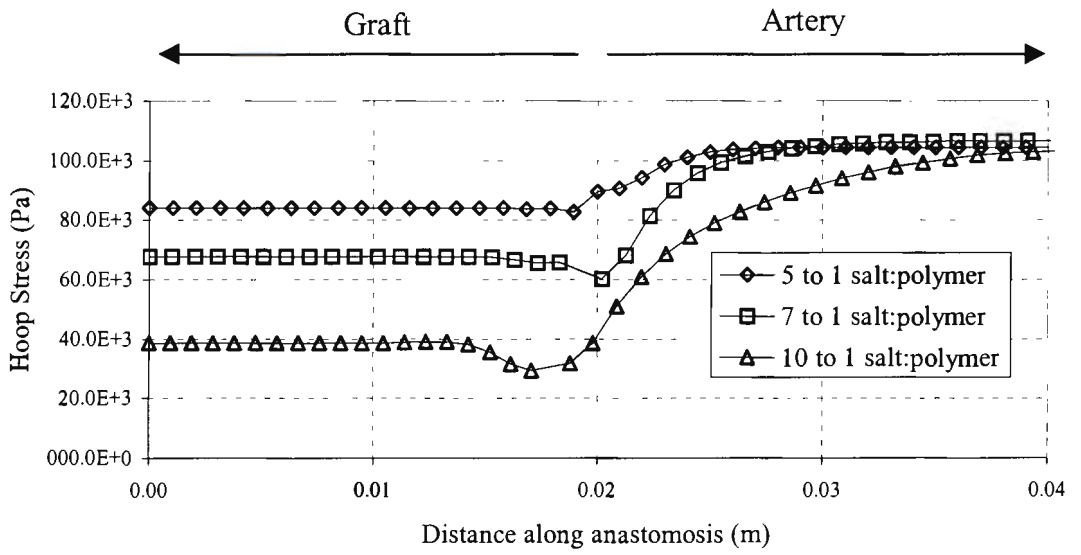

Figure 4.15 Hoop stress plotted along a path on the inner surface at the anastomosis

The hoop stress at the artery - graft anastomosis is displayed in Figure 4.15. There is discontinuity in the stress distribution across the anastomosis. This can be attributed to the difference in mechanical properties of the two materials. The artery is an incompressible material so the volume of the artery must remain constant during deformation, promoting a higher stress than that experienced by the compressible graft. The change in material properties also leads to local deformation that influences the stress distribution at the anastomosis. Chandran *et al.*, (1992) reported a similar phenomenon in their finite element analysis of an artery graft anastomosis. They found a hypercompliant zone in the artery about 0.5mm from the anastomosis. They also report a region of increased stress at the anastomosis.

The hoop stress in the 7 to 1 and 10 to 1 grafts is displayed in Figures 4.16b and 4.16c. The 10 to 1 graft dilates excessively when compared with the artery and for the purposes of matched compliance is not suitable. The 7 to 1 graft is only slightly more dilated and is still a viable option for a compliant graft with external reinforcing.

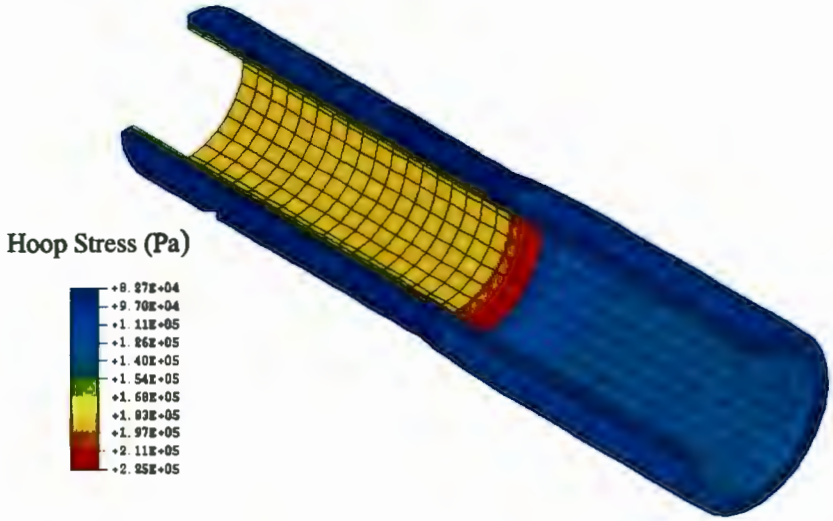

Figure 4.16 (a)

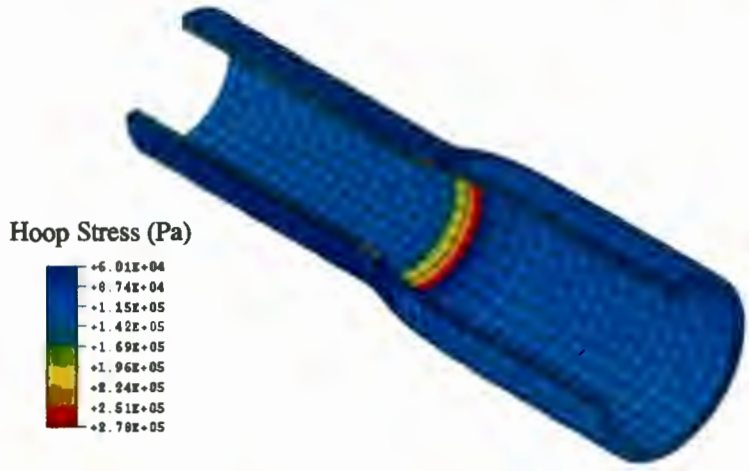

Figure 4.16 (b)

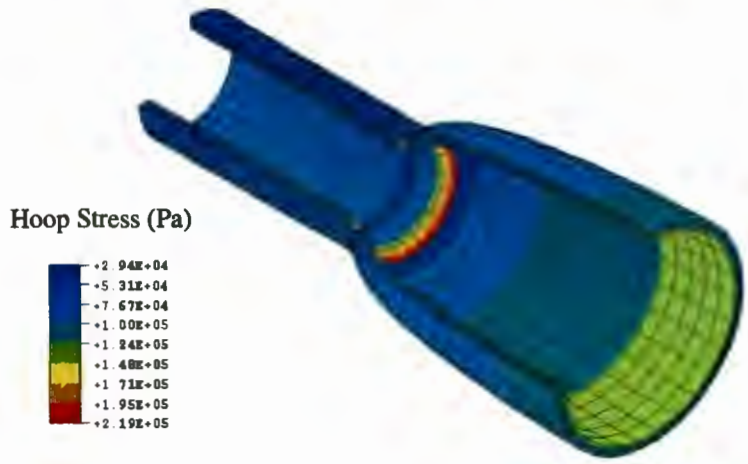

Figure 4.16 (c)

Figure 4.16 Hoop stress at the artery –graft anastomosis with: a) 5:1 graft at 180mmHg, (b) 7:1 graft at 140mmHg, (c) 10:1 graft at 90mmHg

4.5 GRAFTS WITH INTERNAL CHANNELS

A graft with a single spiral-wound internal channel is modelled as a first step in exploring the possibilities of internal channels as a design concept. The objective is to show how a channel influences the behaviour of the graft and to demonstrate the ability of numerical modelling to analyse complex graft structures.

A graft, 6mm internal diameter with a wall thickness of 1mm, is modelled with an internal spiral. The diameter of the channel is 200μm and the pitch of the spiral is 2.5°. The graft is modelled using 3-D 8-noded linear brick elements.

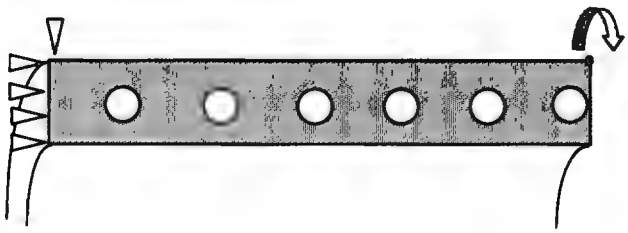

Figure 4.17 Boundary conditions on the finite element model with internal channels.

Two material porosities were investigated, each one using the hyperfoam material law described in the previous sections. The graft is constrained radially and axially at one end. The other end is constrained from rotation into the plane to enforce the symmetry boundary condition (Figure 4.17)

The effect of internal channels on the overall performance of the graft is investigated
To create grafts with an internal channel, a mandrel is coated with a layer of polyurethane and a soluble thread is wound on (Figure 4.18).

Figure 4.18 Porous polyurethane on mandrels with a soluble thread wound on.

The mandrel is then coated with a second layer of polyurethane to create the outside layer. (Figure 4.19).

Figure 4.19 A second coating of polyurethane is applied to the mandrels, covering the soluble thread.

An acid is used to dissolve the soluble thread out and an internal channel remains (Figure 4.20a,b). The finite element model compares well to these scanning electron micrographs, thus the model can be considered an accurate representation of the geometry and a reasonable result can be expected.

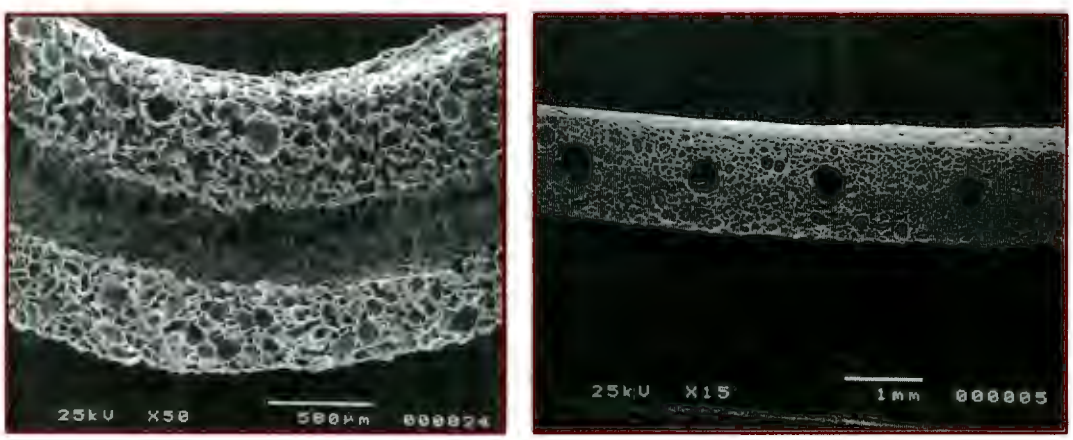

(a) **(b)**

Figure 4.20(a). Scanning electron micrograph, 50 times magnification, of a transverse cross section of the internal channel **(b)** A longitudinal section of the same graft at 15 times magnification.

Figure 4.21 is a contour plot of the axial stress in the finite element model. The stress is slightly higher in these models when compared to a graft without channels, since there is less cross sectional area in the graft wall to carry the load. The close-up detail of an

internal channel in Figures 4.22 a and b, shows the hoop and radial stress contours respectively around a channel. The channels have a minor effect on the hoop stress and a more pronounced stress concentration effect in the radial stress distribution. The radial stress is predominantly compressive throughout the thickness, with a region of tensile stress above the channel (Figure 4.22 b).

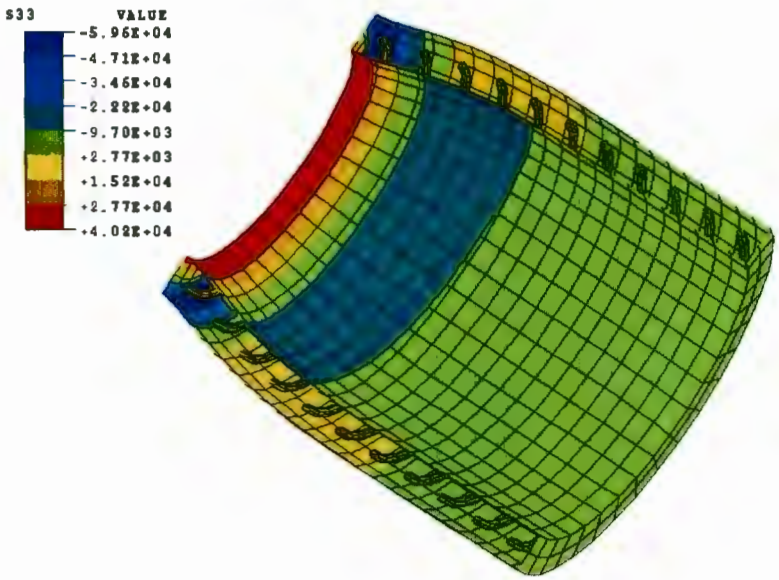

Figure 4.21 A section of a graft with internal channels showing axial stress at 100mmHg. The internal channels are clearly visible and compare well with the actual geometry.

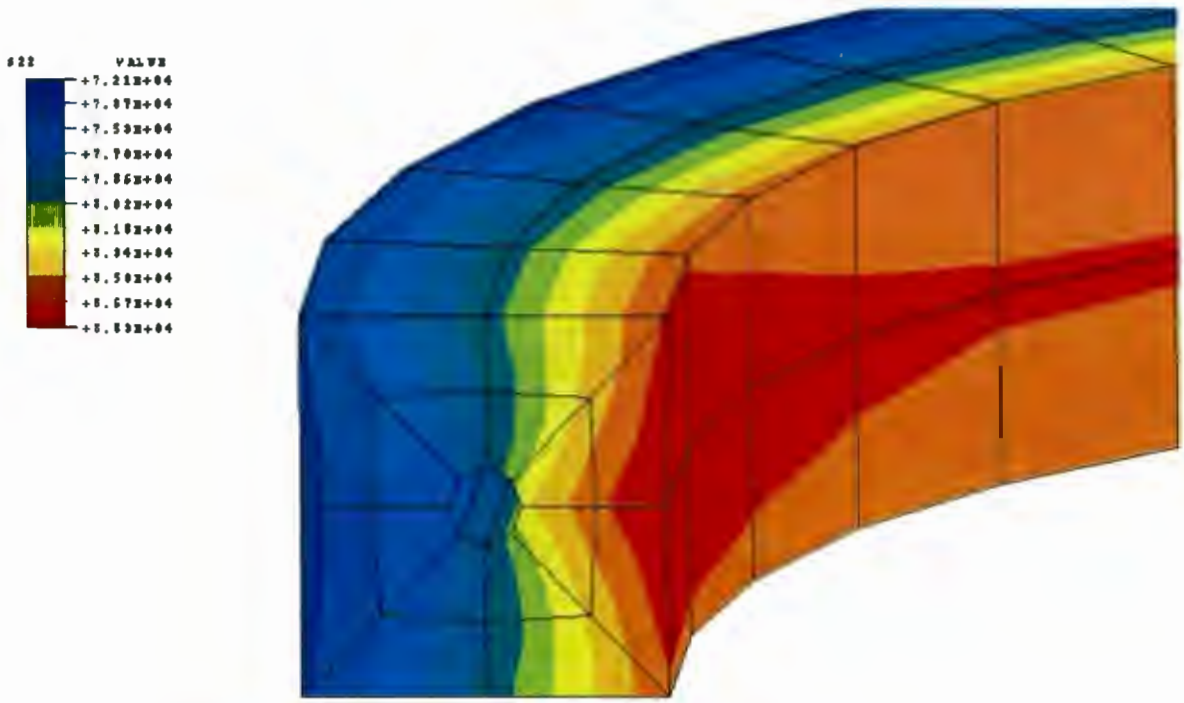

Figure 4.22(a) A detail of a channel in the finite element model, showing hoop stress at 100mmHg

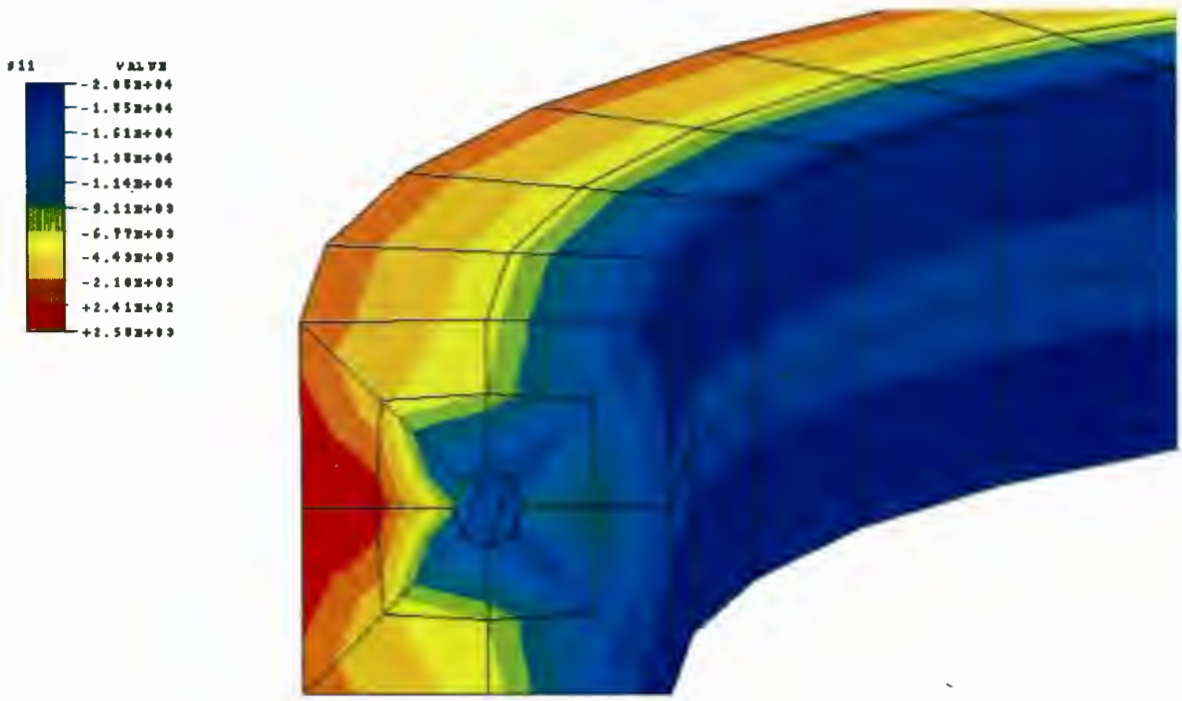

Figure 4.22(b) Radial stress distribution around a channel in the graft pressurized to 100mmHg.

The change in diameter is naturally affected by the inclusion of internal channels since the material is effectively more porous and hence not as strong (Figure 4.23). This has a direct influence on the compliance, which is increased by the inclusion of channels (Figure 4.24). The difference is more visible in the 7:1 porosity graft than the 5:1 graft, showing a compliance that is approximately 50% greater after a pressure of around 25mmHg. The solution becomes unstable after the 7:1 graft has reached a diameter of 10mm and the 5:1 graft 9mm.

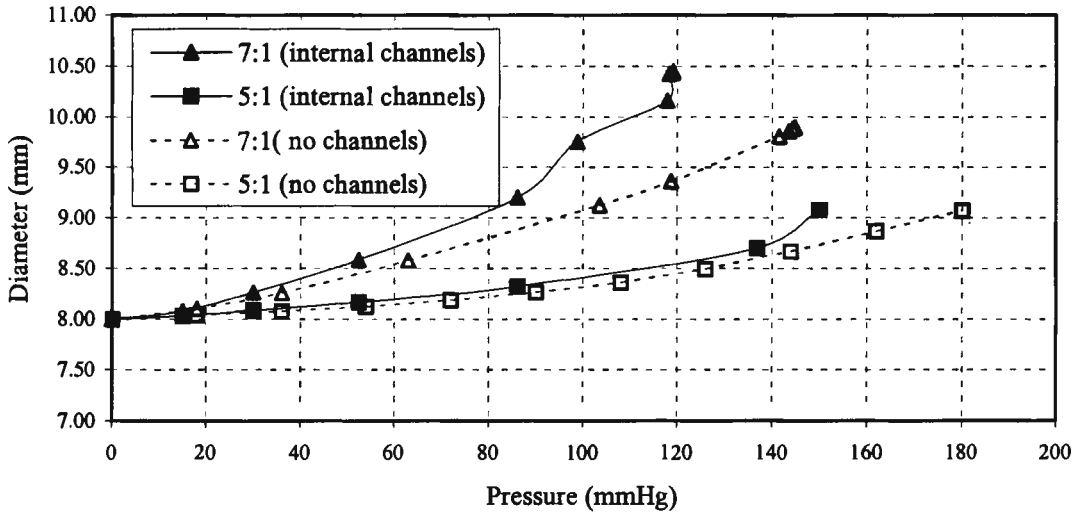

Figure 4.23 The effect of internal channels on the change in diameter for different porosity material.

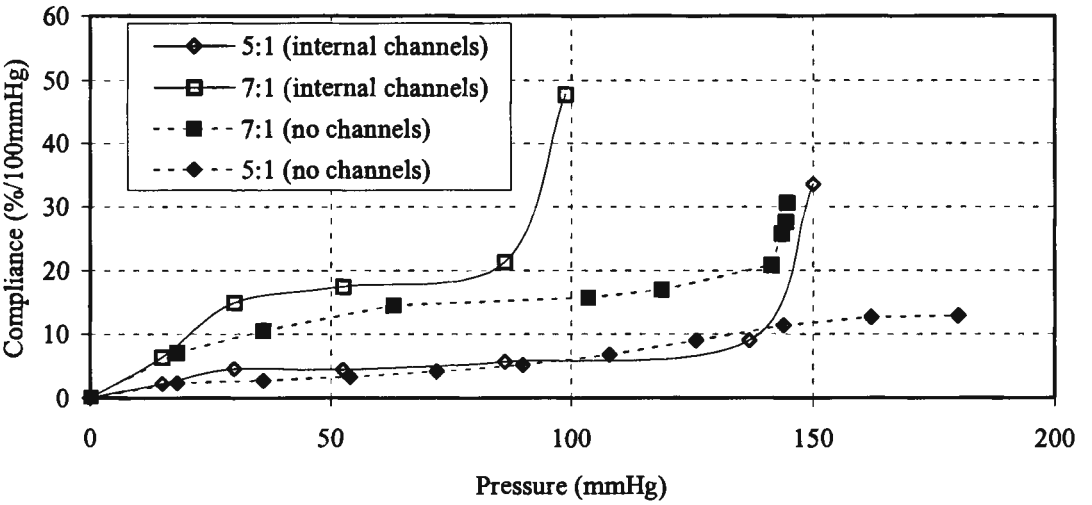

Figure 4.24 Effect of internal channels on compliance for different porosity material.

4.6 Numerical Modelling of Grafts with Spiral Reinforcing

It has been shown that initial compliance can be achieved with a plain porous graft, but in the long term, the viscoelastic effect of the material will predominate and the graft will creep to unacceptable dimensions. One way to overcome this is to use an external winding that prevents the graft from over dilating. The problem is that some compliance is sacrificed due to the stiff nature of the reinforcing. It is thus necessary to investigate the nature of such a wind and to evaluate the effect of parameters such as the diameter of the wind, the wind angle and the wall thickness of the graft. By varying these properties, a compromise can be reached that preserves a certain degree of compliance, while providing the structural support necessary for high loads and long term behaviour.

4.6.1 Numerical Modelling

Grafts with an internal diameter of 6mm and wall thickness of 0.8mm and 1.0mm are modelled. The grafts are modelled using 3D, 8 noded linear brick incompatible mode elements. The incompatible mode option is used since these elements incorporate an enhanced strain formulation that allows for better bending in the elements, resulting in a continuous solution over the element. This is useful where the material bulges out from between the reinforcing spirals.

To model the reinforcement in ABAQUS, a FORTRAN program was written to generate a spiral of truss elements. The input variables of the program include spiral wind diameter, graft diameter, pitch angle, length of the graft and the number and direction of spiral winds. The program then generates the nodes and elements for a spiral wind with the desired parameters and the associated material properties. With this data, the program can generate a number of combinations of spiral reinforcing. The elements used are quadratic truss elements that act only in tension and have the elastic properties of solid polyurethane calculated as a secant modulus of the initial stress-strain behaviour. The problem with truss elements is that they cannot be modelled as hyperelastic in ABAQUS, and cannot be modelled as viscoelastic. However, since the reinforcing is so much stiffer than the graft, the strains experienced by the reinforcing are small and it is assumed that the material will remain mostly linear elastic in behaviour. These truss elements are tied to the surface of the tube, simulating the bonding that occurs between the reinforcing and the tube during manufacture.

The grafts are constrained axially to simulate the *in vivo* conditions and to enforce symmetry i.e. the graft is attached to an artery at either end. The ends are not constrained radially since the graft is expected to expand with the artery. The reinforcing winds are constrained at their ends by a circumferential and axial boundary condition. They are also constrained from rotation in the plane to ensure a symmetric boundary. The graft material

porosity was chosen to be 7 to 1, so that the initial compliance was higher than that of an artery since it is expected that the spiral winds will reduce the compliance. The reinforcing wind is modelled as solid polyurethane with an initial diameter of 100μm.

4.6.2 Results and Discussion

Figure 4.25 shows a graft with a single reinforcing wind, pressurised to 120mmHg. The single helix produces a twisting motion in the graft due to the spiral unwinding as it is forced to expand by the internal pressure. The unwinding effect can clearly be seen here. The graft tends to open up as it unwinds, at the same time twisting the artery to which it is attached. This cyclic twisting motion that would be produced with every pulse will lead to fatigue failure. It is therefor necessary to have two or more winds that have alternating orientations to produce a symmetrical deformation in the graft and prevent the unwinding effect.

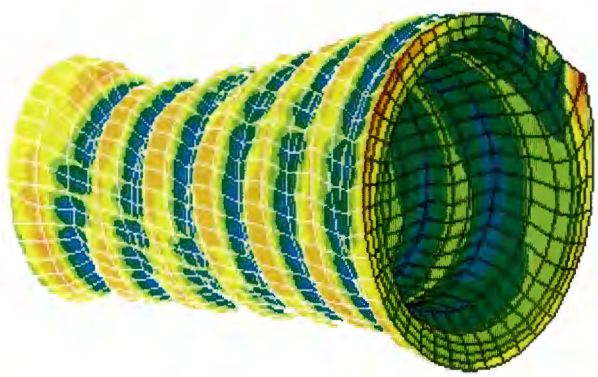

Figure 4.25 Single reinforcing wind at 120mmHg showing a tendency to unwind.

The following figures (Figure 26a,b,c) show the hoop stress and appearance of grafts pressurised to 120mmHg (16kPa) with three different wind angles and thickness.
From the figures, it is apparent that a "loose" wind angle is not ideal because of the excessive bulging of the material between the winds. This is a likely point for failure due to the exaggerated hoop stress produced by the bulging. In the other extreme, the tight wind angle of 5° has over constrained the graft, reducing the compliance dramatically

The maximum hoop stresses occur in the regions of bulging between the spiral winds. The peak stress reported is around 40kPa and is reported in the 15° wind angle. The highest stress reported in the 10° wind angle is around 25kPa. The peak stress in the 5° wind angle model is 3kPa. The peak stresses are lower in the grafts with a steeper wind angle. A steeper wind angle results in more wind material and consequentially more of the stress being absorbed by the stiffer material. These stresses are very much lower than those reported for the un-reinforced grafts. The highest hoop stresses in those models is around 80kPa. Thus, even in the 15° wind, the hoop stress is approximately half. This can also be attributed to the fact that the load is carried in proportion to the moduli of the materials.

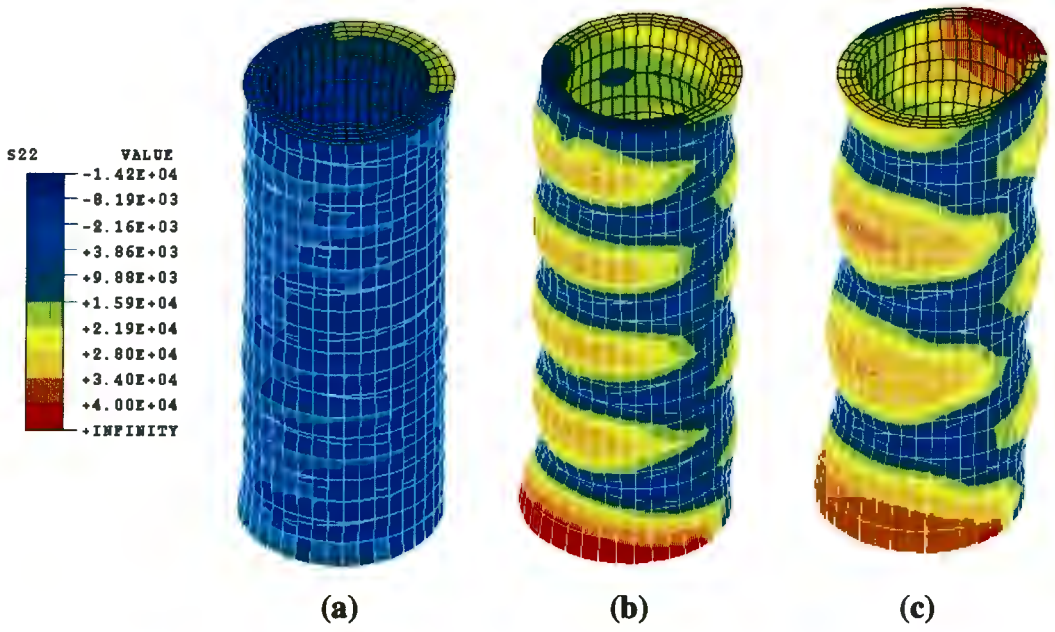

Figure 4.26 Comparison of hoop stress in three reinforced grafts. Wall thickness - 8mm, diameter of reinforcing - 100μm, wind angle (a) 5° , (b) 10° , (c) 15°

Since the reinforcing is so much stiffer than the graft material, the graft takes on an undulating appearance. The compliance of the externally reinforced grafts is measured as the change in diameter between a point where the reinforcing makes contact on the graft surface and a point on the wall directly opposite (Figure 4.27), so that the compliance is taken at the effective flow area. It is pointless to consider the widest part of the graft since it is not a true indication of the diameter change of the graft.

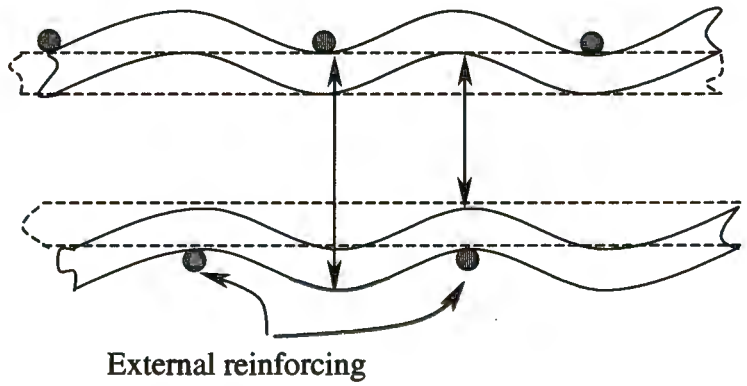

Figure 4.27 Change in diameter taken at the furthest distance from a spiral reinforcing wind.

Figure 4.28 shows a graph of diameter for externally reinforced grafts with wall thickness of 0.8mm and 1mm, with a material porosity of 7 to 1. The spiral reinforcing is 100μm diameter and has material properties of the solid polyurethane. The grafts were pressurised to 150mmHg. Again, a 5° wind over constrains the graft, no matter how thick the wall is.

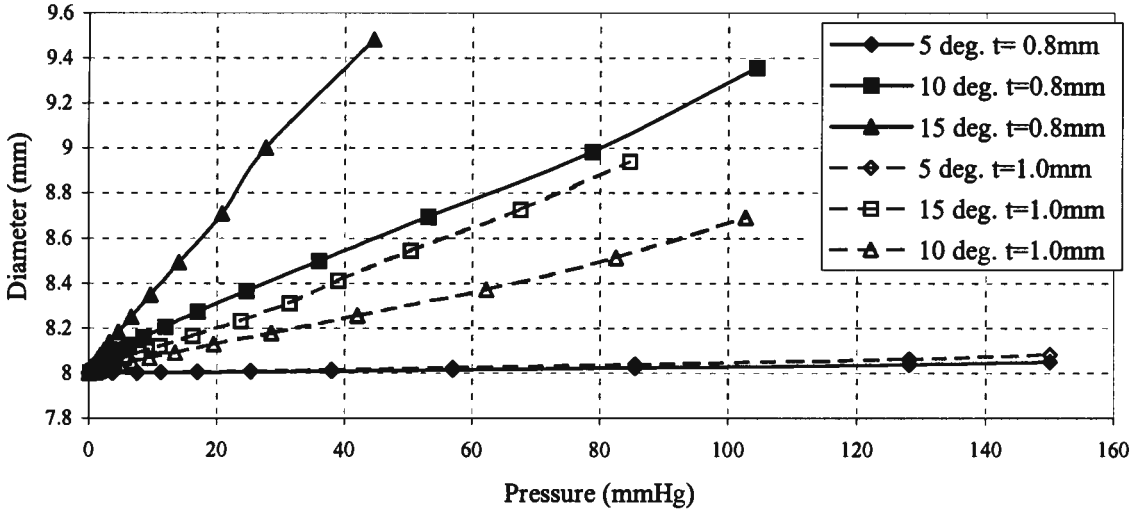

Figure 4.28 Comparison of diameter change in grafts with a 1.0mm and 0.8mm thick walls and different reinforcing wind angles.

The compliance of a graft with a wind angle of 5° produces a very stiff, un-compliant structure, independent of the wall thickness or material porosity. The close wind angle means that there are more winds over the length of the graft and therefore more stiff material to absorb the load (Figures 4.29 and 4.30). Since the load is distributed amongst the compliant and stiff materials in proportion, the reinforcing carries the majority of the load and the graft is consequently un-compliant. At the other extreme, a wind angle of 15° allows too much deformation between the winds and the grafts are thus over compliant. The compliance of the 0.8mm graft with 10° and 15° wind angles is higher

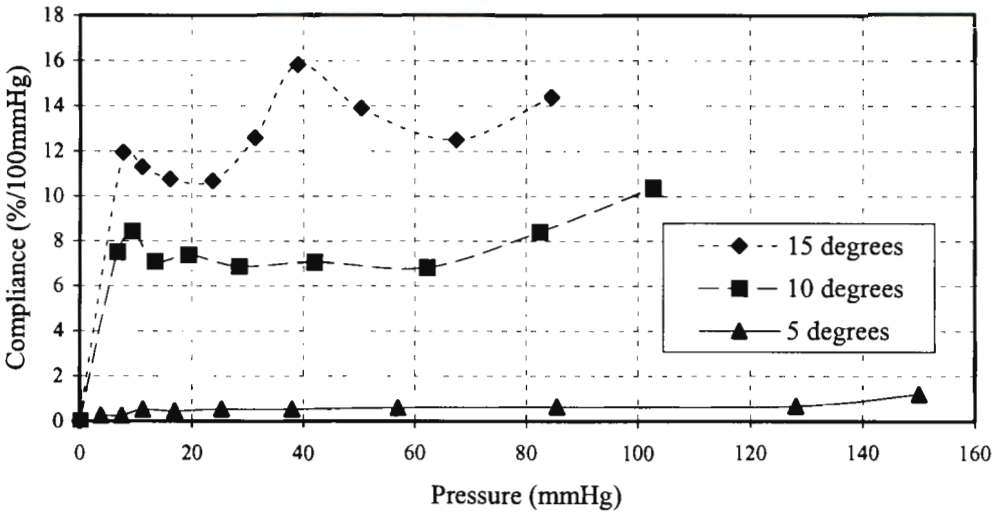

Figure 4.29 Compliance of reinforced graft with a wall thickness of 1.0mm and 100μm diameter reinforcing winds at different pitch angles.

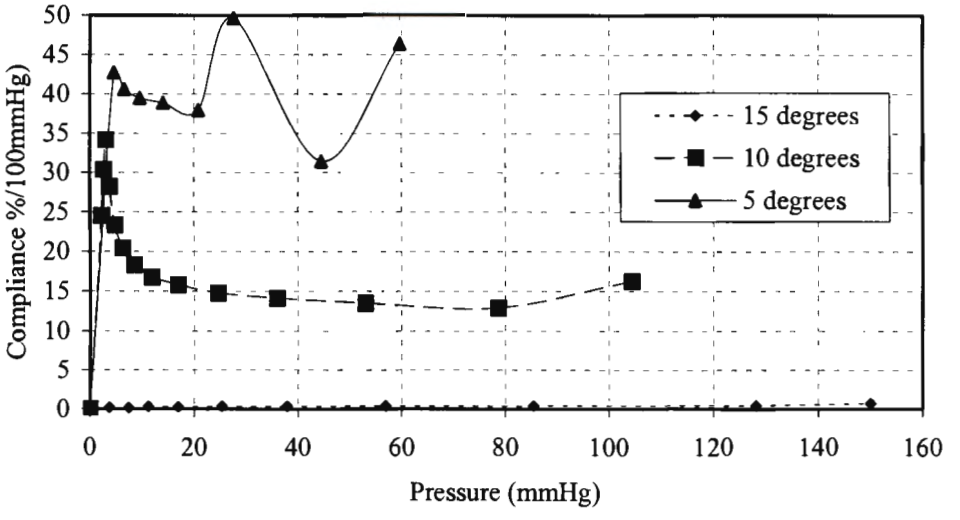

Figure 4.30 Compliance of reinforced graft with a wall thickness of 0.8mm and 100μm diameter reinforcing winds at different pitch angles.

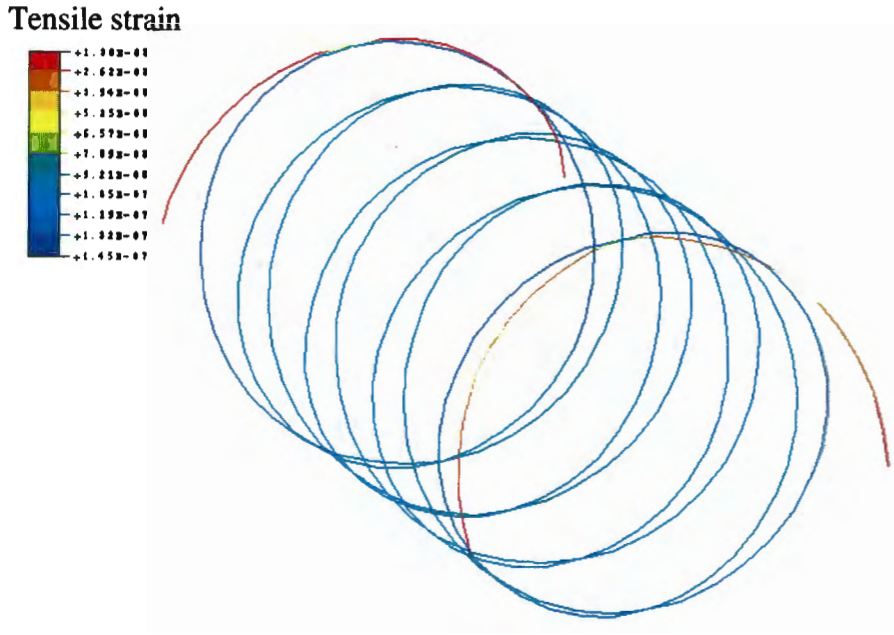

Figure 4.31 Detail of the spiral reinforcing showing tensile stress in 100μm winds at a 10° pitch angle.

The tensile strain in the spiral reinforcing on a 7:1 porosity graft with a 1.0mm wall thickness and a 10° wind angle is shown in Figure 4.31. The maximum strain in the material is around 1.0E-7, which is very, very small. The reinforcing is 100μm diameter and has hardly distended under a pressure of 120mmHg. This indicates that the material is not at all compliant and would have to be very much thinner if it was to maintain any compliance.

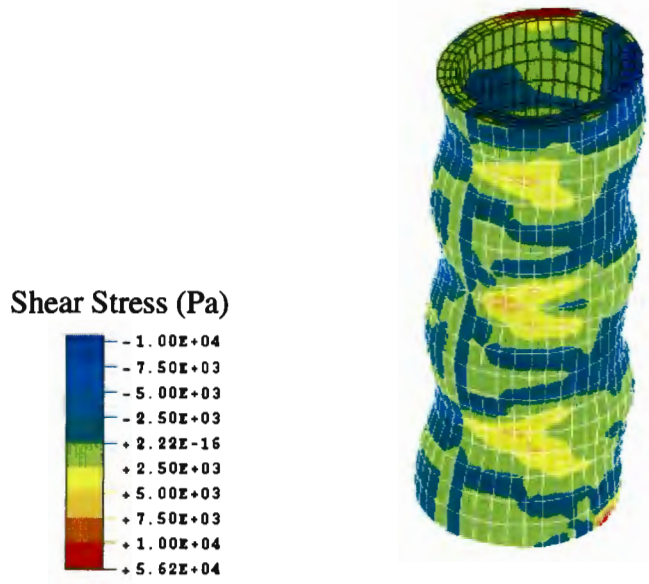

Figure 4.32 Shear stress ($\sigma_{r\theta}$) on a 1.0mm thick 7:1 graft with a 15° reinforcing wind.

The shear stress in the material is important since the creep response of the material is based the shear modulus. Figure 4.32 displays a contour plot of the shear stress in a graft with 1mm wall thickness, 7:1 porosity and 15° wind angle with an internal pressure of 130mmHg. The peak values at the ends are caused by the boundary condition at the reinforcing winds. Stress concentrations also appear on the surface at the point where the windings cross over each other. Bands of higher stress are associated with the elements closest to the reinforcing wind. The shear stress here is around 5kPa.

4.7 LONG-TERM BEHAVIOUR

The viscoelastic model was applied to the 3-D models with spiral reinforcing to examine the influence the windings have on the "creep" response of the material. The grafts are 6mm internal diameter, 1mm thick, with 100μm diameter spiral reinforcing winds at 5 and 10°. The axi-symmetric model with creep is also included here for comparison. All the grafts were modelled as 7:1 porous material. The grafts were pressurised to a constant load of 100mmHg and were constrained in the axial direction. Truss elements cannot be modelled as viscoelastic in ABAQUS. These models are thus a simplification since the reinforcing material is definitely viscoelastic. They do however give an indication as to what would happen if a purely elastic material were used for reinforcing.

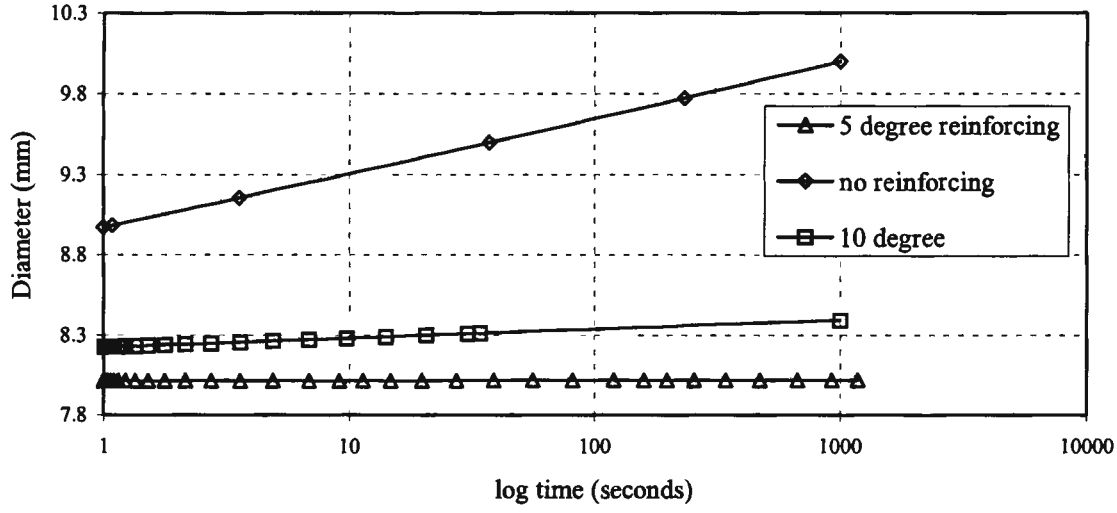

Figure 4.33 "Creep" response of reinforced grafts.

The solution of models with reinforcing at 5° and 10° became unstable after around 40 seconds due to the large strains induced by the bulges. In order to continue the creep prediction, a curve was fitted to the early result from the model. Using this curve, a point was extrapolated for a time of 1000 seconds. Figure 4.33 plots the diameter against time for the three different models. The un-reinforced axi-symmetric model "creeps" the most and reaches a displacement of 10mm after 1000 seconds (16.67 minutes), an increase in diameter of 1.1mm or 13.7%. The effect of the reinforcing is noticeable in the 10 and 5

reinforcing wind angle. The "creep" is much more gradual and almost completely eliminated in the 5° model. This indicates a very stiff graft with almost no compliance at all.

The graph shows that there is a compromise between the amount of reinforcing needed to prevent creep while still maintaining compliance. Figure 4.34 shows the hoop stress in the graft reinforced with 5° winds after 80 000 seconds. The graft has not deformed much except for the slight bulging between the winds. The stress is in the region of 3kPa, which is very low.

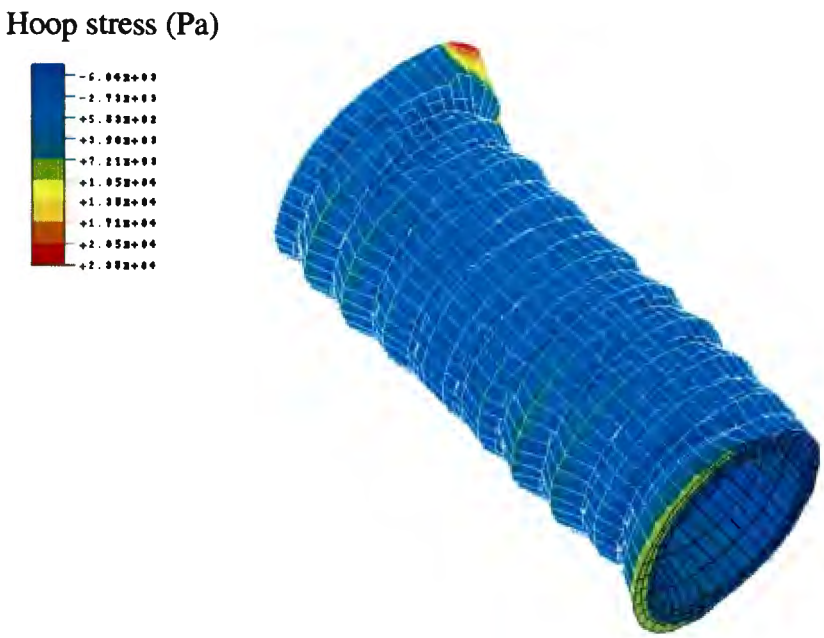

Figure 4.34 Hoop stress in a graft with 5° reinforcing after 80 000 seconds (22 hours).

CHAPTER FIVE

DISCUSSION AND CONCLUSIONS

Significant progress has been made over the past 15 years in the development of vascular grafts. Some of this progress is attributable to the introduction of new bio-stable materials such as ether-free polyurethane elastomers. These materials are well known to the cardiovascular industry where much of their success lies in their excellent blood compatibility, strength, performance and ease of manufacture. However, the development of a cardiovascular implant requires careful assessment of the material properties in order to establish the suitability of the chosen material for the proposed application. The mechanical response of the material will arise from the chemical composition, as well as from the structural characteristics such as porosity and microstructure. Typically the constituency of polymeric materials gives rise to properties such as non-linearity, anisotropy, hyper-elasticity and viscoelasticity. Once the material properties have been adequately characterised, a host of design issues can be addressed by making use of sound numerical methods. These issues include important mechanical characteristics necessary for the development of a successful artery graft, such as compliance matching, long-term dilation, and ultimate failure.

Numerical modelling provides a means for addressing the design issues of a vascular graft. With sound material laws, modelling can aid the design process by allowing the designer to investigate these issues conveniently and with limited prototyping. Furthermore, it is often difficult, if not impossible, to accurately measure quantities such as stress and strain or displacement in experimental models. These quantities are however readily available from numerical models. While numerical modelling can aid the design process, this type of analysis needs to be seen as part of the overall design process.

The work outlined in this report details the material characterisation of a bio-stable polyurethane for use in the fabrication of a small diameter vascular prosthesis. A suitable constitutive law is outlined and implemented in finite element models for the analysis of basic graft designs. These models are extended to examine other more sophisticated graft designs that involve concepts such as internal channels and external reinforcing spirals.

As a consequence of the large displacements that take place in the vessel wall during normal loading, large strain theory is necessary for the description of the deformation

encountered in polyurethane and soft tissue. The material behaviour of both materials is highly non-linear and can best be described by a strain energy function. In Chapter Three, forms of strain energy function used previously by investigators such as Fung, Vaishnav and Hyashi were reviewed. Polyurethanes and soft tissues exhibit time dependant behaviour, which is sensitive to temperature. A polyurethane elastomer has been characterised and implemented in a finite element code using a large strain, compressible hyperelastic material model with viscoelasticity. The mechanical constants in the material model were determined from tensile, simple-shear and viscoelastic material tests.

The numerical formulation of the graft material has been validated by modelling tensile, simple-shear and viscoelastic tests using a single element and comparing the results to those obtained from physical tests (Chapter Three). The models were found to be accurate for loading conditions in the physiological range where a good correlation between experimental and numerical results was reported. However, there were limitations where the finite element solution became unstable at very large strains due to a poor fit to the material data. This was found even using the highest order formulation of the hyperelastic material model available in the finite element code (i.e. using the maximum of six terms in the Ogden hyperfoam material model). The model was found to be accurate up to 40% strain in tension and 65% strain in shear. The single element viscoelastic test showed a very close correlation to the experimental data from physical testing. The normalised shear compliance predicted in the single element test compared very favourably with experimental results, with an error of around 3% after 200 seconds.

Finite element (FE) models were used to predict the performance of various graft structures in Chapter Four, where an axi-symmetric FE model and an *in vitro* experiment are compared and an FE model of an artery-graft anastomosis is analysed. Values for the change in diameter and pressure were recorded and the corresponding compliance and displacements were calculated and found to be accurate in the physiological pressure range for two models with different boundary conditions. The results confirm that, although there is a fairly wide scatter in the experimental results, the finite element result represents the trend of the data accurately. This finding indicates that the scope of the test data used to characterise the material was sufficient to predict a mean range of material response that allows for any minor defects incurred in the graft production process. The viscoelastic material behaviour was accurately modelled for an axi-symmetric load case where a very good correlation was reported with errors of between 7% and 10% compared with the results of the *in vitro* creep test.

The analyses of the artery–graft anastomosis indicate that initial compliance is achievable using the material with a porosity of 5:1. The material displayed a compliance of approximately 5%/100mmHg, equal to the artery compliance at a pressure of 90mmHg. A

feature of the artery not represented by the graft is the increased stiffening of the artery at higher pressures. This feature is produced by the recruitment of collagen fibres in the adventitia at high strains (Chapter One). The graft does not display this behaviour since no external reinforcing was modelled here. The other salt:polymer ratios investigated (the 7:1 and 10:1 materials) are hypercompliant in the physiological pressure range and thus, without modification, these materials are unsatisfactory for use in the manufacture of artery prostheses. These models did not include any viscoelastic effects and are thus simplified elastic representations of the material. The axi-symmetric models discussed earlier were used to analyse a graft including viscoelastic effects and show how the graft creeps and expands with time. External reinforcing was investigated as a means to stem the creep and provide the graft with structural support and increased stiffness at high strains.

In the case of over-compliant grafts and for grafts that experience retarded elastic behaviour (creep), external reinforcing can be introduced to reduce the compliance and stem the creep. The results presented in Chapter Four emphasise some important characteristics of reinforced grafts: Firstly, a single wind is unsatisfactory due to the unwinding effect it produces. Secondly, the reinforcing material is very stiff compared to the porous material of the graft (maximum strain reported in the reinforcing at 120kPa was 1.0E-7). This occurred at a reinforcing diameter of 100μm, which implies that the reinforcing has to be even thinner or there must be very few reinforcing winds to ensure an acceptable compliance. So compliance is achievable using fewer winds. But using fewer reinforcing winds creates an undulating graft. Since the objective is to create a vessel similar to an artery, this undulating effect is not desired. The bulges that appear in the graft, due to the reinforcing winds, are points of localised shear and hoop stress that will lead to excessive dilation. This effect will be magnified if the material creeps and may also initiate localised fatigue failure. The reinforcing also creates an uneven flow surface in the models when the wind angle is large (10°–15°), which creates large disturbances in the local haemodynamics. Corrugations and surface roughness are both undesirable features that add to the formation of a fibrous build up (Sauvage *et al.*, 1974). A finely spun material would provide a better overall reinforcing, creating a more even, less undulating graft.

Viscoelastic effects in a graft with and without external reinforcing were analysed. The un-reinforced graft displayed an increase in diameter of 1.1mm after 1000 seconds (16.67 minutes). This corresponds to an increase of 13.7%. With external reinforcing spirally wound at a pitch angle of 10°, the graft is initially noticeably stiffer and the diameter has not increased by more than 4% after 1000 seconds.

Internal channels were modelled in a graft and found not to affect the hoop stresses in the wall dramatically and have the effect of increasing the overall graft compliance. The model with internal channels is a simple approach that demonstrates the influence of geometry on compliance. Further development of this type of model can be used to analyse more complicated designs such as those mentioned in Chapter Three, where the graft porosity is entirely created by internal channels in a solid polyurethane tube. These models can provide an insight to the development of strain sensitive biological cells in the channels by examining the stress distribution around the channel. They also show how versatile and useful the finite element method is in designing complex structures.

There may be many biological advantages for using this particular polyurethane for the manufacture of artery prostheses, but on a mechanical level, the material has some limitations. At the porosity necessary for a compliant, normal size graft, the material lacks the structural strength. Although the material is well within its limits for physiological conditions, at elevated pressures, such as those that may be encountered in a hypertensive patient, the material is too close to its ultimate failure strength for safe operation. This is unacceptable since ultimately the graft should be stable under any applied loading condition and should in fact be over designed rather than on the design limit for its application. This is even more evident in the case where the material bulges out from between the reinforcing spirals. The stress concentration due to these bulges, which will worsen with the cyclic loading, may lead to fatigue failure.

In addition, most segmented polyurethanes are highly viscoelastic and display retarded elastic response (creep) to loading. From the viscoelastic test results (Chapter Three) the material clearly displays significant time dependant behaviour. The fact that this material shows any sign of creep limits its usefulness as a graft material. In Chapter Four, an un-reinforced graft is shown to creep at a steady rate. In previous cases where the material has displayed similar creep characteristics (i.e. Teflon), the solution has been to reinforce the tube with a cross-linked (no creep) material such as Dacron (eg. Hyashi *et al.* 1989). This prevents the material from over dilation in the long term by carrying most of the load in the reinforcing, thereby reducing the amount of strain in the graft material. The effect reinforcing has on the creep is demonstrated in Chapter Four where a graft with 5° reinforcing winds hardly displays any creep displacement after 22 hours. Although the creep has been significantly reduced, the compliance is very poor due to the added stiffness provided by the reinforcing winds.
If the reinforcing is much stiffer than the graft material the reinforcing will govern the overall compliance of the vessel. Thus, the reinforcing material must have a similar compliance to the graft material and cannot be viscoelastic.

To this end, reinforcing could be more effectively used if it was applied as a reinforcing against excessive distension as opposed to a prevention of creep. Much like the collagen fibres in the adventitia of a natural artery, loose bundles of reinforcing attached to the surface of the graft would become active only once the graft has distended beyond a certain critical amount (Gupta *et al.*, 1997). The bundles of reinforcing would align themselves and provide the stiffening necessary to prevent excessive dilation in the vessel at high strains.

Using the finite element method as a design tool, many different graft geometries can be modelled using a wide variety of material properties. The time and cost of prototyping can be significantly reduced and new designs can be formulated and validated. By coupling the FE model to a cell growth algorithm, (Beattie *et al.*, 1995), the proliferation of cell evolution in the wall could be predicted. If the material properties of the cell ingrowth were known, then it would be possible to predict the graft behaviour *in vitro*. This would be useful in the prediction of long term compliance.

In this work, several important graft design issues have been successfully examined. It was shown that numerical analysis provides meaningful insight to aid the graft design process. A polyurethane elastomer was sufficiently tested and characterised for numerical analysis. From this data, a compressible hyperelastic material model with viscoelasticity was successfully implemented in the finite element code. Results show that there is a good correlation between analytical models and physical experiments. An artery–graft anastomosis was modelled using an incompressible isotropic hyperelastic material model for the artery. This approximation gives a reasonable indication to the interaction between artery and graft regarding compliance. Some more complex design concepts incorporating an internal channel structure and external reinforcing were also modelled. The inclusion of viscoelastic effects in the numerical model shows that the polyurethane analysed in this work displays a significant propensity to creep, which would affect the long-term behaviour of a graft. Reinforcing does restrict the creep, but also increases the graft stiffness, thus reducing the compliance. The results show that compliance is achievable using a porous version of the polyurethane, but this is lost with the inclusion of external reinforcing.

REFERENCES

1. Annis D, Bornat A, Edwards RO, Higham A, Loveday B, Wilson J, An elastomeric vascular prosthesis, *Trans.Am.Soc.Artif.Intern.Organs* ,**XXIV**, 1978
2. AAMI Standard, Cardiovascular implants – Vascular prostheses, *American National Standard, Assoc. for the Advancement of Med. Instrumentation* 1994
3. Baird R N, Kidson I G, L'Italien G J, Abbott W M, Dynamic compliance of arterial grafts, *Am. J. Physiol.*, **233**, H568-H572, 1977
4. Baker LD, Impragraft (expanded PTFE) early clinical results, in Vascular Grafts edited by Sawyer PN, Kaplitt MJ, *Appleton-Century-Crofts, New York* ch.**32**, 349-358, 1978
5. Ballyk P D, Ojha M, Walsh C and Butany J, Suture-induced intramural stresses and intimal hyperplasia, *Advances in Bioengineering*, **ASME BED-Vol 33**, 213-214, 1996
6. Ballyk P D, Walsh C, Ojha M, Effect of intimal thickening on the stress distribution of an end-to-side graft-artery junction, *Advances in Bioengineering*, **ASME BED-Vol 31**, 327-328, 1995
7. Ballyk P D, Ojha M, Walsh C, Butany J, Suture induced intramural stresses and intimal hyperplasia, *Advances in Bioengineering*, **ASME BED-Vol. 33**, 213-214, 1996
8. Beattie DK, Vito RP, Xu C, Determination of stresses and strains in heterogeneous, diseased human aorta, *Advances in Bioengineering*, **ASME BED-Vol. 33**, 215-216, 1996
9. Burkel W, The challenge of small diameter vascular grafts, *Medical progress through technology*, **14**, 165-175, 1988
10. Campbell CD, Brooks DH, Bahnson HT, Expanded microporous PTFE (Gore Tex) as a vascular graft, in Vascular Grafts edited by Sawyer PN, Kaplitt MJ, *Appleton-Century-Crofts, New York* ch.**31**, 335-348, 1978
11. Carmines D V, McElhaney J H, Stack R, A piece-wise non-linear elastic stress expression of human and pig coronary arteries tested *in vitro*, *J. Biomech.*, **24**, 899-906, 1991
12. Chandran K B, Gao D, Han G, Baraniewski H, Corson J D, Finite element analysis of arterial anastomoses with vein, Dacron and PTFE grafts, *Medical and Biological Engineering and Computing*, **30**, 413-418, 1992
13. Christensen R M, Theory of Viscoelasticity: An Introduction, *Academic Press*, 1971
14. Chuong C J and Fung Y C, Compressibility and constitutive equations of arterial wall in radial compression experiments, *J. Biomech.*, **17**, 35-50, 1984

15. Chuong C J and Fung Y C, On residual stresses in arteries, *J. Biomech. Eng.*, **108**, 189-192, 1986

16. Crisfield, M A, Non-linear Finite Element Analysis of Solids and Structures, **vol. 2** Advanced Topics, John Wiley and Sons, NY, 1997

17. Decraemer W F, Maes M A, Van Huyes V J, Van Peperstraete P, A non-linear viscoelastic constitutive equation for soft biological tissues, *J. Biomech.* **13**, 559-564 , 1980

18. Dehoff P H, On the nonlinear viscoelastic behaviour of soft biological tissues, *J. Biomech.*, **11**, 35-40, 1978

19. Demiray H, A quasi-linear constitutive relation for arterial wall materials, *J. Biomech.*, **29**, 1011-1014, 1996

20. Deweese J A, Anastomotic neointimal fibrous hyperplasia. In *Complications in vascular surgery*, 2nd edition, 157-170, Grune and Stratton, Orlando,1985

21. De Cooman R, Vandeweerdt P, Berghmans H, Koningsveld R, Solution spinning of fibres with oriented porosity, *J. Appl. Pol. Science*, **60**, 1127-1135, 1996

22. Van Dijk A M, Vascular single smooth muscle cells and whole tissue. Mechanical properties and response of stimuli. PhD thesis, University of Leiden, Netherlands, 1983

23. Doi K, Nakayama Y, Matsuda T, Novel compliant and tissue permeable microporous polyurethane vascular prosthesis fabricated using an excimer laser technique, *J. Biomed. Mat. Research,* **31**, 27-33, 1996

24. Edwards A and Carson RJ, Bowald S, Quist WC, Development of a microporous compliant small bore vascular graft, *J. Biomat. Applications*, **10**, October 1995

25. Flemma RJ, Mullen DC, Leply D, Artocoronary vein bypass grafting, in Vascular Grafts edited by Sawyer PN, Kaplitt MJ, *Appleton-Century-Crofts, New York* ch.**33**, 369-371, 1978

26. Ferry J D, Viscoelastic properties of polymers, *Wiley, New York*, 1961

27. Fry D L, Acute vascular endothelial changes associated with increased blood velocity gradients, *Circ. Res.*, **22**, 165-197, 1968

28. Fung Y C, Stress-strain history relations of soft tissues in simple elongation. Biomechanics, its foundations and objectives (Edited by Fung Y C, Perrone N, and Anliker M), Prentice-Hall, Englewood Cliffs, New York, 1972

29. Fung Y C and Liu S Q, Strain distribution in small blood vessels with zero stress state taken into consideration, *Am. J. Physiol.*, **264**, H544-H552, 1992

30. Fung Y C, Fronek K, Patitucci P, Pseudoelasticity of arteries and the choice of its mathematical expression, *Am. J. Physiol.*, **237**, H620-H631, 1979

31. Fung, Biomechanics: Circulation 2nd Edition, *Springer*,1996

32. Fung, Biomechanics: Mechanical properties of living tissue 2nd Edition, *Springer*,1993
33. Gibson L J and Ashby M F, Cellular solids: Structure and properties, Pergamon Press, 1988
34. Greenwald S E, Newman D L, Denyer H T, Effect of smooth muscle activity on the static and dynamic elastic propertries of the rabbit carotid artery., *Cardiovasc. Res.*, **16**, 86-94, 1982
35. Gow B S and Taylor M G, Measurement of viscoelastic properties of arteries in the living dog, *Circ. Res.*, **23**, 111 - 122, 1968
36. Greenwald S E, Rachev A, Moore J E, Meister J J, The contribution of the structural components of the arterial wall to residual strain, *Advances in Bioengineering*, **ASME BED-Vol 28**, 63-64, 1994
37. Greer L S, Vito R P, Nerem R M, Material property testing of a collage-smooth muscle cell lattice for the construction of a bioartificial vascular graft, *Advances in Bioengineering*, **ASME BED-Vol 28**, 69-70, 1994
38. Hasson J E, Megerman J, Abbott W A, Increased compliance near vascular anastomosis, *J. Vasc. Surg.*, **2**, 419 - 423, 1985
39. Haut R C and Little R W, A constitutive equation for collagen fibres, *J. Biomech.* **5**, 423-430, 1972
40. Hayashi K, Elastic properties and strength of a novel small-diameter compliant polyurethane vascular graft, *J. Biomed. Mater. Res.*, **23**, 229-244, 1989
41. Hayashi K, Experimental approaches on measuring the mechanical properties and constitutive laws of arterial walls, *J. Biomech. Eng.*, **115**, 481-487, 1993
42. Hess F, Jerusalem C, Braun B, The Endothelialisation of a fibrous polyurethane microvascular prosthesis after implantation in the abdominal aorta of the rat, *J. Cardiovasc. Surgery*, **24**, 198?
43. Hibbit, Karlsson and Sorensen, ABAQUS Theory Manual, *v5.6*, 1996
44. Hibbit, Karlsson and Sorensen, ABAQUS Users Manual Volume1 and 2, *v5.6*, 1996
45. Hiratzka L F, Goeken J A, White R A, Wright C B, In vivo comparison of replamineform, silastic and bioelectric polyurethane arterial grafts, *Arch. Surg.* **114**, 699-7-1, 1979
46. How TV, Guidon R, Young SK, Engineering design of vascular prostheses, *Proc Instn Mech Engrs* **206** 1992
47. Hokanson DE and Strandness DE, Stress-strain characteristics of various arterial grafts, *J. Surgery, Gynacology and Obstetrics*, 1968
48. Humphrey J D, Strumpf R K, Yin F C P, Determination of a constitutive relation for passive myocardium: I. A new functional form, *J. Biomech. Eng.*, **112**, 333 - 339, 1990a

49. Humphrey J D, Strumpf R K, Yin F C P, Determination of a constitutive relation for passive myocardium: II. - Parameter estimation, *J. Biomech. Eng.*, **112**, 340 - 345, 1990b

50. Humphery JD, Mechanics of the arterial wall: Review and Directions, C*ritical Reviews in Biomedical Engineering* vol.**23**, issues 1 and 2, 1995

51. Hutchinson K J, Effect of variation of transmural pressure on the frequency response of isolated segments of canine carotid arteries, *Cirulation Res.*, **35**, 742-751, 1974

52. Huyghe J M, Van Campen D H, Arts T, Heethaar R M, The constitutive behaviour of passive heart muscle tissue: A quasi-linear viscoelastic formulation, *J. Biomech.* **24**, 841-849, 1991

53. Ishibashi H, Park H, Ojha M, Langdon S and Langille L, Shear-intimal thickening on the bed of an end-to-end anastomosis model, *Advances in Bioengineering*, **ASME BED-Vol 33**, 475-476, 1996

54. Johnson G A, Livesay G A, Woo S L-Y, Rajagopal K R, A single integral finite strain viscoelastic model of ligaments and tendons, *J. Biomech. Eng.* **118**, 221-226, 1996

55. Kowligi RR, von Maltzahn WW, Eberhart RC, Synthetic vascular graft fabrication by a precipitation-flotation method, **XXXIV**, *Trans Am Soc Artif Intern Organs* 1988

56. Langewouters G J, Wesseling K H, Goedhard W J A, The static elastic properties of 45 human thoracic and 20 abdominal aortas *in vitro* and the parameters of a new model, *J. Biomech.*, **17**, 425-435, 1984

57. Langewouters G J, Wesseling K H, Goedhard W J A, The pressure dependent dynamic elasticity of 35 thoracic and 16 abdominal human aortas *in vitro* described by a five component model, *J. Biomech.*, **18**, 613-620, 1985

58. Lanir Y, A microstructural model for the rheology of mammalian tendon, *J. Biomech. Eng.*, **102**, 332-339, 1980

59. Lanir Y, Constitutive equations for fibrous connective tissue, *J. Biomech.*, **16**, 1-12, 1983

60. Lockett F J, Nonlinear Viscoelastic Solids, Academic Press, New York, 1972

61. Lyman DJ, Albo D, Jackson R, Knutsen K, Development of small diameter vascular prostheses, *Trans Am Soc Artif Intern Organs* **XXIII**, 1977

62. Lyman D J, Fazzio F J, Voorhees H, Robinson G, Compliance as a factor effecting the patency of a copolyurethene vascular graft, *J Biomed. Mater. Res.*, **12**, 337-345, 1978

63. Malvern L E, Introduction to the Mechanics of a Continuum Medium, Prentice-Hall, Englewood Cliffs, New Jersey, 1969

64. McAfee M A, Kaufmann M V, Simon B R, Baldwin A L, Experimental/numerical approach to the determination of material properties of large arteries, *Advances in Bioengineering*, **ASME BED-Vol 28**, 111-112, 1994

65. Minns R J, Soden P D, Jackson D S, The role of the fibrous components and ground substance in the mechanical properties of biological tissues: a preliminary investigation, *J. Biomech.*, **6**, 153-165, 1973

66. Mohan D, Melvin J W, Failure properties of passive human aortic tissue I – uniaxial tension tests, *J. Biomech*, vol.**15** no.11, 887-902, 1982

67. Mooney DJ, Baldwin DF, Suh NP, Vacanti JP, Langer R, Novel approach to fabricate porous sponges of poly(D,L-lactic-co-glycolic acid) without the use of organic solvents, *Biomaterials*, **17**, no.14 1996

68. Myers B S, McElhaney J H, Doherty B J, The viscoelastic responses of the human cervical spine in torsion: experimental limitations of quasi-linear theory, and a method for reducing these effects, *J. Biomech.*, **24**, 811-817, 1991

69. Murabyashi S, Kambic H, Harasaki H, Morimoto T, Yozu R, Nose T, Fabrication and long-term implantation of semi-compliant small vascular prosthesis, *Trans Am Soc Artif Intern Organs* Vol. **XXXI**, 52-53, 1985

70. Newman D L, Bowden N L R, Gosling R G, The dynamic and static elastic properties of the aorta of the dog, *Cardiovasc. Res.*, **9**, 679-684, 1975

71. Noishiki Y, Yamane Y, Miyata T, Long term evaluation of a growable graft, **ASAIO Trans**, **35**, 267-270, 1989

72. Paasche P E, Kinley C E, Dolan F G, Gonza E R, Marble A E, Consideration of suture line stresses in the selection of synthetic grafts for implantation, *J. Biomech.*, **6**, 253-259,1973

73. Reed A M, Potter J, Szucher M, A solution grade biostable polyurethane elastomer: Chronoflex AR, *J. Biomaterials Applications,* **8**, 210-236, 1994

74. Rodgers V G J, Teodori M F, Borovetz H S, Experimental determination of mechanical shear stress about an anastomotic junction, *J. Biomech.*, **20**, 795-803, 1987

75. Sauvage LR, Berger KE, Mansfield PB, Wood SJ, Smith JC, Overton JB, Future directions in the development of arterial prostheses for small and medium calibre arteries, Symposium on Vascular surgery, *Surgical clinics of N. America*, **54**, no.1, Feb 1974

76. Sauvage L R, Walker M W, Berger K, Robel S B, Lischko M M, Yates, S G, Logan G A, Current arterial prostheses, *Arch. Surg.* **114** 687-691,1979

77. Seifert K B, Albo D, Knowlton H, Lyman D J, Effect of elasticity of prosthetic wall on patency of small-diameter arterial prostheses, *Surg. Forum.*, **30**, 206 - 208, 1979

78. Simon B R, Kaufmann M V, McAfee M A, Baldwin A L, Finite element models for the arterial wall mechanics, *J. Biomech. Eng.*, **115**, 489 - 496, 1993

79. Stewart S F C and Lyman D J, Effects of vascular graft/natural artery compliance mismatch on pulsatile flow, *J. Biomech.*, 25, 297-310,1992

80. Sternstein S S, Mechanical properties of glassy polymers: Treatise on Materials Science and Technology, Volume 10, part B, Edited: Schultz J M, Academic Press, New York

81. Takamizawa K and Hayashi K, Strain energy density function and uniform strain hypothesis for arterial mechanics, *J. Biomech.*, **9**, 293-300, 1987

82. Vaishnav R N, Young J T, Patel D J, Distribution of stresses and of strain-energy-density through the wall thickness in a canine aortic segment, *Circ. Res.*, **32**, 577-583, 1973

83. Vito R P, Hickey J, The mechanical properties of soft tissues – II: The elastic properties of arterial segments, *J. Biomech.* **13**, 951-956, 1980

84. von Maltzahn WW, Besdo D, Wiemer W, Elastic properties of arteries: A non-linear two-layer cylindrical model, *J. Biomech.*, **14**, 389-397, 1981

85. von Maltzahn WW, Warriyar R G, Kietzer WF, Experimental determination of the elastic properties of media and adventitia of bovine carotid arteries, *J. Biomech.*, **17**, 839-847, 1984

86. Ward I M, Mechanical properties of solid polymers, *John Wiley & Sons*, 1971

87. Weston M W, Rhee K, Tarbell J M, Compliance and diameter mismatch affect the wall shear rate distribution near an end-to-end anastomosis, *J. Biomech.*, **29**, 187-198, 1996

88. Wong A J and Pollard T D, Herman I M, Actin filament stress fibres in vascular endothelial cells *in vivo*, *Science*, **219**, 867-869, 1983

89. Wu S G and Lee G C, On nonlinear viscoelastic properties of arterial tissue, *ASME J. Biomech. Eng.*, **106**, 42 - 47, 1984

90. Young J T, Vaishnav R N, Patel D J, Non-linear anisotropic viscoelastic properties of canine arterial segments, *J. Biomech.*, **10**, 549-559, 1977

91. Zhang Z, Marois Y, Guidoin RG, Bull P, Marois M, How T, Laroche G, King MW, Vascugraft polyurethane arterial prosthesis as femoro-popliteal and femoro-peroneal, structural and chemical analyses of four excised grafts, *Biomaterials*, **18**, no.2 1997